

# LEVELS AND GAMMA DEEXCITATION MODES IN SOME NUCLEI

A Thesis Submitted  
In Partial Fulfilment of the Requirements  
for the Degree of  
DOCTOR OF PHILOSOPHY

BY

*C. Rangacharyulu*

to the

DEPARTMENT OF PHYSICS  
INDIAN INSTITUTE OF TECHNOLOGY KANPUR  
AUGUST 1972

100-100000-100000

100-100000-100000

100-100000-100000

422158



ii

CERTIFICATE

Certified that the work presented in this thesis entitled 'LEVELS AND GAMMA DEEXCITATION MODES IN SOME NUCLEI' by C. Rangacharyulu has been carried out under my supervision and it has not been submitted elsewhere for a degree.

*G.K. Mehta*

G.K. Mehta  
Assistant Professor  
Department of Physics  
Indian Institute of Technology Kanpur

POST GRADUATE OFFICE
This thesis is approved
for the award of the Degree of
Doctor of Philosophy (Ph.D.)
in the subject of
Physics
Indian Institute of Technology Kanpur
Date: 29/9/72 <i>M</i>

### ACKNOWLEDGEMENTS

I would like to express my gratitude to Dr. G.K. Mehta for introducing me to this field and for his valuable guidance during the course of this work. I am indebted to Dr. R.M. Singru for his constant encouragement and many helpful suggestions. The kind interest and useful suggestions of Dr. G.N. Rao are gratefully acknowledged. I wish to thank Dr. Y.R. Waghmare for many stimulating discussions. I am thankful to Professor G. Srikanthiah for providing me the facilities of Van de Graaff accelerator laboratories.

I extend my thanks to Dr. B.V.N. Rao for many valuable suggestions. My sincere thanks are due to Mr. V.G. Jadhao for his help in the measurements and also many fruitful discussions.

My thanks are due to the technical staff of Nuclear Physics and Central Nuclear Laboratories for their help. Help received from Mr. B.K. Jain is acknowledged.

Several of my friends made my stay at IIT/K a memorable one and my thanks are due to all of them. Special mention should be made of Messrs. S. Krishna, M.S. Prasad and Dr. B.L. Deopura.



Sincere thanks are due to Mr. N. Ahmad for his excellent typing of the manuscript.

Financial assistance received from CSIR (India) and DAE (India) organizations is gratefully acknowledged.

.

C. RANGACHARYULU

# TABLE OF CONTENTS

<u>Chapter</u>	<u>Page</u>
LIST OF TABLES	viii
LIST OF FIGURES	ix
SYNOPSIS	xiv
I. INTRODUCTION	1
II. EXPERIMENTAL DETAILS	9
2.1 Introduction	9
2.2 Detectors	9
2.3 Coincidence Measurements	13
2.4 Fast-Slow Coincidence Set-up	15
2.5 Sum-coincidence Spectrometer	18
A. Description of the technique	19
B. Description of the spectrometer	25
C. Performance	28
D. Fictitious cascades	32
2.6 Target Holder and Collimator System	36
III. SUM COINCIDENCE STUDIES ON $^{131}\text{Cs}$	42
3.1 Introduction	42
3.2 Measurements of Singles Spectra	43
3.3 Sum-coincidence Measurements	44
3.4 Conclusions	55

<u>Chapter</u>	<u>Page</u>
IV. DECAY SCHEME STUDIES OF $^{147}\text{Nd}$	58
4.1 Introduction	58
4.2 Ge(Li) Spectra of Gamma Transitions	59
4.3 Coincidence Measurements	59
4.4 Discussion	71
4.5 Summary	72
V. DECAY OF $^{115\text{m}}\text{Cd}$	76
5.1 Introduction	76
5.2 Details of the Measurements	76
5.3 Summary	83
VI. NUCLEAR LEVEL STRUCTURE STUDIES OF $^{99}\text{Ru}$	86
6.1 Introduction	86
6.2 Gamma Ray Transitions and Intensities	87
6.3 Sum-coincidence Spectra	96
6.4 Summary	105
6.5 Comments on the Level Structure of $^{99}\text{Ru}$	107
VII. DECAY OF $^{63}\text{Zn}$	116
7.1 Introduction	116
7.2 Details of Measurement	116
7.3 Results	117
7.4 Discussion	127
APPENDIX	130

<u>Chapter</u>	<u>Page</u>
VIII. STUDY OF $^{27}\text{Al}(\text{p},\gamma)^{28}\text{Si}$ RESONANCE DECAYS	134
8.1 Introduction	134
8.2 Stability etc. of the Proton Beam	135
8.3 Study of the Gamma Decay of 992 and 1261 keV Resonances in $^{27}\text{Al}(\text{p},\gamma)^{28}\text{Si}$ Reaction	145
8.4 Gamma Decay of 992 keV Resonance	147
8.5 Gamma Decay of 1261 keV Resonance	155
8.6 Summary	155

# LIST OF TABLES

<u>Number</u>	<u>Caption</u>	<u>Page</u>
2.1	Energy calibration standards of gamma rays	12
3.1	Gamma rays observed in the decay of $^{131}\text{Ba}$	49
4.1	Gamma rays observed in the decay of $^{147}\text{Nd}$	62
4.2	Summary of sum-coincidence measurements of $^{147}\text{Nd}$	64
5.1	Gamma rays observed in the decay of $^{115\text{m}}\text{Cd}$	80
5.2	Summary of sum-coincidence measurements of $^{115\text{m}}\text{Cd}$	82
6.1	Gamma ray observed in the 16.1 d decay of $^{99}\text{Rh}$ and their relative intensities	94
6.2	Summary of sum-coincidence measurements	103
7.1	Gamma ray energies in the 38.4 m decay of $^{63}\text{Zn}$	125
8.1	Summary of sum-coincidence measurements at resonance for $E_p = 992 \text{ keV}$	153
8.2	Summary of sum-coincidence measurements at resonance for $E_p = 1261 \text{ keV}$	160

# LIST OF FIGURES

<u>Number</u>	<u>Caption</u>	<u>Page</u>
2.1	Efficiency curve of Ge(Li) detector	11
2.2	Ge(Li)-NaI(Tl) fast-slow coincidence assembly	16
2.3	Block diagram of sum-coincidence spectrometer	20
2.4	Decay scheme to explain sum-coincidence technique	21
2.5	Sum-coincidence spectrometer	26
2.6	Sum-coincidence spectrum of $^{22}\text{Na}$	29
2.7	Sum-coincidence spectrum of $^{60}\text{Co}$	30
2.8	Decay Scheme to explain the origin of fictitious cascades	33
2.9	The target holder	38
2.10	The Collimator system	39
3.1	Ge(Li) spectrum of $^{131}\text{Cs}$ in 0-280 keV energy range	45
3.2	Ge(Li) spectrum of $^{131}\text{Cs}$ in 280-390 keV energy range	46
3.3	Ge(Li) spectrum of $^{131}\text{Cs}$ in 390-510 keV energy range	47
3.4	Ge(Li) spectrum of $^{131}\text{Cs}$ in 510-1060 keV energy range	48
3.5	Sum-coincidence spectrum of $^{131}\text{Cs}$ with gate at 1048 keV	51
3.6	Sum-coincidence spectrum of $^{131}\text{Cs}$ with gate at 585 keV	52
3.7	Sum-coincidence spectrum of $^{131}\text{Cs}$ with gate at 585 keV taken after four half lives	53

<u>Number</u>	<u>Caption</u>	<u>Page</u>
3.8	Level scheme of $^{131}\text{Cs}$	56
4.1	Ge(Li) spectrum of $^{147}\text{Nd}$ in 0-460 keV energy range	60
4.2	Ge(Li) spectrum of $^{147}\text{Nd}$ in 460-700 keV energy range	61
4.3	Sum-coincidence spectrum of $^{147}\text{Nd}$ with gate at 595 keV	67
4.4	Sum-coincidence spectrum of $^{147}\text{Nd}$ with gate at 685 keV	68
4.5	Sum-coincidence spectrum of $^{147}\text{Nd}$ with gate at 725 keV	69
4.6	Level scheme of $^{147}\text{Pm}$	73
5.1	Ge(Li) spectrum of $^{115\text{m}}\text{Cd}$ in 0-900 keV energy range	78
5.2	Ge(Li) spectrum of $^{115\text{m}}\text{Cd}$ in 900-1500 keV energy range	79
5.3	Sum-coincidence spectrum of $^{115\text{m}}\text{Cd}$ with gate at 598 keV	81
5.4	Level scheme of $^{115}\text{In}$	84
6.1	Ge(Li) spectrum of $^{99}\text{Rh}$ in 0-400 keV energy range	88
6.2a	Ge(Li) spectrum of $^{99}\text{Rh}$ in 400-700 keV energy range	89
6.2b	Ge(Li) spectrum of $^{99}\text{Rh}$ in 700-1150 keV energy range	90
6.3	Ge(Li) spectrum of $^{99}\text{Rh}$ in 1150-1680 keV energy range	91
6.4	Ge(Li) spectrum of $^{99}\text{Rh}$ in energy range >1700 keV	92
6.5	Sum-coincidence spectrum of $^{99}\text{Rh}$ with gate at 575 keV	97

<u>Number</u>	<u>Caption</u>	<u>Page</u>
6.6	Sum-coincidence spectrum of $^{99}\text{Rh}$ with gate at 618 keV	98
6.7	Sum-coincidence spectrum of $^{99}\text{Rh}$ with gate at 850 keV	99
6.8	Sum-coincidence spectrum of $^{99}\text{Rh}$ with gate at 941 keV	100
6.9	Sum-coincidence spectrum of $^{99}\text{Rh}$ with gate at 1000 keV	101
6.10	Sum-coincidence spectrum of $^{99}\text{Rh}$ with gate at 1295 keV	102
6.11	Gamma decay scheme of $^{99}\text{Rh}$ (16.1 days) and levels of $^{99}\text{Ru}$	108
6.12	Systematics of even parity states in odd A Mo and Ru isotopes	111
6.13	Systematics of odd parity states in odd A Mo and Ru isotopes	112
7.1	Ge(Li) Spectrum of $^{63}\text{Zn}$ in 400-700 keV energy range	118
7.2	Ge(Li) spectrum of $^{63}\text{Zn}$ in 700-1050 keV energy range	119
7.3	Ge(Li) spectrum of $^{63}\text{Zn}$ in 1050-1250 keV energy range	120
7.4	Ge(Li) spectrum of $^{63}\text{Zn}$ in 1300-2100 keV energy range	121
7.5	Ge(Li) spectrum of $^{63}\text{Zn}$ in 2100-2800 keV energy range	122
7.6	Ge(Li) spectrum of $^{63}\text{Zn}$ in 2820-3300 keV energy range	123
7.7	Half life plots of annihilation quantum (511 keV) and 1716, 1734 and 2103 keV gamma rays of $^{63}\text{Zn}$	124
7.8	Gamma decay scheme of $^{63}\text{Zn}$ and levels of $^{63}\text{Cu}$	128



<u>Number</u>	<u>Caption</u>	<u>Page</u>
8.1	Experimental layout	136
8.2	Reproducibility test of beam energy	138
8.3	Threshold spectrum of ${}^3\text{H}(p,n){}^3\text{He}$ reaction	-141
8.4	Resonances in ${}^{27}\text{Al}(p,\gamma){}^{28}\text{Si}$ and ${}^{19}\text{F}(p,\alpha\gamma){}^{16}\text{O}$ reaction for calibration	142
8.5	Voltage calibration plot	144
8.6	Excitation function of ${}^{27}\text{Al}(p,\gamma){}^{28}\text{Si}$ reaction	146
8.7a	Ge(Li) spectrum of gamma rays from $E_p=992$ keV resonance in ${}^{27}\text{Al}(p,\gamma){}^{28}\text{Si}$ reaction in the energy region 2.5-6.5 MeV	148
8.7b	Ge(Li) spectrum of gamma rays from $E_p=992$ keV resonance in ${}^{27}\text{Al}(p,\gamma){}^{28}\text{Si}$ reaction in the energy region 6.5-11.0 MeV	149
8.8	1-3 MeV gamma ray spectrum of ${}^{27}\text{Al}(p,\gamma){}^{28}\text{Si}$ with $E_p = 992$ keV	150
8.9	Sum-coincidence spectrum with gate at 10.76 MeV for 992 keV resonance	151
8.10	Sum-coincidence spectrum with gate at 6.28 MeV resonance	152
8.11	Gamma decay scheme of resonant capturing state in ${}^{27}\text{Al}(p,\gamma){}^{28}\text{Si}$ at $E_p = 992$ keV	155
8.12a	Ge(Li) spectrum of gamma rays from $E_p = 1261$ keV resonance in ${}^{27}\text{Al}(p,\gamma){}^{28}\text{Si}$ reaction in the energy region 0-4 MeV	156
8.12b	Ge(Li) spectrum of gamma rays from $E_p = 1261$ keV resonance in ${}^{27}\text{Al}(p,\gamma){}^{28}\text{Si}$ reaction in the energy region 4-11 MeV	157

<u>Number</u>	<u>Caption</u>	<u>Page</u>
8.13	Sum-coincidence spectrum with gate at 11.02 MeV for 1261 keV resonance	158
8.14	Sum-coincidence spectrum with gate at 8.1 MeV for 1261 keV resonance	159
8.15	Gamma decay scheme of resonant capturing state in $^{27}\text{Al}(p,\gamma)^{28}\text{Si}$ at $E_p = 1261$ keV	161

## SYNOPSIS

### LEVELS AND GAMMA DEEXCITATION MODES IN SOME NUCLEI

G. RANGACHARYULU  
Ph.D.

Department of Physics  
Indian Institute of Technology, Kanpur  
August 1972

One of the aims in gamma ray spectroscopy is the determination of the energies and the intensities of gamma transitions emitted from a radioactive isotope or from a nuclear level populated in a nuclear reaction. It also attempts to establish the genetic relations among the gamma rays to determine unambiguously the positions of energy levels and their cascade modes of decay. Precise information of energies and intensities along with the data of coincidence relations of gamma rays leads to unique level schemes in many cases. Such studies with a Ge(Li) detector and NaI(Tl) scintillation detectors used for gamma ray energy measurements and to establish the deexcitation modes of nuclear levels were undertaken in the present study. The decay schemes of  $^{131}\text{Ba}$ ,  $^{147}\text{Nd}$ ,  $^{115\text{m}}\text{Cd}$ ,  $^{99}\text{Rh}$  and  $^{63}\text{Zn}$  were studied to arrive at the level schemes of  $^{131}\text{Cs}$ ,  $^{147}\text{Pm}$ ,  $^{115}\text{In}$ ,

$^{99}\text{Ru}$  and  $^{63}\text{Cu}$  respectively. The gamma decay measurements on the 992 and 1261 keV resonances of  $^{27}\text{Al}(p,\gamma)^{28}\text{Si}$  were also carried out.

The first chapter forms a general introduction. The importance of different detector assemblies is discussed. The methods of the present investigation are pointed out. A brief discussion of the problems of the present study follows.

Chapter II provides the experimental details of the present investigation. The characteristics of the radiation detectors are presented. The coincidence assemblies are described. A detailed description of the sum-coincidence set-up and the discussion of the origin of fictitious cascades in sum-coincidence spectra is also given. Lastly, the target holding systems used for the experiments with the 2 MV Van de Graaff accelerator are described.

Gamma decay measurements of  $^{131}\text{Ba}$  isotope form the subject matter of Chapter III. Two recent investigations on the decay of  $^{131}\text{Ba}$ , using sum-coincidence assemblies, are far from consistent. The existence of a few gamma rays has been in dispute. Sum-coincidence and Ge(Li) spectra measurements were carried out to resolve these discrepancies.

A recent investigation on the decay of  $^{147}\text{Nd}$  indicated several new gamma transitions and levels, unknown earlier.

Chapter IV describes the measurements carried out to arrive at an unambiguous decay scheme of  $^{147}\text{Nd}$ . The present study of the decay of  $^{115\text{m}}\text{Cd}$ , not well understood from the measurements of earlier workers, is described in Chapter V.

Chapter VI describes the studies of the  $^{99}\text{Rh}$  decay (16.1 days), motivated to establish the cascade relations of gamma rays of the decay. Detailed calculations of the level structure of  $^{99}\text{Ru}$  are not available in literature. Systematics of odd A Ru and Mo nuclear levels are compared to offer a few qualitative comments on the level structure of  $^{99}\text{Ru}$ .

The structure of  $^{63}\text{Cu}$  levels has been studied by many nuclear reactions and also from the decay of 38.4 minute activity of  $^{63}\text{Zn}$ . The structure has also been the subject of many theoretical investigations. The agreement between the theory and experiment is rather unsatisfactory. Besides, the two recent investigations of this decay differ in many details. Chapter VII describes the study of this decay, with an attempt to resolve the discrepancies. A possible test for the core-excitation model from the knowledge of ft values of the population to the core-multiplet members in the nuclear beta decay is proposed and the explicit calculation is shown in the Appendix. The same test is applied to the multiplet in  $^{63}\text{Cu}$  and the results are discussed.

Although the 992 and 1261 keV resonances in  $^{27}\text{Al}(p,\gamma)^{28}\text{Si}$  have been extensively studied with scintillation detectors, the recent measurements with Ge(Li) detectors disagree about the population of certain levels. An attempt is made, in the present investigation, to clarify these doubts with the help of singles and coincidence measurements. Chapter VIII deals with the details of measurements and results. A few performance tests of the newly installed 2 MV Van de Graaff accelerator carried out to establish the stability, reproducibility etc. of proton beam, are also described in Chapter VIII.

## CHAPTER I

### INTRODUCTION

Nuclear spectroscopy concerns the study of properties of nuclear levels, which constitute the measurements of the properties of nuclear radiations, emitted from them. One needs to measure the energies and intensities of the radiations and also their angular distributions and polarization properties to determine the positions of the energy levels, their modes of deexcitations, spins and parities. The first aspect of such studies is to locate the nuclear energy levels. This is done from the studies of the nuclear disintegration processes, in which the levels of interest are populated. It can either be a nuclear reaction study or the study of induced radioactivities. The artificial radioactivities can be produced either in a reactor or by using a particle accelerator. Each disintegration study of the present investigation involved either one of these processes. The gamma ray studies, a major branch of nuclear spectroscopy, was the method of investigation of this work.

The first stage of these gamma rays spectroscopic studies is to measure the gamma ray energies. Before the advent of Ge(Li) detectors, NaI (Tl) scintillation detectors were the best ones available for these measurements. But due to their poor energy resolution, it was always a

difficult problem to identify the gamma rays properly, especially for closely separated transitions. The Ge(Li) detectors have practically revolutionized the gamma ray spectroscopy due to the order of magnitude improvement in energy resolution. This has made precise determination of energies and intensities of gamma rays possible. However, the gamma rays of low intensities still escape detection, especially when they are submerged in the Compton background of gamma rays of larger intensities. Anticompton spectrometers, which make use of a Ge(Li) detector enclosed in a large scintillation detector, decrease the Compton background from the spectra and help to identify the gamma rays of low intensities. The removal of Compton background is, of course, not complete. The expenditure and the amount of efforts needed to optimize the performance of such an assembly are perhaps not worthwhile in view of the very limited amount of additional information obtainable from them.

Even if the total number of gamma rays emanating from the nuclear levels are known, one can hope to get a reasonable information about the energy levels from these simple measurements only when the number of gamma rays are not many. However, in general, the number of levels being populated are themselves many and the various possible modes of deexcitation of each level produce numerous gamma transitions. A data of gamma ray



energies can, in many cases, be explained by various combinations of energy levels. To establish the level scheme unambiguously, further knowledge of genetic relations of gamma rays is, therefore, necessary. This information is obtainable from the measurements of gamma ray coincidence spectra. From the consideration of energy resolutions, a coincidence assembly of two Ge(Li) detectors is most desirable. But the detection efficiency of the system is so low, that such a spectrometer results in unduly long data collection times. When one undertakes coincidence measurements one, therefore, naturally prefers scintillation detector assemblies, as long as energy resolution is not of primary concern. If good energy resolution is essential, the measurements have to be done by replacing one or both of the scintillation detectors by Ge(Li) detectors.

The true/chance coincidence ratio of a coincidence assembly is a measure of its superiority. The assemblies with poor ratios do not provide meaningful spectra. This ratio is equal to  $1/2\tau N$ , where  $2\tau$  is the time resolution of the coincidence assembly and  $N$  is the radioactive source strength. Slow coincidence systems, with large  $2\tau$ , result in poor true/chance ratios. Strong radioactive sources cannot be used with these systems. However, for linearity of energy response, one has to retain the slow coincidence systems. These conflicting requirements are

satisfied in fast-slow coincidence assemblies. In these systems, the true/chance coincidence ratios are governed by the fast sections with shorter resolving times and the energy information is retained in the slow sections. The fast-slow systems, which are conventional by now, provide the genetic relations of the gamma rays and also reduce the compton background to some extent by not recording the spectra of gamma rays non-coincident with the gamma rays of gate settings. However, the compton background of the gamma rays in coincidence, is still troublesome. The sum-coincidence technique proves more useful in the decay scheme studies, as it provides the data of genetic relations of gamma rays and also removes the compton background to a fairly large extent. In favourable cases, the removal of compton background is almost complete. It, thus, helps to establish weak branching modes of deexcitation of nuclear levels.

The above considerations indicate that the measurements of the radiations with a Ge(Li) detector along with the results of coincidence measurements provide, in most of the cases, unambiguous level schemes. With this point of view, the present studies made use of a Ge(Li) detector and coincidence systems with NaI(Tl) scintillation detectors. A sum-coincidence set up, incorporating the fast-slow coincidence condition, was assembled for the present measurements. Very extensive use was made of

these two assemblies. In some cases, conventional fast-slow coincidence spectrometers were also used.

The following general procedure was adopted in the present investigations of the decay schemes: First stage of the study was the measurement of Ge(Li) detector spectra. The spectra were recorded in expanded energy scales to obtain precise energies and intensities of gamma rays. Spectra were measured over regular periods of time to assign the decay rate of each gamma ray. This was necessary to make sure that the gamma rays being considered do really have their origin in the isotope of interest and are not from any impurity. In many cases, peaks due to the presence of impurities were observed. However, they were identified and taken into account during the analysis of the data.

The second stage was the measurement of coincidence spectra. The sum-coincidence spectrometer was mostly used for this purpose. In each study, spectra were recorded with several gate settings, to obtain all possible genetic relations. A decay scheme, in each case, was arrived at with the help of results from these two sets of measurements.

### Problems of the Present Study

The following problems were investigated during the present studies.

- i)  $^{131}\text{Cs}$  level scheme : Horen et al.<sup>1</sup> measured the internal conversion spectra of the decay of  $^{131}\text{Ba}$  and proposed a level scheme. Later studies of Kucarova et al.<sup>2</sup> report two new gamma rays of 506 and 563 keV gamma ray energies. The sum-coincidence studies of Murthy et al.<sup>3</sup> and Mangal et al.<sup>4</sup> disagree on the existence of 969 keV gamma ray. Besides, Mangal et al. report a new gamma transition. Our measurements aim at resolving these discrepancies.
- ii)  $^{147}\text{Nd}$  decay : In the study of this decay, Bashandy et al.<sup>5</sup> reported several new gamma transitions and levels from the measurements of electron spectra with an iron free double focussing spectrometer, which was disturbing. It was felt that there is a need to study the decay scheme to examine the situation.
- iii)  $^{115\text{m}}\text{Cd}$  decay : Visweswara Rao et al.<sup>6</sup> investigated this decay scheme with a sum-coincidence spectrometer and Graeffe et al.<sup>7</sup> studied it with a Ge(Li) detector. These two reports disagree about the existence of a few levels and transitions. For example, the 650 and 1560 keV levels observed by Rao et al.<sup>6</sup> were not observed by Graeffe et al. In stead, Graeffe et al. proposed a new level at 828 keV. The measurements of the present study

aim at clarifying these doubtful aspects.

- iv)  $^{99}\text{Rh}$  decay : Very limited amount of information is available on the genetic relations of the gamma rays, arising from this decay. The present study was aimed at providing a firm basis for the decay scheme, with the help of coincidence measurements. Furthermore, the level structure of  $^{99}\text{Ru}$  is also not well understood from theoretical point of view. A qualitative description of the systematics of odd A Mo and Ru nuclei was, therefore, attempted.
- v)  $^{63}\text{Zn}$  decay : The two recent investigations of the decay disagree in details. The existence of many gamma rays is controversial. The present study was carried out to resolve these discrepancies. An attempt is also made to test the applicability of core-excitation model for this nucleus.
- vi)  $^{28}\text{Si}$  resonances : In spite of many investigations on the 992 keV resonance decay in  $^{27}\text{Al}(p,\gamma)^{28}\text{Si}$  reaction, certain aspects of this decay are still not understood. For example, the existence of 10.27 MeV level has been in doubt. Similarly, the 1261 keV resonance decay reported by Meyer et al.<sup>8</sup> differs from the reports of Gibson et al.<sup>9</sup> in details. The present measurements were aimed at examining these aspects.

REFERENCES

1. D.J. Horen, J.M. Hollander and R.L. Graham, Phys. Rev. 135 (1964) B301.
2. T. Kucarova, B. Kracik and V. Zvolaska, Sov. J. Nucl. Phys. 7 (1968) 433.
3. V.R.K. Murthy and S. Jnanananda, Proc. Phys. Soc. 91 (1967) 600.
4. P.C. Mangal and P.N. Trehan, Proc. Nucl. Phys. and Sol. Sta. Phys. Symp. [DAE, Bombay (India)] Vol. 2 (1968) 188.
5. E. Bashandy and A.A. El-Haliem, Z. Naturf. 22A (1967) 154.
6. V. Visweswara Rao, V. Lakshminarayana and S. Jnanananda, Nucl. Phys. 51 (1964) 442.
7. G. Graeffe, C.W. Tang, C.D. Coryell and G.E. Gordon Phys. Rev. 149 (1967) 884.
8. M.A. Meyer, N.S. Wolmarans and D. Reitmann, Nucl. Phys. A144 (1970) 261.
9. E.F. Gibson, K. Battleson and D.K. McDaniels, Phys. Rev. 172 (1968) 1004.

## CHAPTER II

### EXPERIMENTAL DETAILS

#### II.1 Introduction

In the present investigation, an extensive use was made of NaI(Tl) scintillators, Ge(Li) detectors and different types of coincidence arrangements with these detectors. For precise energy definition of gamma rays and their intensity evaluations, Ge(Li) detectors were used. In the coincidence set-ups, generally NaI(Tl) scintillation detectors were preferred because of their higher efficiencies. However, for some measurements it was found necessary to use Ge(Li) detector at least as one of the detectors in coincidence system, where better energy resolution was needed.

#### II.2 Detectors

The excellent energy resolution of Ge(Li) detectors, which is an order of magnitude better than the scintillation detectors, give accuracies in energy measurements which could previously be obtained only with bent crystal spectrometers. The Ge(Li) detectors are, therefore, generally used for precise energy and intensity assignments of gamma rays.

The Ge(Li) detector, used in the present studies, is of 4.2 c.c. effective volume. It is a planar diode of

7 mm depletion depth. It has the energy resolution  $\text{FWHM} = 3 \text{ keV}$  at 662 keV gamma energy. The relative photopeak efficiency curve for a fixed source to detector geometry was determined upto 2 MeV gamma energies. Standard calibration sources, procured from the International Atomic Energy Agency [IAEA, Vienna], were used in the measurement. The efficiency curve is shown in Fig. 2.1.

Gamma ray spectra were recorded with sources of different strengths to measure the change in the position of photopeak with source strength, due to pile up effects. The variation was found to be negligibly small, being about .02%, when the countrates were changed by a factor of 10 from  $10^3$  to  $10^4$  counts per second. The energy calibration for the later experiments were, however, done at about the same counting rates as in the actual experiment. The most commonly used calibration standards are listed in Table 2.1. Internal calibrations, whenever possible, were used as a check over the external calibrations.

For intensity assignments, gamma ray spectra were measured in the same source to detector geometry, as was used in the determination of relative photopeak efficiency of the detector. The measured photopeak areas were corrected for the relative efficiencies of detection. The intensities, thus measured, were normalized with respect to a specific gamma ray of the spectrum.



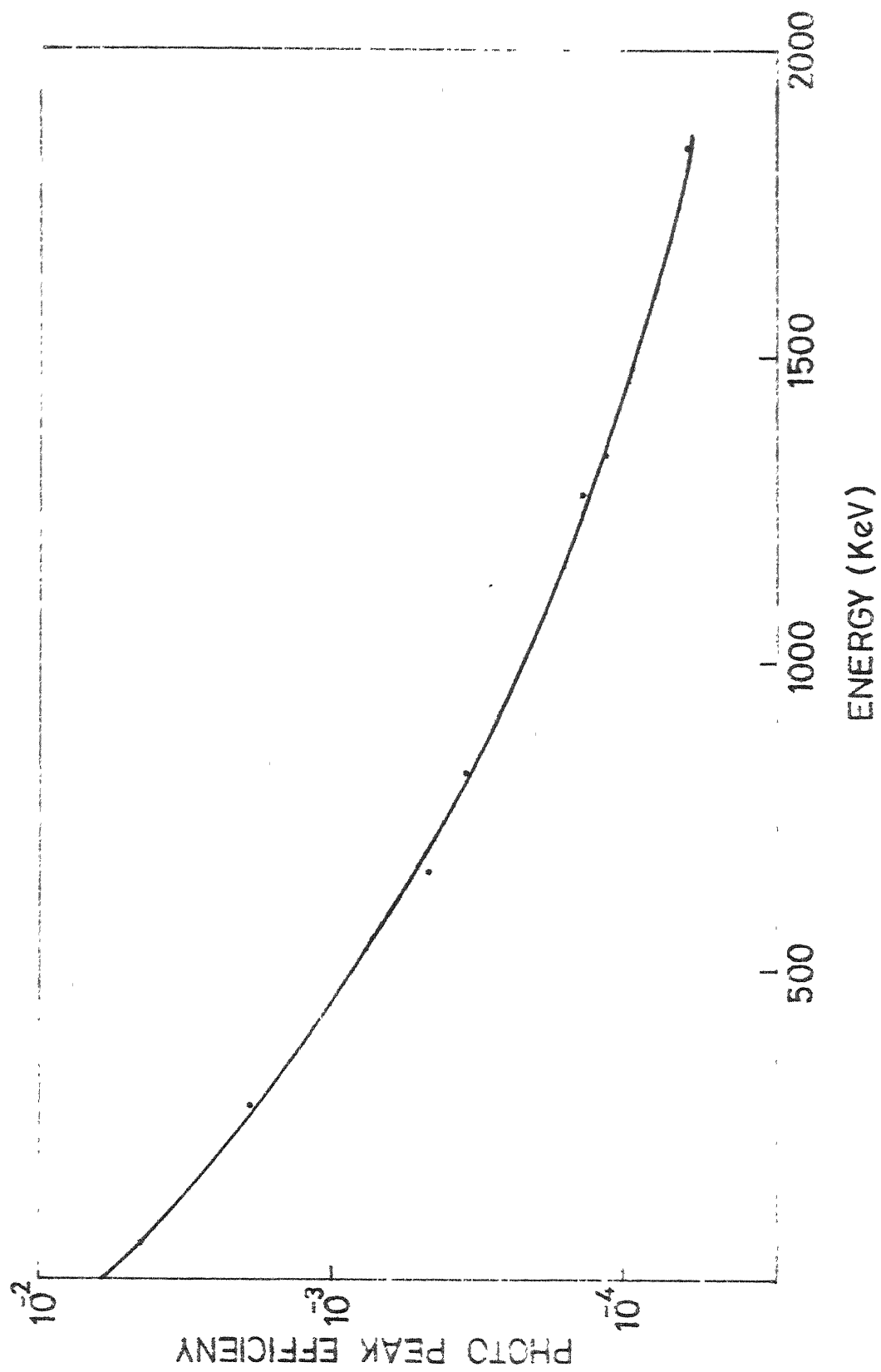


FIG. 2.1 RELATIVE PHOTOPEAK EFFICIENCY CURVE OF Ge(Li) DETECTOR

Table 2.1. Energy Calibration Standards<sup>(a)</sup>

<u>Radioactive isotope</u>	<u>Energy of the <math>\gamma</math>-ray (keV)</u>
$^{241}\text{Am}$	59.543
$^{57}\text{Co}$	121.97
$^{141}\text{Ce}$	145.43
$^{203}\text{Hg}$	279.17
$^{22}\text{Na}$	511.006
$^{137}\text{Cs}$	661.59
$^{54}\text{Mn}$	834.85
$^{89}\text{Y}$	897.96
$^{65}\text{Zn}$	1115.44
$^{60}\text{Co}$	1173.226
$^{22}\text{Na}$	1274.53
$^{60}\text{Co}$	1332.48
$^{88}\text{Y}$	1836.08

(a) Taken from Table of isotopes (1967 Edition) by C.M. Lederer, J.M. Hollander and I. Perlman, page 561.

### II.3 Coincidence Measurements

The measurements using a single detector will only provide the energies and intensities of different gamma rays emitted from an isotope. To know the genetic relations among the gammas, time coincidence measurements are necessary. A coincidence set up is of finite resolving time ( $2\tau$ ), such that two events in the detectors separated by less than the time  $2\tau$ , are recorded as coincident. The finite resolving time also gives rise to undesirable random coincidences. The choice of the resolving time and the source strength are made to optimise the true/chance coincidence ratio.

If a source of strength  $N$  is used, then the countrate of each detector is

$$N_1 = N\epsilon_1\Omega_1 \quad (2.1a)$$

$$N_2 = N\epsilon_2\Omega_2 \quad (2.1b)$$

and the genuine coincidence rate is

$$N_{\text{true}} = N\epsilon_1\Omega_1\epsilon_2\Omega_2 \quad (2.2)$$

where  $\epsilon_1, \epsilon_2$  are the efficiencies of the detectors  $\Omega_1, \Omega_2$  are the solid angles subtended by the source on the two detectors respectively and  $N_1, N_2$  are the observed contrates in the two detectors.

The accidental coincidence rate is given by

$$N_{\text{chance}} = 2\tau N^2\epsilon_1\Omega_1\epsilon_2\Omega_2 \quad (2.3)$$

The ratio true/chance coincidence is

$$\frac{N_{\text{true}}}{N_{\text{chance}}} = \frac{1}{2\tau N} \quad (2.4)$$

The experiment aims at maximizing this ratio. So  $2\tau N$  should be as small as possible. It can be achieved by using coincidence units of very short resolving times and sufficiently weak radioactive sources. Use of weak sources results in prolonged data collection times, which are undesirable. Very short resolving time for coincidence system also result in the loss of detection efficiency. So an optimum condition should be arrived at.

The fast-slow coincidence spectrometers solve this problem quite satisfactorily. The energy processing section of the assembly is a slow type, retaining the linearity of response. The time processing section is of fast type, which essentially decides the true/chance ratios of the set up. Finally slow coincidence is sought between the fast section and slow section, thus retaining both energy and time information. This assembly is very useful, as reasonably strong sources can be used without loosing any information.

In the present investigation, two coincidence set ups incorporating the fast-slow coincidence condition were used. The same are described in the following sections.

## II.4 Ge(Li)-NaI(Tl) fast-slow Coincidence Assembly

A fast-slow coincidence assembly with two Ge(Li) detectors would have been much favoured in gamma ray spectroscopy, but for the low efficiency of detection. A Ge(Li)-NaI(Tl) fast-slow coincidence system is a good compromise due to the fact that it is superior to NaI(Tl)-NaI(Tl) system in energy resolution and to Ge(Li)-Ge(Li) system in the efficiency of detection. A Ge(Li)-NaI(Tl) fast-slow coincidence assembly is set up to derive the advantages of the system.

The block diagram of the system is shown in Fig. 2.2. The 4.2 c.c. Ge(Li) detector, the characteristics of which are described earlier, was used as one of the detectors. A NaI(Tl) crystal of 4.4 cm diameter and 5 cm thickness was mounted on a 56 AVP photomultiplier tube. This forms the second detector of the assembly. The anode pulses of the scintillation detector were clipped to get the risetime  $tr \approx 15$  nsec and width  $T = 150$  nsec. The linear pulses were drawn from the eighth dynode.

Linear pulses carrying the energy information are the only output pulses available from the Ge(Li) detector. To achieve good timing and also energy information, the detector output is simultaneously fed to a time pickoff unit and a linear amplifier. The output of time pickoff unit is further processed in a time pickoff control unit.

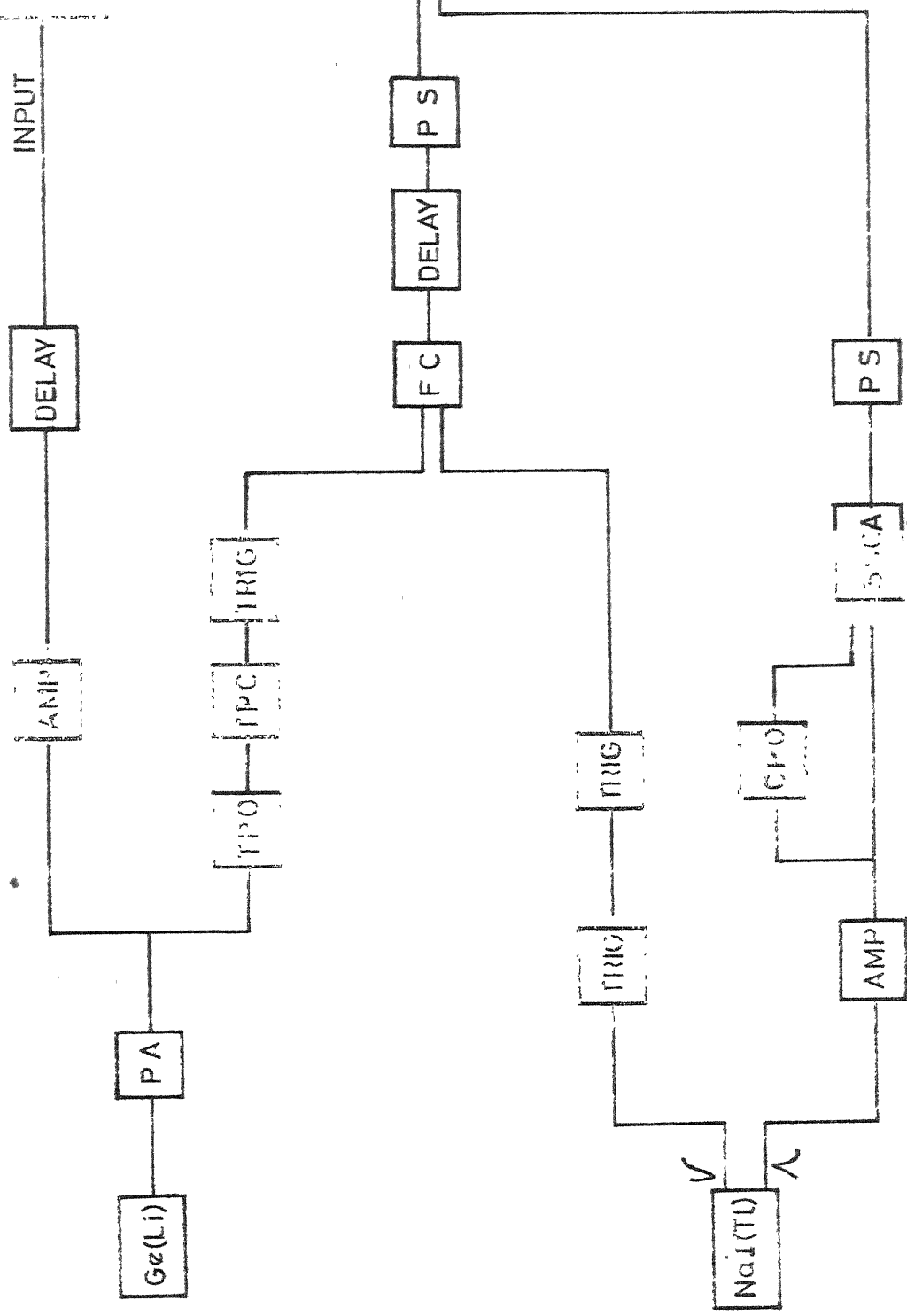


FIG.2.2 Ge(Li)-NaI(Tl) FAST-SLOW COINCIDENCE ASSEMBLY

The fast pulses from pickoff control are stretched to a width of 40 nsec in a pulse shaper circuit. The output of pulse shaper forms one input of the fast coincidence circuit. The anode pulse of the NaI(Tl) detector is discriminated against the noise and the output of the discriminator is of 40 nsec width. It forms the other input for the fast coincidence circuit.

The linear pulses from NaI(Tl) detector feed simultaneously a strobed single channel analyzer and also a crossover pickoff unit. The single channel analyzer is used in external strobing mode, with the output pulses of crossover pickoff unit as its strober pulses. The output pulse of crossover pickoff unit is generated when the input pulse crosses from a positive to a negative value. The discriminator of crossover pickoff unit is set at the point on the output pulse from the amplifier, having minimum walk as a function of amplitude. This arrangement minimizes the variation in the timing of output pulses from single channel analyzer.

The output pulses from single channel analyzer are shaped in a pulse shaper unit. The output of it is an input to the slow coincidence circuit. The fast coincidence output is delayed to match in time with the single channel analyzer output and stretched to a width of .5  $\mu$ s. The stretched pulses form the other input of the slow coincidence circuit. Both the input pulses of the slow coincidence

circuit are of  $0.5 \mu\text{s}$  width. The coincidence circuit, being of overlapping type, is of time resolution  $2\tau = 1 \mu\text{sec}$ . The output of the slow coincidence circuit is shaped to meet the requirements of the gate pulse of multichannel analyzer. The output pulses of the linear amplifier are properly delayed in time and used as the input to multichannel analyzer.

Thus, the Ge(Li) spectra in coincidence with the selected gamma ray in the NaI(Tl) detector are recorded on multichannel analyzer. Energy calibrations of the set up are done as described in the earlier sections. The system was found to operate quite satisfactorily with true/chance ratio of the order of 50, for the spectrum recorded with the radioactive isotope  $^{22}\text{Na}$ , energy gating being at 511 keV, strength of the source being a few micro curies.

## II.5 Sum-coincidence Set-up

The sum-coincidence technique<sup>1</sup> provides a means of studying the genetic relations in complicated gamma cascades and the spectra obtained are more or less free of compton background. The technique consists of demanding an extra condition to be met by the pulses from the two detectors used in coincidence set-up that the sum of the two pulses should always add up to the energy of a level whose decay characteristics are being investigated. The



same technique can, of course, be used to study the cascades between two levels, say  $E_1$  and  $E_2$  by demanding the sum of the two pulses to be equal to the energy  $[E_2 - E_1]$ .

A. Description of the technique: The block diagram of a sum-coincidence spectrometer in its simplest form is shown in Fig. 2.3. The linear signals from the two detectors are summed in a 'Linear-Adder' circuit. The single channel analyzer is used to set the energy window on the sum pulse. Thus the output from the single channel analyzer comes only when the sum of the two pulses is equal to the energy of interest, which is the energy of the level being investigated or the difference between two energy levels between which cascades are to be studied. The energy spectrum from one of the detectors is analyzed on a multichannel analyzer, gated with the sum window. The spectrum, thus recorded, consists of only the photo-peaks of gamma rays corresponding to the different cascade modes of decay in the selected energy region.

The operational principles of the set-up can be illustrated by considering a simple decay scheme shown in Fig. 2.4. It consists of two levels at  $E_1$  and  $E_2$ , with three gamma rays of energies  $E_2$ ,  $E_2 - E_1$  and  $E_1$ . To study this decay scheme by the present technique, one makes use of a two detector assembly. The linear outputs of the two detectors are perfectly matched in shape and size to achieve

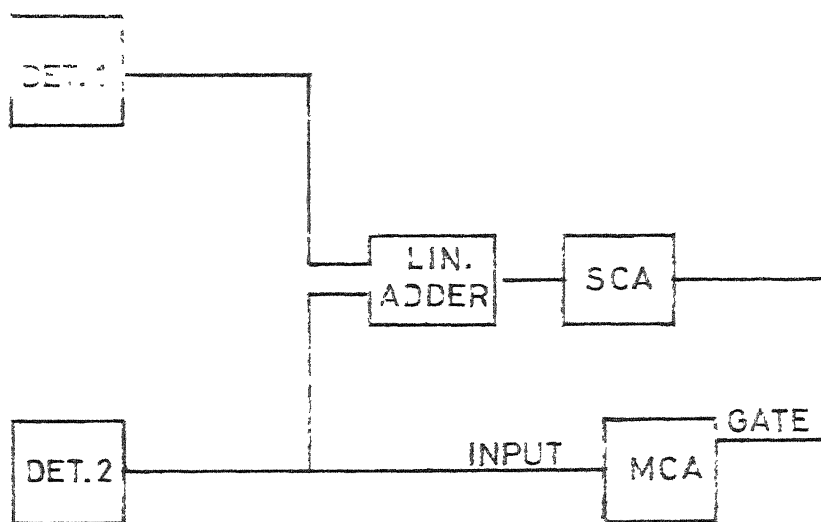


FIG. 2.3 BLOCK DIAGRAM OF SIMPLE SUM COINCIDENCE SPECTROMETER

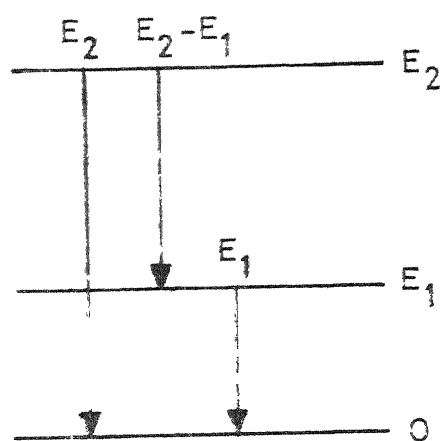


FIG. 2.4 DECAY SCHEME TO EXPLAIN SUM-COINCIDENCE TECHNIQUE

the same energy calibration and proper summing of the pulses. The pulses, thus matched, are linearly summed in an adder circuit, the output of which is used for energy selection. To study the decay modes of level  $E_2$ , the energy selection is made to accept pulses corresponding to energy  $E_2 \pm \delta E$ . The linear spectrum from one of the detectors is scanned on a multichannel analyzer, which is gated with the pulses of energy selection. The energy condition can be satisfied only when either  $E_2$  spends its entire energy in the detector recording the spectrum or both of  $E_1$  and  $E_2 - E_1$  spend their total energy in either of the detectors. The spectrum observed on multichannel analyzer, therefore, shows only three full energy peaks corresponding to  $E_2$ ,  $E_1$  and  $E_2 - E_1$  energies, their Compton and other portions of the spectrum being absent.

The two detectors employed are carefully made identical in all respects. So the detection efficiency of a particular event is same for both the detectors. Let us assume that a gamma ray  $\gamma_1$ , and the complementary gamma ray  $\gamma_2$  are detected with the efficiencies  $\epsilon_1$  and  $\epsilon_2$  respectively. The recording of  $\gamma_1$  in the spectrum corresponds to the detection of  $\gamma_1$  in one crystal and  $\gamma_2$  in the other. Similarly, recording of  $\gamma_2$  corresponds to the detection of  $\gamma_2$  in the former and  $\gamma_1$  in the latter. Thus, the efficiency of recording  $\gamma_1$  and  $\gamma_2$  is same and is

proportional to the product of efficiencies of detection for individual gamma rays,  $\epsilon_1 \epsilon_2$ . It is, thus, clear that both the event and its complementary event are recorded with the same efficiency. This results in the same area for a gamma ray peak as is for its complementary gamma ray peak.

In sum-coincidence spectra, the width of a photopeak is same as in the single spectra, (i.e., without coincidence requirement) for wide window settings. As the window setting is narrowed down further and further, the width of the peaks becomes smaller and smaller. In the limiting case of very small window widths, the width of the peak corresponding to a particular cascade gamma becomes same as that of its complementary peak. This can be understood quantitatively<sup>1</sup> as follows. The widths of the two complementary gamma ray peaks in sum-coincidence spectrum are given by the expressions:

$$\Gamma_{1s} = \frac{\Gamma_1 \sqrt{\Gamma_2^2 + \Gamma_s^2}}{\sqrt{\Gamma_1^2 + \Gamma_2^2 + \Gamma_s^2}} \quad (2.5)$$

$$\text{and} \quad \Gamma_{2s} = \frac{\Gamma_2 \sqrt{\Gamma_1^2 + \Gamma_s^2}}{\sqrt{\Gamma_1^2 + \Gamma_2^2 + \Gamma_s^2}} \quad (2.6)$$

where  $\Gamma_{1s}$  and  $\Gamma_{2s}$  are the widths of the two gamma rays in a particular sum-coincidence spectrum.

$\Gamma_1$  and  $\Gamma_2$  are the widths of the same gamma rays in single spectrum, without any coincidence requirement and  $\Gamma_s$  is sum-window width.

In the limiting case where  $\Gamma_s \ll \Gamma_1$  and  $\Gamma_2$

$$\Gamma_{1s} = \Gamma_{2s} = \frac{\Gamma_1 \Gamma_2}{\sqrt{\Gamma_1^2 + \Gamma_2^2}} \quad (2.7)$$

Thus, the complementary peaks, observed in the sum-coincidence spectra with very narrow window settings are of equal width. However, in practice, the window setting is never kept so narrow because of the loss of efficiency. One has to choose a window setting to compromise between the energy resolution and efficiency.

As seen above, in this simple version of the spectrometer, the recorded spectrum shows sum peak besides the peaks corresponding to cascade modes. The origins of the sum peak are the following:

- i) A crossover transition of the level being considered,
- ii) summing of both the gamma ray events in the same crystal, recording the spectrum, and
- iii) accidental coincidences.

Furthermore, since this simple sum-coincidence arrangement requires a good linear summing circuit, which can only be achieved by slow pulses, it is clear from the discussion of section II.3 that the true/chance ratio obtainable from such an arrangement cannot be good. However, this difficulty can be solved by incorporating an additional fast coincidence requirement (as discussed in section II.3).

B. Description of the spectrometer : The sum-coincidence spectrometer, with fast-slow coincidence condition, set up for our measurements is shown in Fig. 2.5 and the details are given below:

Two NaI(Tl) crystals of 4.4 cm diameter and 5 cm thickness each coupled to a 56 AVP photomultiplier tube, are used as the detectors. As explained earlier, it is essential that the linear pulses from the two detectors are identical in shape. To achieve this, two carefully matched bleeder circuits were assembled for the two photomultipliers and linear pulses are drawn from the eighth dynode of each detector. Potentiometric arrangements are made to adjust the pulse shapes. The pulses are further amplified in linear amplifiers, which also have the provision of adjusting the shapes of the output pulses. The gains of the pulse shaping amplifiers are adjusted to have the same energy calibration for both the detectors. The pulses are then linear added up in an adder circuit. The adder circuit is a linear signal mixer [EG&G, AN 100]. It is a current summing unit, including an operational amplifier and an impedance matching circuit. This summed pulse is then fed to a crossover pickoff unit and also to a strobed single channel analyzer (SSCA). The SSCA is externally strobed with the output pulses from the crossover pickoff unit. The external strobing is done to eliminate the time jitter effects, described in the earlier

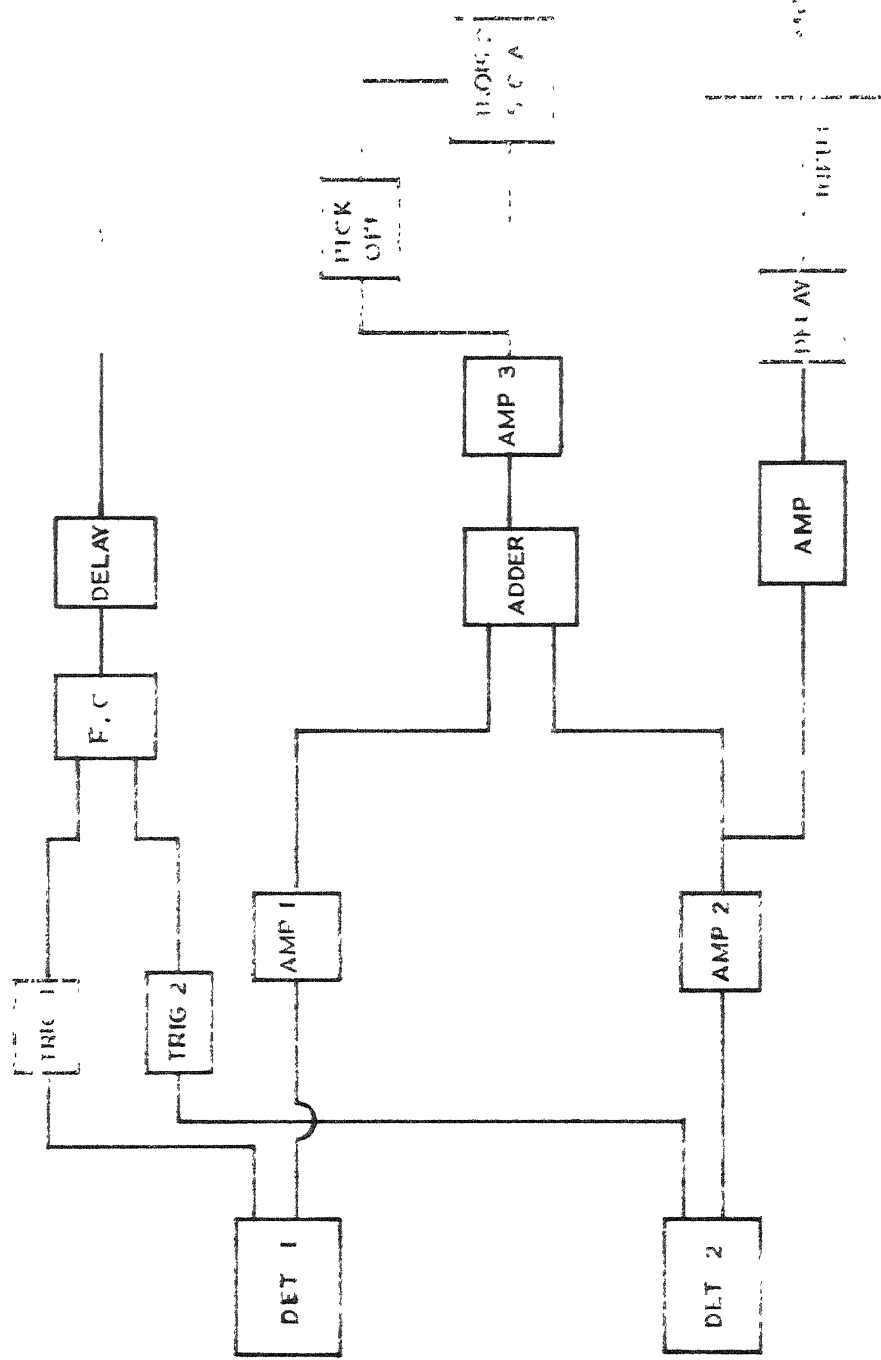


FIG. 2.5 SUM-COINCIDENCE SET-UP



section. The output of the single channel analyzer is properly shaped and used as one of the inputs to the slow coincidence circuit.

Fast coincidence is sought between the anode pulses of the two detectors. The anode pulses are clipped to get the rise time  $t_r \approx 15$  nsec and width  $T \approx 150$  nsec. The fast coincidence circuit being of overlapping type, the input pulses of 15 nsec give the fast resolving time  $2\tau = 30$  nsec. The fast clipping of anode pulses produces problem of multiple triggering in the discriminator. To solve this problem of multiple triggering, two fast discriminators are used in series for each detector. The output of the first discriminator is 100 nsec wide. It is RC differentiated with a time constant  $RC = 2$  nsec. The negative part of the differentiated pulse triggers the second discriminator, with output width adjusted to 15 nsec. This arrangement solves the problem of multiple triggering. A fast resolving time of  $2\tau = 30$  nsec is achieved.

As seen earlier, the smaller the resolving time, better is the true/chance coincidence ratio. But very small resolving times result in the reduction of true coincidence counts. Moreover, for shorter resolving times, the percentage jitter is more and thus even small variation in timing will be troublesome. It is found that for our present set-up the

30 nsec resolving time makes the system free from the above two limitations.

The output pulses of the fast coincidence circuit are stretched to a width of  $0.5 \mu\text{s}$  and are delayed to match the timing with the single channel analyzer output pulses. The properly shaped single channel analyzer output and fast coincidence output make the two inputs required for the slow coincidence. Both the inputs being of  $0.5 \mu\text{s}$  width, the resolving time of the slow coincidence circuit  $2\tau = 1 \mu\text{s}$ . The output of slow coincidence circuit is shaped to match the requirements of gate pulse of multi-channel analyzer.

The dynode output of one of the detectors after amplification, is delayed to match the timing with the gating pulse and is analyzed on multichannel analyzer, in the coincidence mode.

C. Performance : The performance of the set-up was checked with the spectra recorded for gamma radiation from the radioactive isotopes of  $^{60}\text{Co}$  and  $^{22}\text{Na}$  separately. The pulses corresponding to 2.5 MeV and 1.785 MeV with a window width of 50 keV were accepted in the single channel analyzer respectively. In each case, true/chance ratio of better than 100 was achieved. The spectra recorded with these two sources are shown in Figs. 2.6 and 2.7. In the decay of  $^{60}\text{Co}$ , 2.5 MeV level of  $^{60}\text{Ni}$  is populated, which gets

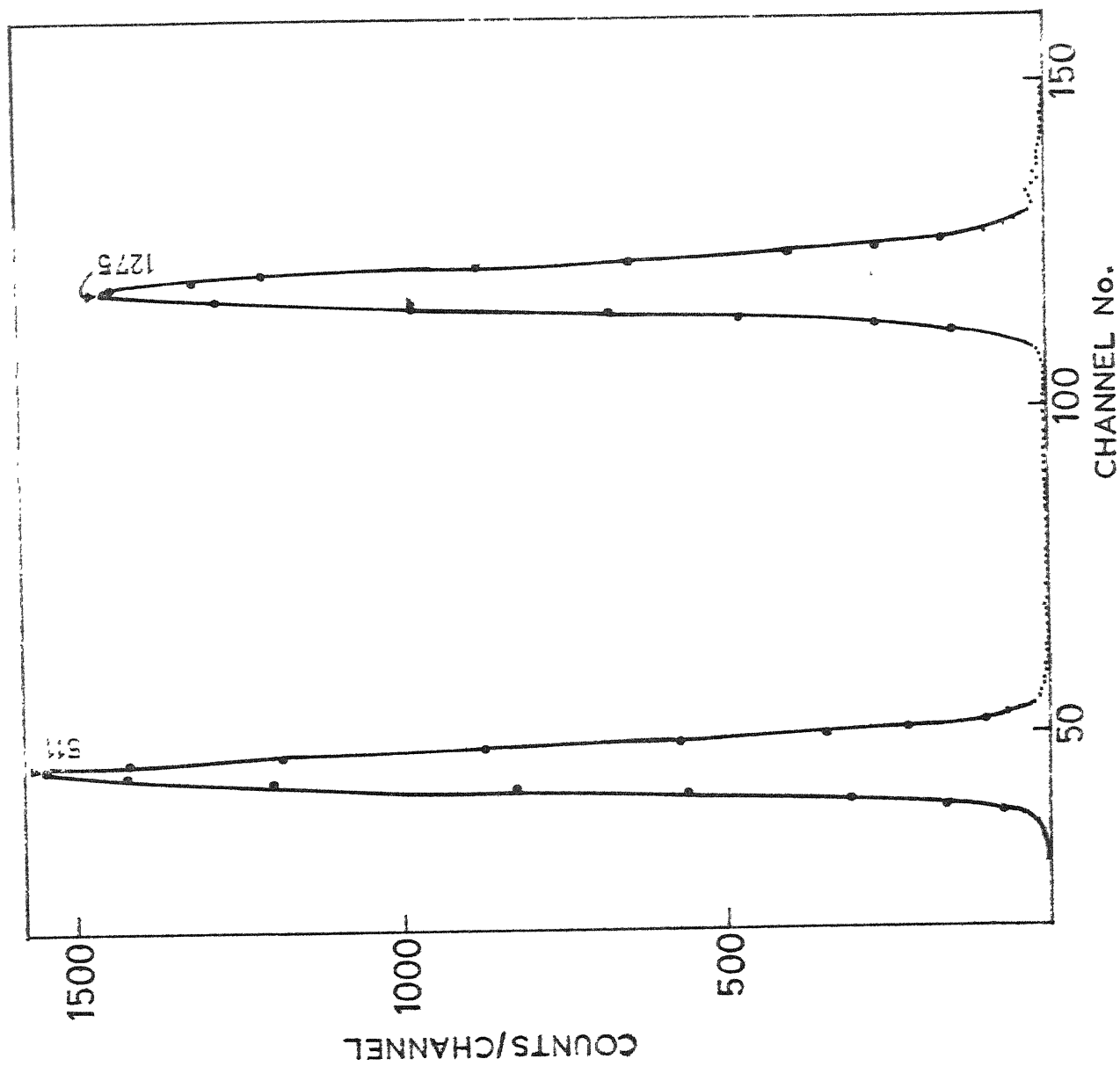


FIG.2.6 SUM-COINCIDENCE OF SPECTRUM OF  $^{22}\text{Na}$  WITH

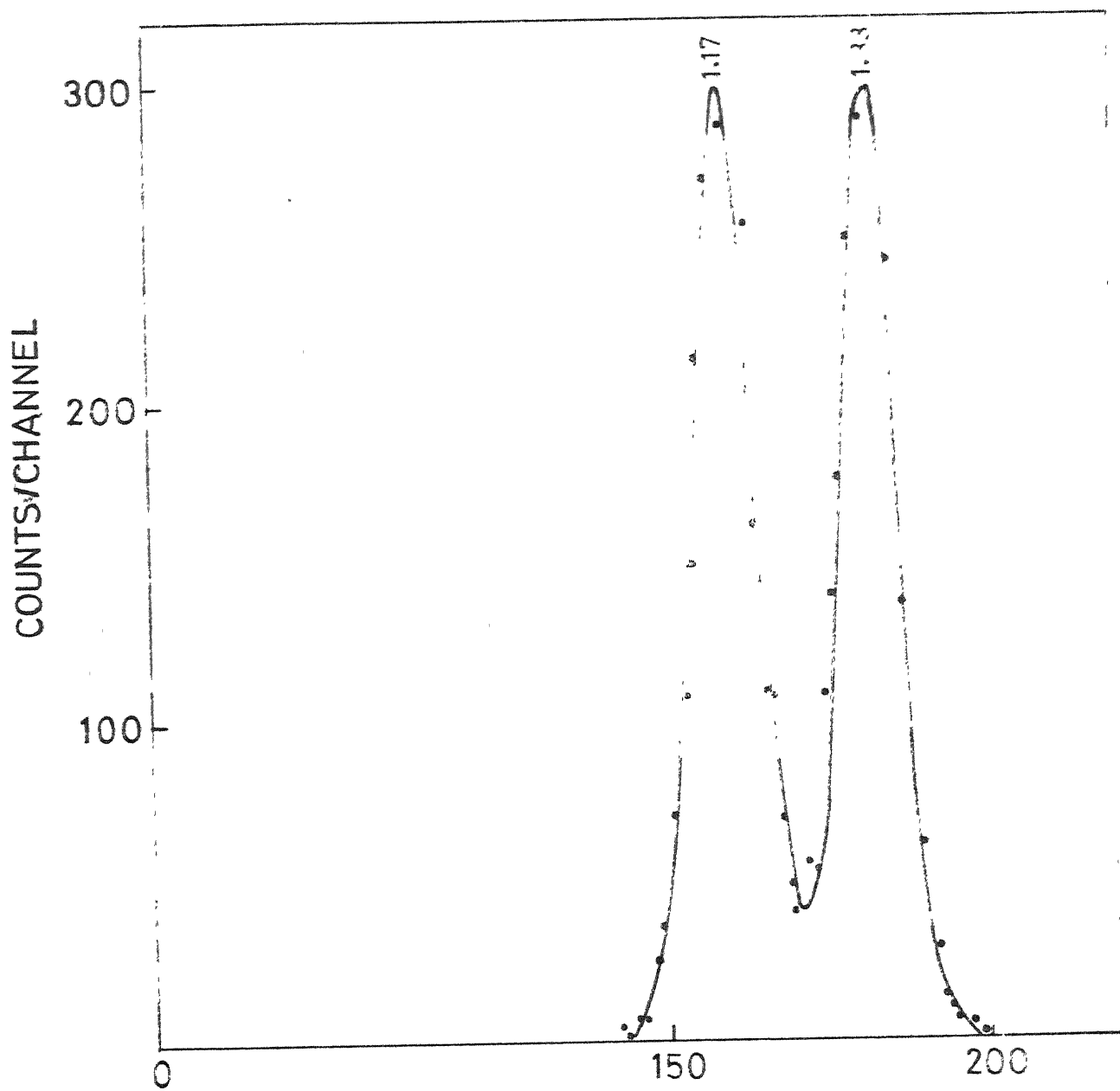


FIG. 2.7 SUM-COINCIDENCE SPECTRUM OF  $^{60}\text{Co}$

deexcited by emitting two gamma rays of energies 1.17 and 1.33 MeV. The sum-coincidence spectrum clearly shows two well resolved ( $\sim 5\%$ ) peaks at 1.17 and 1.33 MeV energies, the countrate in the other channels being negligible. In the decay of  $^{22}\text{Na}$ , 1.275 MeV level of  $^{22}\text{Ne}$  is populated, resulting in the emission of 1.275 MeV gamma ray. The positron decay of  $^{22}\text{Na}$  gives rise to two annihilation quanta, which are in time coincidence with the 1.275 MeV gamma ray. Thus, the spectrum of  $^{22}\text{Na}$  recorded with gate at 1.785 MeV shows two peaks corresponding to energies 0.511 and 1.275 MeV. The sum-coincidence spectrum clearly shows these two peaks and very small countrate in the other channels (peak/base  $\approx 100$ ). To ensure that there is no asymmetry, the detectors were interchanged to check that the spectrum obtained is independent of the choice of one or the other detector in the spectrometer. To make sure that electronic drifts of the system are insignificant, the stability of the set-up was checked over periods of 50 hours. During this period, the stability of calibration of each detector, the fast trigger cut off positions, the single channel analyzer window position and the time delays are checked periodically. The overall shifts are found to be negligibly small so that the recorded spectra do not show any observable distortion.

D. Fictitious cascades and their elimination : In sum-coincidence experiments, any wrong sum window setting can, obviously, give rise to fictitious cascades and lead to erroneous conclusions regarding the deexcitation process. Thus, one has to be very careful in choosing and correctly setting the desired sum window. Moreover, presence of excited states at energies higher than the level under investigation can also give rise to fictitious cascades, due to the possibility of obtaining the sum pulse of correct amplitude through the addition of a compton scattered gamma originating from higher energy gammas, and a photoelectrically absorbed gamma of low energy.

Let us consider the decay scheme shown in Fig. 2.8 to elaborate the photo-compton summing effects. It consists of levels at  $E_1$ ,  $E_2$  and  $E_3$  which can give gamma rays of energies  $E_3$ ,  $E_3-E_2$ ,  $E_2$ ,  $E_2-E_1$  and  $E_1$ . If one is investigating the decay modes of level  $E_3$  by setting window at  $E_3 \pm \delta E$ , then the photopeaks at energies  $E_3-E_2$  and  $E_2$  are expected. Similarly, in the investigation of level  $E_2$ , peaks corresponding to energies  $E_2-E_1$  and  $E_1$  are expected. But it might so happen that the  $E_3-E_2$  gamma ray spends its entire energy in one detector and  $E_2$  interacts by compton effect in the other detector, spending a part of its energy such that

$$E_3-E_2 + E_{2_{\text{compt}}} = E_2 \quad (2.8a)$$

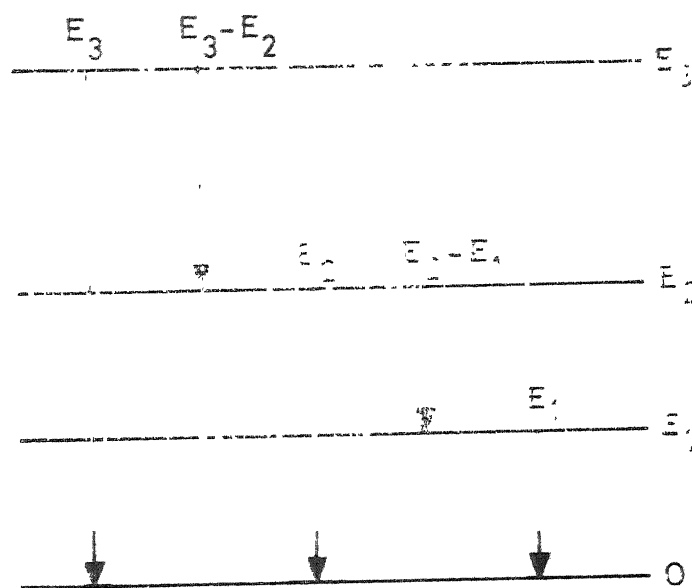


FIG. 2.8 DECAY SCHEME TO EXPLAIN FICTITIOUS CASCADES

$$\text{or } E_{2\text{compt}} = 2E_2 - E_3 \text{ for } E_2 > E_3/2 \quad (2.8b)$$

So one would observe four peaks in the sum-coincidence spectrum with sum gate set at energy  $E_2$ , which would be at energies  $E_2 - E_1$ ,  $E_1$ ,  $E_3 - E_2$  and  $2E_2 - E_3$ . Thus, one can be led to assign two different cascade modes of decay of level at  $E_2$ , whereas in reality only one cascade mode is present. This warrants for a very careful analysis of the spectra.

Even when one is investigating the highest level, one should make sure that the selection of the sum window is exact. If not, fictitious cascades of different origin can arise. For example, in the investigation of the decay of level  $E_3$ , if the gate is set at  $E'_3 \pm \delta E$  such that  $E'_3 \neq E_3$ , then there will be two possibilities. One is that the gamma ray of energy  $E_3 - E_2$  may get added with the compton scattered gamma originating from  $E_2$  to give the sum  $E'_3$ , that is

$$E_3 - E_2 + E_{2\text{compt}} = E'_3 \quad (2.9a)$$

$$\text{or } E_{2\text{compt}} = E'_3 - (E_3 - E_2) \quad (2.9b)$$

and the second alternative is that the gamma ray with energy  $E_2$  may get added with the compton scattered gamma ray of energy  $E_3 - E_2$  to give the sum of  $E'_3$ , that is

$$E_2 + (E_3 - E_2)_{\text{compt}} = E'_3 \quad (2.10a)$$

$$\text{or } (E_3 - E_2)_{\text{compt}} = E'_3 - E_2 \quad (2.10b)$$



Thus, the sum-coincidence spectrum will show peaks corresponding to energies  $E_2$ ,  $E'_3 - E_2$ ,  $E'_3 - (E_3 - E_2)$  and  $(E_3 - E_2)$  and would lead once again to the conclusion of two different cascade modes of decay. But a careful analysis can prevent erroneous conclusions, because the sum of the complementary gamma ray energies would, now, be  $E'_3$  in stead of being  $E_3$ .

These effects have been discussed in detail by Schriber and Hogg<sup>2</sup> and they have suggested that these fictitious cascades could be identified by scanning the spectra for different sum window settings. The peak due to the total absorption remains fixed in its position, while the compton peak moves along with the window setting. In this way, one can identify these fictitious peaks. However, this procedure is practical only when the study involves a simple gamma decay scheme or in those cases where the levels are well separated from each other. In general, one has to take due care in gate settings and consider the possibilities of peaks in sum coincidence spectra due to photo-compton summing during the analysis. The gate settings are not difficult when the level of interest has a reasonably strong crossover transition. Otherwise external calibration with the use of standard radioactive isotopes can be employed. However, the calibration is subject to errors due to pileup effects, described earlier. The calibrations should, therefore, be done with the same counting rates as used in the actual experiments.

The gates, thus set, are found to be proper in all the cases. The fictitious cascades are not troublesome in cases where the level under investigation is reasonably well populated and the crossover transition is not its predominant mode of decay. The difficulties arise only when the level is weakly populated, with some level at higher energies being strongly populated. The difficulty also arises when the level of interest has mainly a crossover transition as its deexcitation mode. Such cases were subjected to a critical analysis.

As mentioned earlier, the data from sum-coincidence spectra was supplemented with that from the spectra of the Ge(Li) detector and only those decay modes, which were observed in both the studies, were taken into account. If a gamma ray was observed in a sum-coincidence spectrum and was not found in the Ge(Li) detector spectrum, every care was taken to find out if it was fictitious.

F. Target holder and collimator system : A target holder, a beam collimating system and other auxiliary systems were designed and made for the experiments performed on the Van de Graaff accelerator.

(i) Target holder : The target holder basically consists of a circular brass flange of 10 cm diameter and 1 cm thickness, having a circular groove appropriate to

fix an O-ring of 5.6 cm diameter and 0.3 cm thickness. The flange has a circular step (concentric with the flange) of 2.5 cm diameter and 0.1 cm depth, which is made to be just sufficient to house the target. A circular brass plate of 2 mm thickness and 4 cm diameter with a hole of 2 cm diameter in the center is fixed on the flange with countersunk screws. This provides a rigid hold for the target in position without interrupting the beam path. The brass plate is easily removable and hence replacement of old targets by fresh ones is a simple operation.

The arrangements for the target cooling are incorporated to minimise the contamination build-up on the target and also to slow down the target deterioration. A cylindrical brass stud of dimension 3.8 x 3.8 cm with a blind hole along a diameter is soldered on to the other face of the target flange. A brass tube of 5 cm diameter and 7 cm length is soldered on the same face of the flange so that the stud is enclosed in it. A vertical copper rod passes through a hole in the cylinder into the stud and is soldered to the cylinder. The remote face of the brass tube is closed by soldering a brass plate to the same. The tube has been provided with water inlet and outlet nozzles.

The target cooling can be affected either by running water through the cylindrical tube or by inserting the copper

- 1 TARGET
- 2 BRASS PLATE
- 3 COATED SUNK NUT
- 4 CLAMP GROOVE
- 5 BRASS STUD
- 6 COPPER ROD
- 7 BRASS TUBE

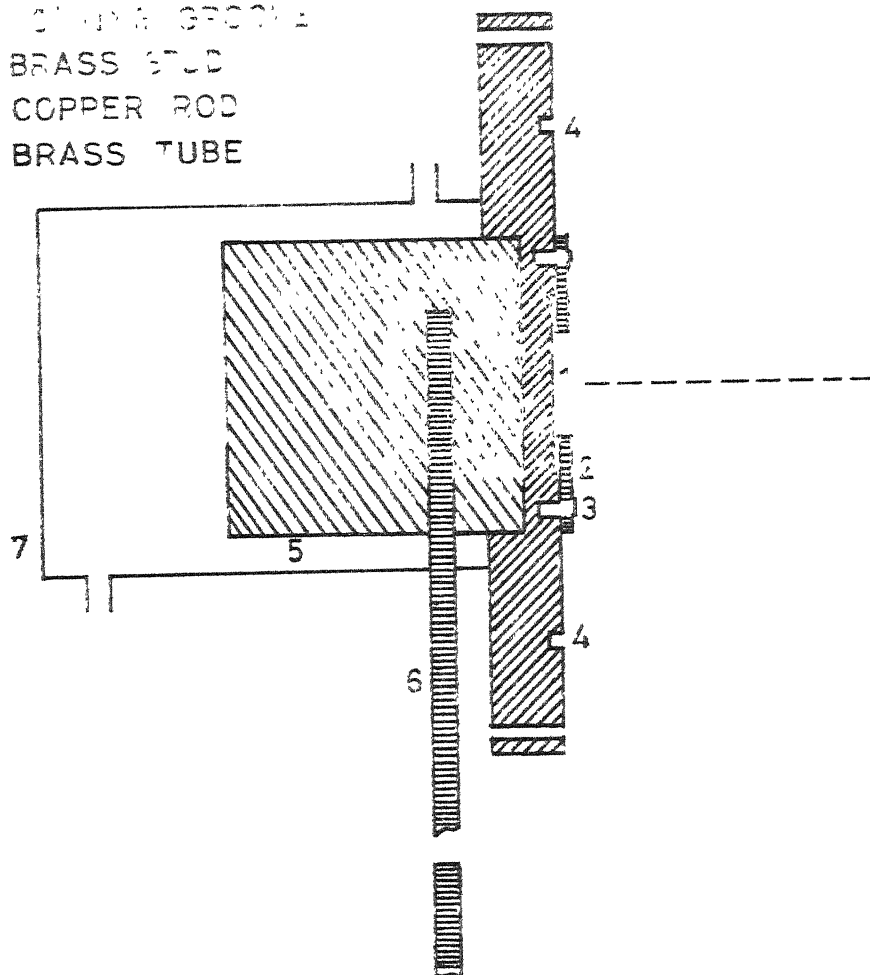


FIG. 2.9 TARGET HOLDER

- 1 TANTALUM PIECES
- 2 SCREW SYSTEM
- 3 BRASS FLANGES
- 4 'O' RING GROOVE
- 5 BRASS TUBE
- 6 BEAM AXIS

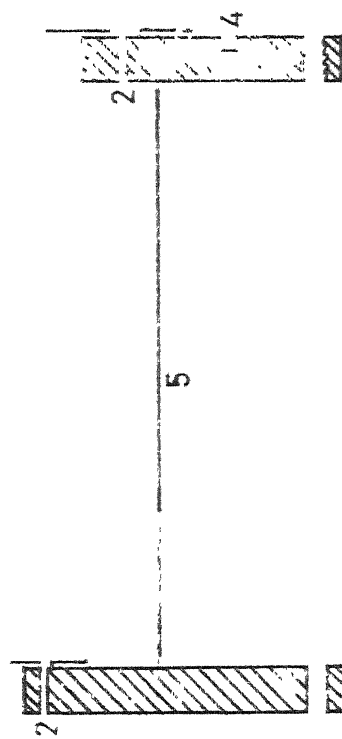
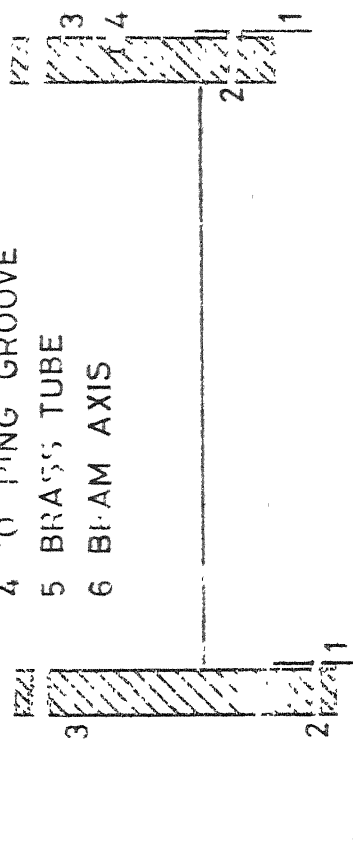


FIG. 2.10 COLLIMATOR SYSTEM

rod in liquid nitrogen. With liquid nitrogen cooling, the temperatures of  $\sim 10^{\circ}\text{C}$  are obtained. The target holder along with the cooling arrangements is shown in Fig. 2.9.

(ii) Collimator system : A collimator system was designed to ensure that the particle beam strikes the active target area only and not the other parts of the target holder. The system is shown in Fig. 2.10. It consists of two circular brass flanges of 10 cm diameter and 1.0 cm thickness soldered to the either ends of a brass tube. The brass tube is of 5 cm internal diameter and 7.5 cm length. A central circular hole of 3 cm diameter is made on one of the flanges and of 1.5 cm on the others. Two circular tantalum pieces, one with a central circular hole of 2 cm diameter and the other with a hole of 1 cm diameter are fixed on to the respective brass flanges. The tantalum piece of smaller hole is nearer to the target. These tantalum pieces can be replaced by others of different hole sizes to meet the requirements.

In general, it is necessary to measure the beam current on the target and also on the collimator separately. The electrical insulation, thus needed, is achieved by using perspex flanges before and after the collimator system. Care has been taken to ensure that beam never falls on the perspex flanges during its travel to avoid the out-gassing and associated problems. The geometry of the system is such that the beam can only strike the effective area of the target and nothing else.

REFERENCES

1. A.M. Hoogenboom, Nucl. Instr. Methods 3 (1958) 57.
2. S.O. Schriber and B.G. Hogg, Nucl. Instr. Methods 26 (1964) 141.

CHAPTER III

SUM-COINCIDENCE STUDIES ON  $^{131}\text{Cs}$

III.1 Introduction

The 11.5 day electron capture decay of  $^{131}\text{Ba}$  populates the levels of  $^{131}\text{Cs}$ . This decay has been the subject of many investigations because of the considerable interest in understanding the structure of excited states in  $^{131}\text{Cs}$ . Various attempts, with different nuclear models, have been made to explain the structure. But none of them is successful in providing a quantitative explanation of the observed properties. Primarily, it is necessary to have the decay scheme established beyond doubt. The scheme proposed by Horen et al.<sup>1</sup> from the study of internal conversion electrons is the one commonly used, but there are several controversies. Recently, some investigations<sup>2,3</sup> have been made with Ge(Li) detectors, but they take the gamma ray energies from Horen et al. Two groups of workers<sup>4,5</sup> also measured sum-coincidence spectra, but there are major disagreements between these two reports. The present investigation is, therefore, undertaken to make precise energy assignments with the help of the Ge(Li) detector and to measure the sum-coincidence spectra to resolve the discrepancies. After the present investigation was completed, Hasselgren et al.<sup>6</sup> reported their measurements, wherein they used a Ge(Li) detector for gamma ray energy assignments. Our results are compared with their measurements also.



The  $^{131}\text{Ba}$  source was obtained from Bhabha Atomic Research Centre, Bombay, India. It was in liquid form as barium chloride in hydrochloric acid solution. The sources were prepared by taking a few measured drops of the solution onto perspex holders. The sources were evaporated to dryness under infrared lamp and wrapped in cellotape to avoid surface contaminations and to prevent the source material from falling out. Sources of different strengths were, thus, prepared for the experiment.

The measurements consist of recording singles spectra with the Ge(Li) detector and sum-coincidence spectra at different energy gates. These two experimental set-ups are described in Chapter II.

### III.2 Measurement of Singles Spectra :

The measurements were done in two stages. In the first stage, the spectrum covering the entire range of interest (0-1050 keV) was recorded. In a fixed source to detector geometry, the spectra were recorded at regular intervals to ensure that all the gamma rays belong to the 11.5 day decay of  $^{131}\text{Ba}$ . Gamma rays due to the presence of long lived impurities of  $^{133}\text{Ba}$ ,  $^{134}\text{Cs}$  and an unidentified activity were observed. The radiation due to  $^{131}\text{Ba}$  could be easily distinguished from that due to the impurities because of the large difference in the half lives of  $^{131}\text{Ba}$  activity and others.

In the second stage, the spectra were recorded in two parts by expanding the energy scale for precise energy measurements. The energy calibrations were done using standard sources giving gammas upto 1.3 MeV. The single spectra recorded with Ge(Li) detectors are shown in Figs. 3.1 to 3.4. The peaks due to identified impurities are marked with the name of the isotope and those due to the unidentified one are marked with an astrix. The gamma ray energies reported in the present investigation agree well with the results of earlier workers except for the following minor differences. The 137.4 keV gamma ray reported by Horen et al. and the 324 keV gamma ray reported by Karlsson<sup>2</sup> are not observed. The 969.6 keV gamma ray reported by Horen et al. and later discarded by Mangal et al.<sup>5</sup> is observed in the present investigation. There is no indication for the existence of 797.0 and 954.6 keV gamma rays reported by Hasselgren et al. In fact, the spectra recorded after four half lives of the activity showed these peaks, thus indicating that these were due to the unidentified impurity. The gamma ray energies as measured in the present investigation are shown in Table 3.1, along with the results of earlier workers.

### III.3 Sum-coincidence Measurements

The sum coincidence spectra were taken at 1048, 925, 832, 696, 620, 585, 404, 373 and 216 keV sum gates. In <sup>131</sup>Cs, there are no levels at the excitation energies of

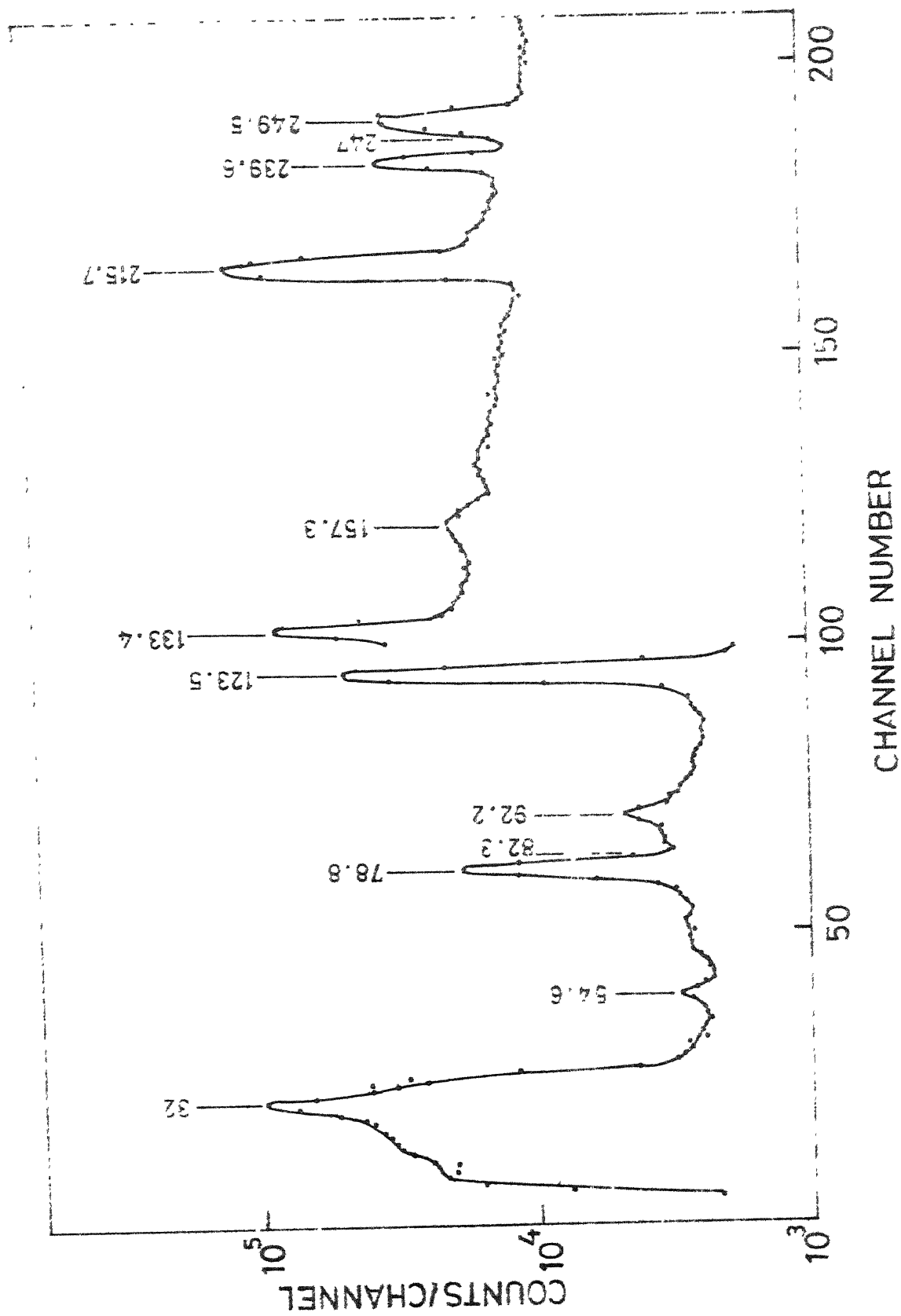


FIG. 3.1 Ge(Li) SPECTRUM OF  $^{131}\text{Cs}$  0-280 KeV ENERGY RANGE

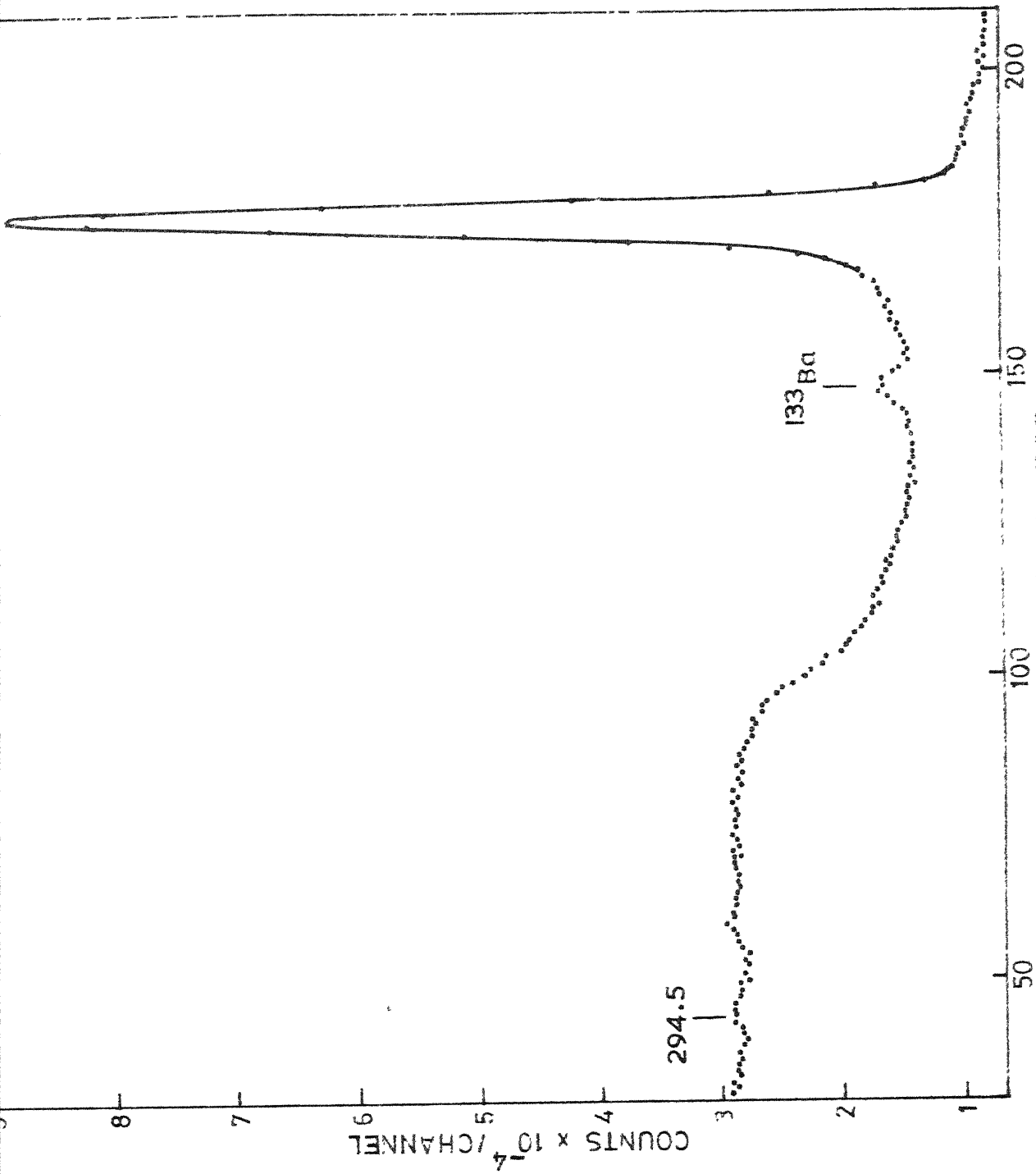


FIG. 3.2 Ge(Li) SPECTRUM OF  $^{131}\text{Cs}$  280-190 KEV ENERGY RANGE

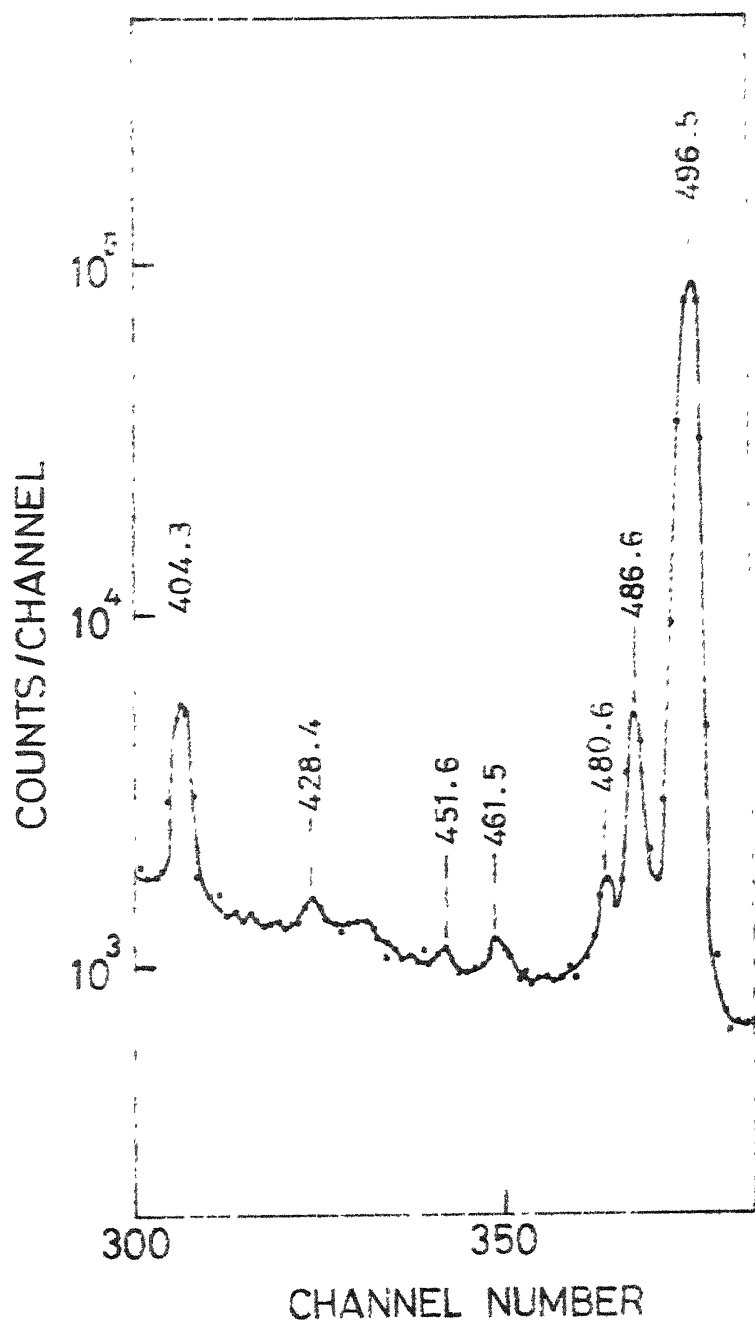


FIG.3.3 Ge(Li) SPECTRUM OF  $^{131}\text{Cs}$   
390-510 KeV ENERGY RANGE

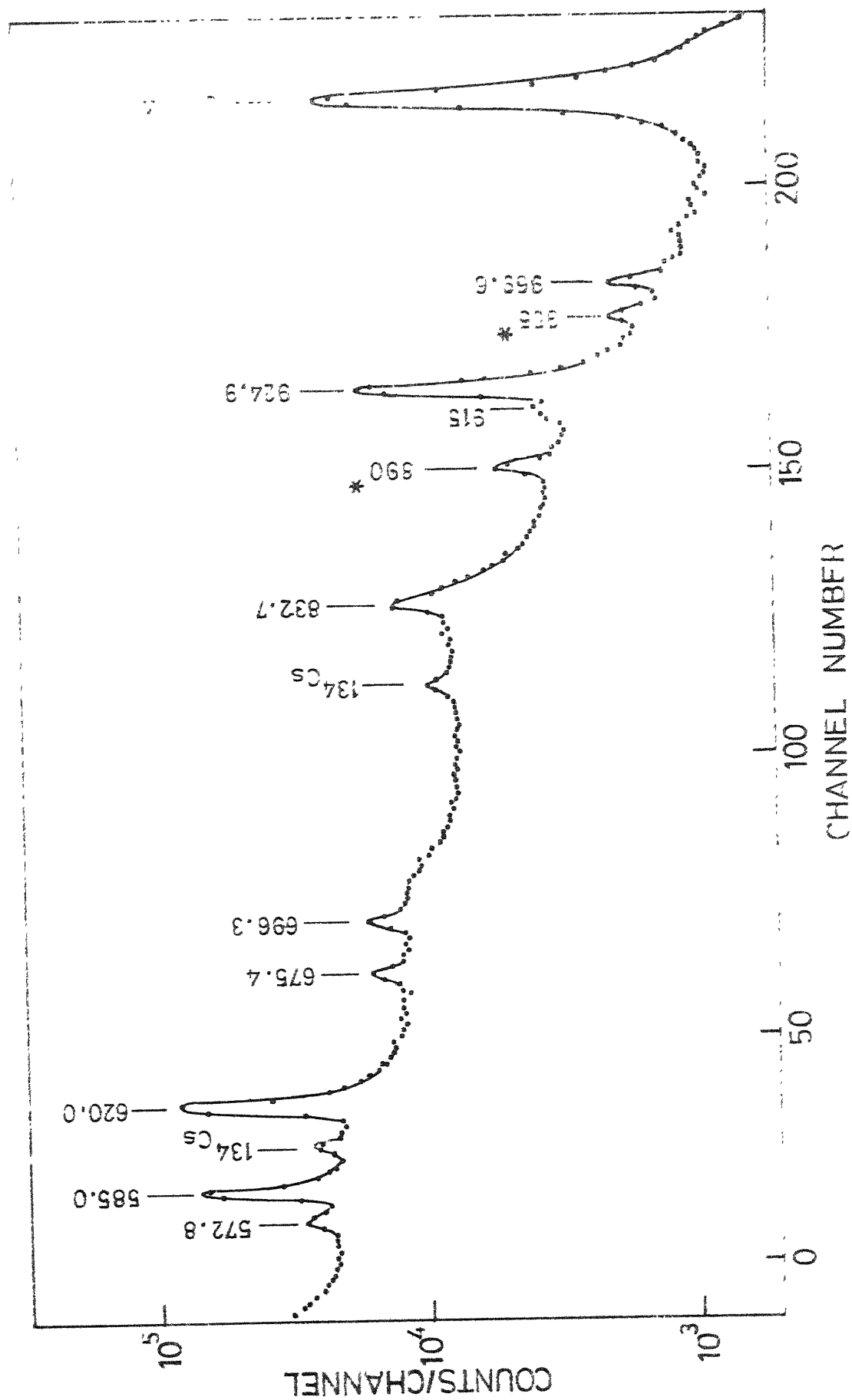


FIG. 3.4 Ge (Li) SPECTRUM OF  $^{131}\text{Cs}$  510-1060 keV ENERGY RANGE

Table 3.1. Gamma Rays Observed in the Decay of  $^{131}\text{Ba}$

<u>Horen et al.</u> <sup>1</sup>	<u>Hasselgren et al.</u> <sup>6</sup>	<u>Present</u>
54.84	55.02	54.6
78.69	78.68	78.8
82.43	82.4	82.3
92.25	92.25	92.2
123.73	123.73	123.5
133.54	133.54	133.4
137.26	-	-
157.01	157.13	157.3
216.01	216.01	215.7
239.56	239.45	239.6
246.83	247.05	247.0
249.36	249.34	249.5
294.45	294.46	294.5
351.21	351.66	352.1
373.15	373.15	373.0
404.3	404.09	404.3
427.7	427.71	428.3
451.7	451.36	451.6
461.3	461.1	461.5
462.9	462.87	-
480.6	480.52	480.6
486.6	486.52	486.5
496.3	496.23	496.5
-	572.95	572.8
585.1	585.01	585.0
620.2	620.2	620.0
-	674.72	675.4
-	696.54	696.3
832.0	831.95	832.7
-	914.66	915.7
924.4	924.4	924.9
969.1	969.19	969.8
1048.2	1048.29	1048.4

925, 832 and 404 keV. The spectra with these energy gates were, however, recorded to establish the double cascades in  $1048.4 \rightarrow 123.5$ ,  $1048.4 \rightarrow 215.7$  and  $620.0 \rightarrow 215.7$  keV modes of decay. At the gate setting of 620 keV, one observes the cascades in the  $620 \rightarrow 0$  keV decay as well as in the  $696.3 \rightarrow 78.8$  keV decay. In all the sum-coincidence spectra two x-ray peaks were observed due to the summing of x-rays with the compton of a gamma ray making up the sum gate. These aspects are carefully noted during the analysis.

The results of the measurements at most of the gate settings are in fair agreement with the reports of earlier workers<sup>4,5</sup>, except for the spectra with gates at 1048 and 585 keV, which require special comments. The sum-coincidence spectrum with gate at 1048 keV is shown in Fig. 3.5. It indicates the presence of  $1048.4 \xrightarrow{969.6} 78.8$  keV transition, which was one of the discrepancies in the earlier measurements. The 969.6 keV gamma is observed in our Ge(Li) spectrum also and is found to have the correct decay rate. However, the presence of a broad peak around 500 keV, in the sum-coincidence spectrum, is not clearly understood. It is possibly due to the presence of impurities.

The spectrum with gate at 585 keV has been recorded twice. The first spectrum is recorded within a week of procurement of the isotope and the other after about 4 half lives. The two spectra are shown in Figs. 3.6 and 3.7 respectively.



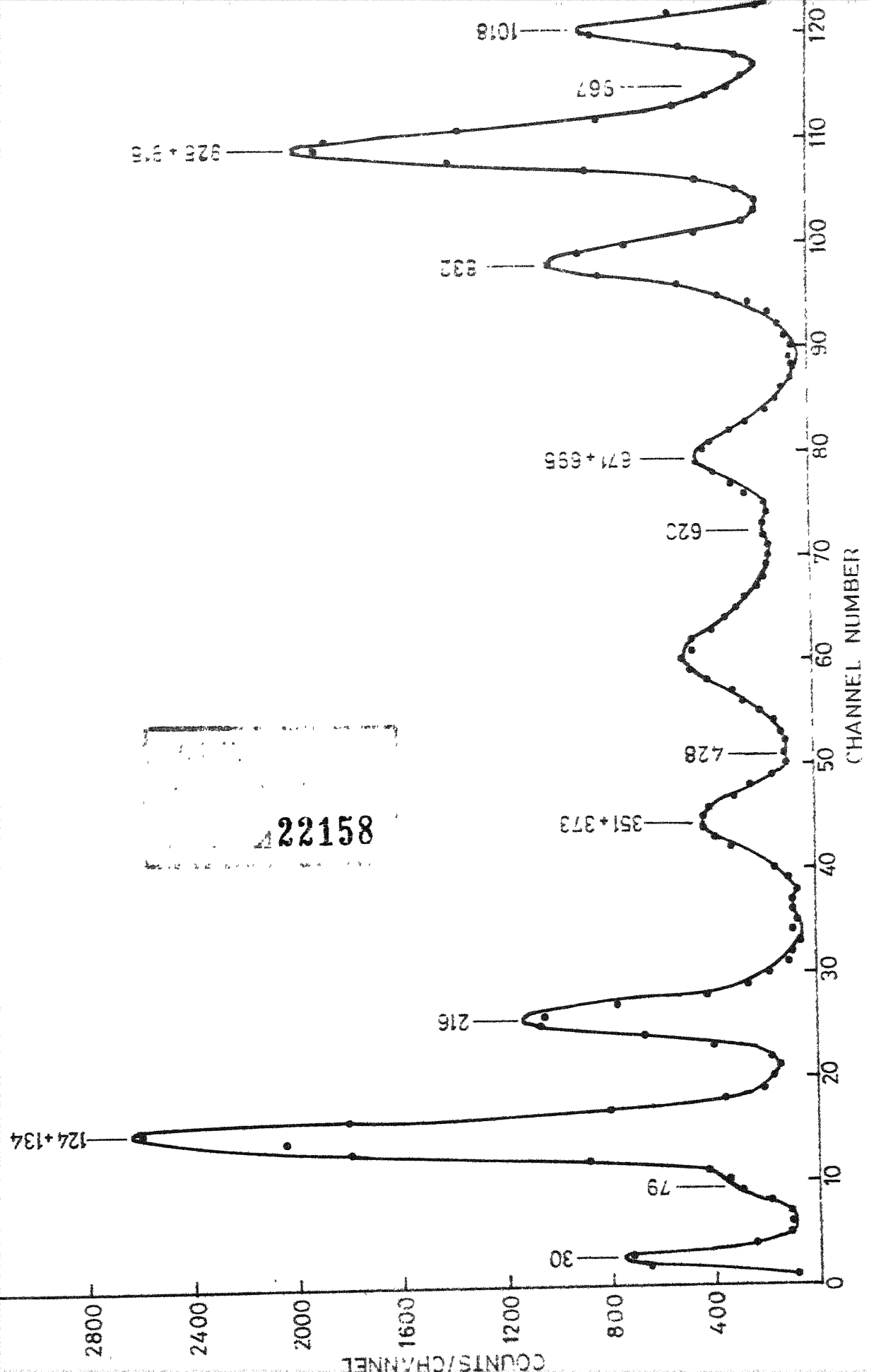


FIG.3.5 SUM-COINCIDENCE SPECTRUM OF  $^{131}\text{Cs}$  WITH GATE AT 1048 KeV

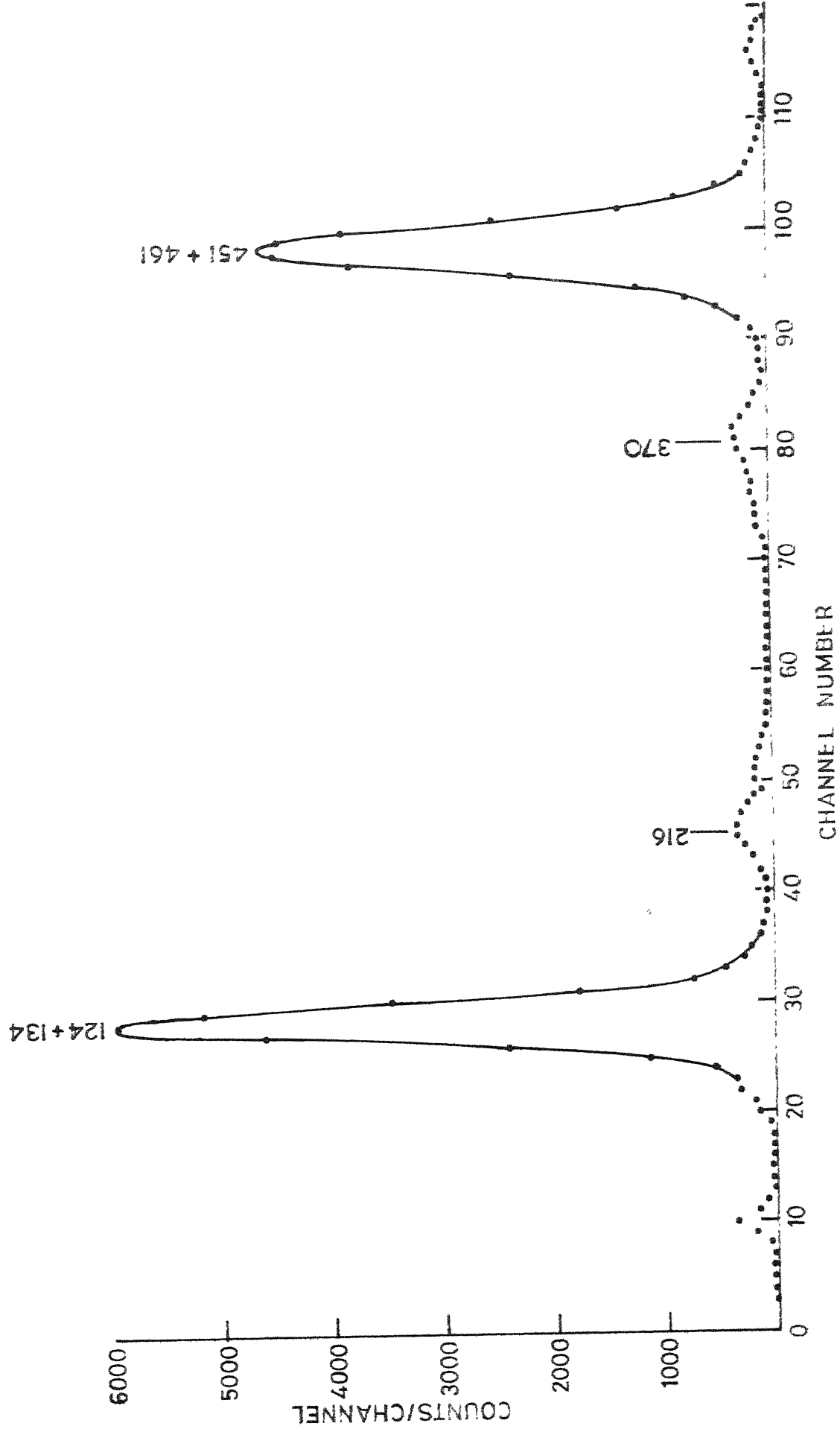
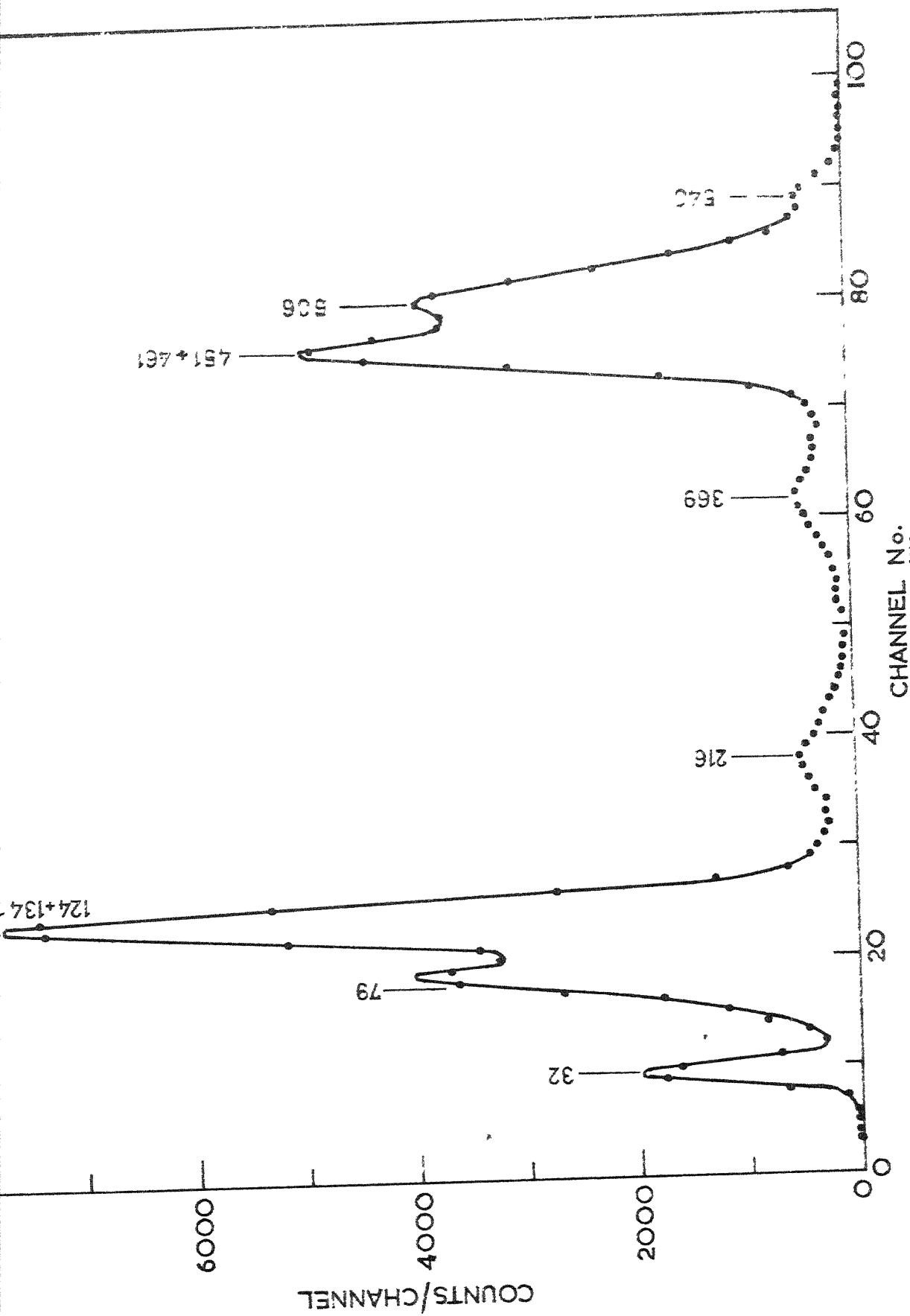


FIG. 3.6 SUM-COINCIDENCE SPECTRUM OF  $^{131}\text{Cs}$  ENERGY GATE AT 585 KeV



CHANNEL No.

FIG. 3.7 SUM COINCIDENCE SPECTRUM OF  $^{131}\text{Cs}$  WITH GATE AT 585 KeV. SPECTRUM RECORDED AFTER 4 HALF LIVES (45 DAYS)

The spectrum which was recorded at the first instance showed peaks at 32, 124 + 134, 216, 239, 346, 370, 451+461 and 553 keV. The spectrum recorded later under identical gate settings, shows additional peaks at energies 79 and 506 keV. Obviously, the 79 and 506 keV pair occurs due to a long lived impurity, which becomes dominant as the source decays. We, therefore, conclude that 506 keV gamma ray reported by Kucarova et al. also should be from an impurity present in the source.

The other peaks in this spectrum have their origin in  $^{131}\text{Ba}$  isotope. Of these, it is concluded that only the pairs 124+134 and 451+461 are due to photo-photo summings. The 32 and 553 keV pair is due to x-ray and compton of a coincident gamma ray summing. The rest two pairs are due to photo-compton summings. As can be seen from the singles spectrum, the 215.7 and 373.0 keV gamma rays are of high intensities. Thus the 215.7 keV gamma ray could sum up with the compton background of a coincidence gamma ray (404, 481 or 832 keV) to make up the sum gate setting and could provide peaks at 216 and 369 keV. Similarly, 373 keV gamma ray could sum up with the compton of a coincident gamma ray (675 and 247 keV) and gives rise to peaks at 212 and 373 keV. Hence, we infer that the peaks observed at 216 and 370 keV, in the present investigation and that of Mangal et al. are of this nature. We, therefore, conclude that there is no transition between 585 and 373 keV levels.

Similarly, we conclude that the peaks at 239 and 346 keV energies are also due to photo-compton summings.

### III.4 Conclusions

1. The 137.4 keV gamma reported by Horen et al. as a transition between  $215.7 \rightarrow 78.8$  and the 324.3 keV gamma reported by Karlsson as the transition between  $696.3 \rightarrow 373.0$  keV levels are not observed.
2. The 506 and 563 keV gamma rays reported by Kucarova et al. are found to be connected with impurities present in the radioactive isotope.
3. The 797.0 and 954.6 keV gamma rays observed by Hasselgren et al. were not seen and thus we conclude that there is no level at 1170 keV.
4. The coincident gamma pair of 212 and 373 keV energies reported by Mangal et al. is found to be due to photo-compton summings and hence the conclusion is that there is no transition between the 585 and 373 keV levels.

The proposed level scheme, on the basis of the present measurements is shown in Fig. 3.8. The doubtful gamma ray is indicated by a dashed lines. The other gamma rays are shown by continuous line. The spins and parities of the levels, as reported by Hasselgren et al., are included in Fig. 3.8.

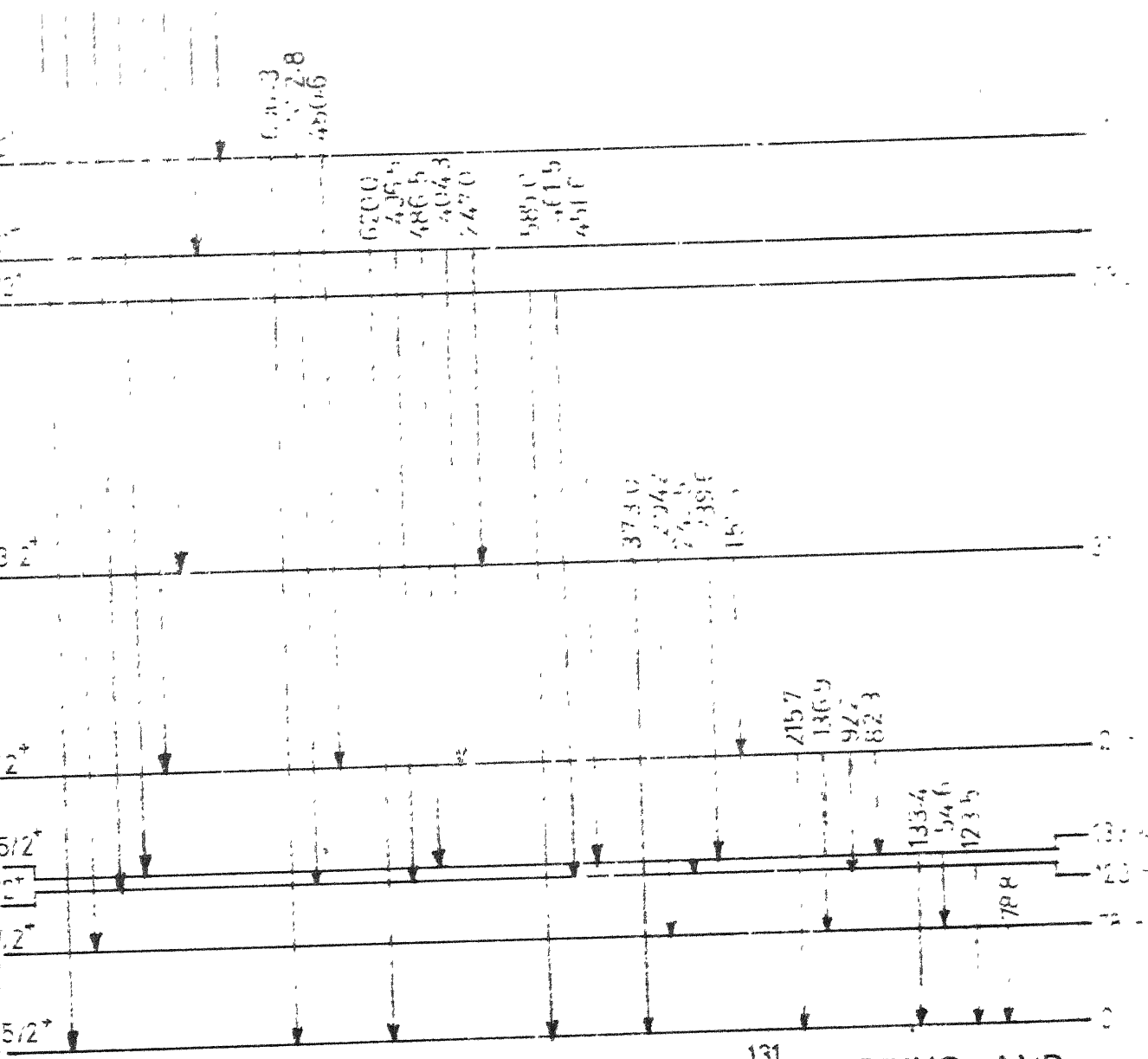


FIG. 3.8 GAMMA DECAY SCHEME OF  $^{131}\text{Ba}$ . SPINS AND PARITIES OF  $^{131}\text{Cs}$  LEVELS ARE FROM HASSELGREN et al.<sup>6)</sup>

REFERENCES

1. D.J. Horen, J.M. Hollander and R.L. Graham, Phys. Rev. 135 (1964) B301.
2. K. Karlsson, Ark.Fys. 33 (1966) 47.
3. T. Kucarova, B. Kracik and V. Zvoliska, Sov. J. Nucl. Phys. 7 (1968) 433.
4. V.R.K. Murthy and S. Jnanananda, Proc. Phys. Soc. 91 (1967) 600.
5. P.C. Mangal and P.N. Trehan, Proc. Nucl. Phys. and Sol. Sta. Phys. Symp. (DAE, Bombay, India), Vol.II (1968) 188.
6. L. Hasselgren, S. Antman, H.S. Sahota and J.E. Thun, Nucl. Phys. A 153 (1970) 625.

CHAPTER IV  
DECAY SCHEME STUDIES OF  $^{147}\text{Nd}$

IV.1 Introduction

The level structure of  $^{147}\text{Pm}$  using the  $^{147}\text{Nd}$  source, has been studied by many investigators<sup>1-18</sup> employing various techniques. Considerable disagreement exists in the number of existing levels of  $^{147}\text{Pm}$  and their possible decay modes. Bashandy et al.<sup>13</sup> with their iron-free double focussing spectrometer predicted new levels at 120, 208, 231, 273, 298, 552, 724 and 763 keV in addition to already well established levels. Besides, there is a considerable interest in the level structure of nuclides around mass number 150, where one expects rather sudden change from near spherical to deformed structure. To check the validity of various theoretical interpretations of nuclear structure in this region there is a general need of detailed and precise experimental data. This theoretical interest together with the discrepancies in the reports of several investigations prompted us to carry out the detailed investigation on the decay of  $^{147}\text{Nd}$ .

The  $^{147}\text{Nd}$  source was obtained from Bhabha Atomic Research Centre, Bombay, India. Sources of different strengths were made onto perspex holders.



## IV.2 Ge(Li) Spectra

Various Ge(Li) spectra were recorded at different intervals to determine the energies of gamma rays precisely and to follow their decay in order to ensure that they originate from the 11 day decay of  $^{147}\text{Nd}$ . The entire range of gamma ray spectrum was recorded in two different energy regions and the typical spectra obtained are shown in Figs. 4.1 and 4.2. The energies of gamma ray observed are listed in Table 4.1, wherein the values from earlier workers are also quoted for comparison.

## IV.3 Coincidence Measurements

Sum-coincidence measurements were done at the following gate settings: 182, 275, 319.5, 410.5, 489.9, 531, 594.8, 685.8 and 725 keV. Some measurements were made with simple fast-slow coincidence requirement, using the same NaI(Tl) detectors, to check a few transitions. In all the sum-coincidence spectra, the 39 and 43 keV x-rays are expected to appear, adding up with some gamma component satisfying the sum gate condition. Their presence is ignored while assigning observed gamma transitions. The results of sum-coincidence measurements are summarized in Table 4.2 and are discussed below.

The spectrum with gate at 182 keV shows a peak at 91 keV. This is explained as due to  $182 \rightarrow 91 \rightarrow 0$  mode of decay.

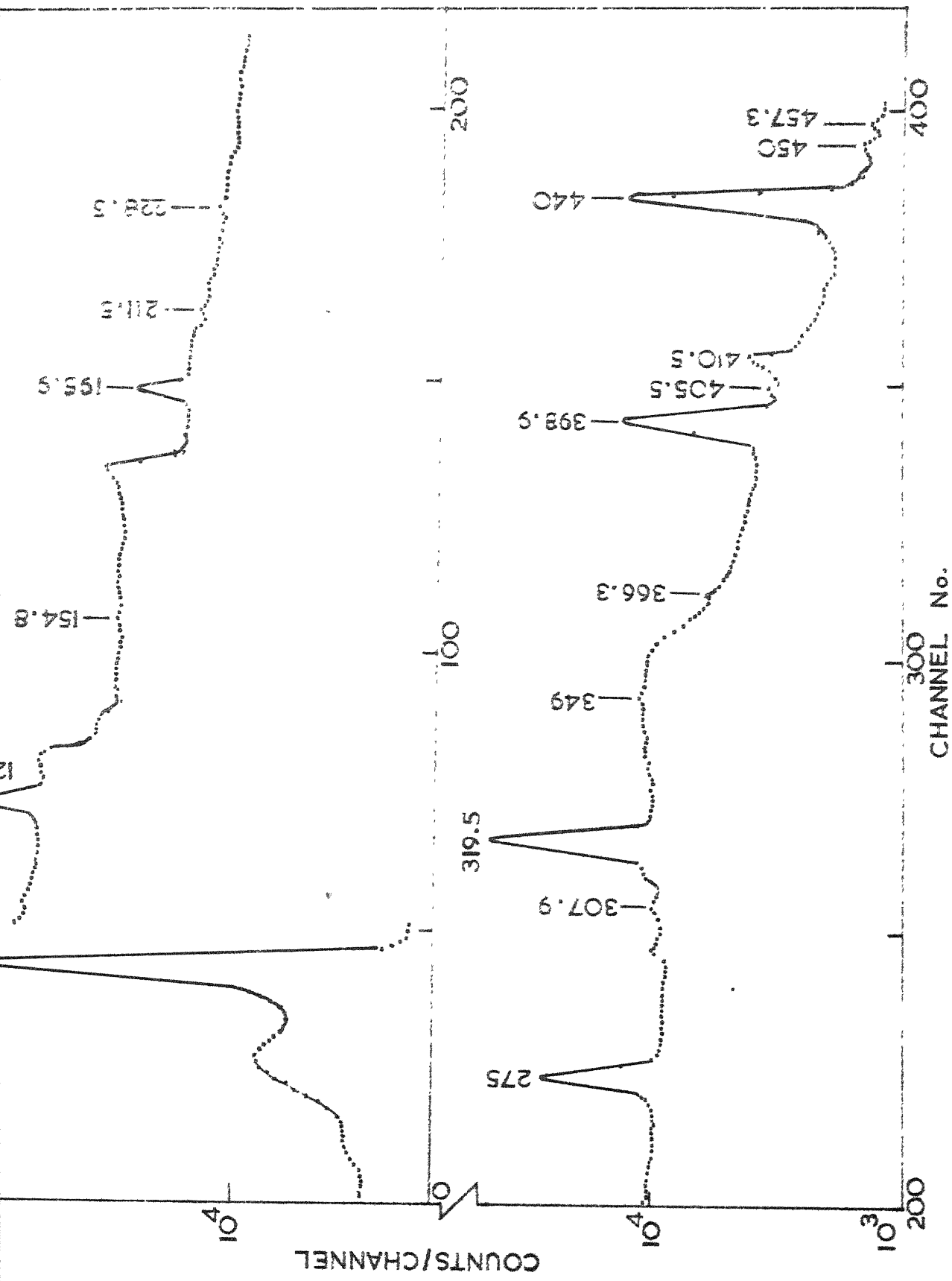


FIG.4.1 Ge(Li) SPECTRUM OF  $^{147}\text{Nd}$  IN 0-460 KEV ENERGY RANGE

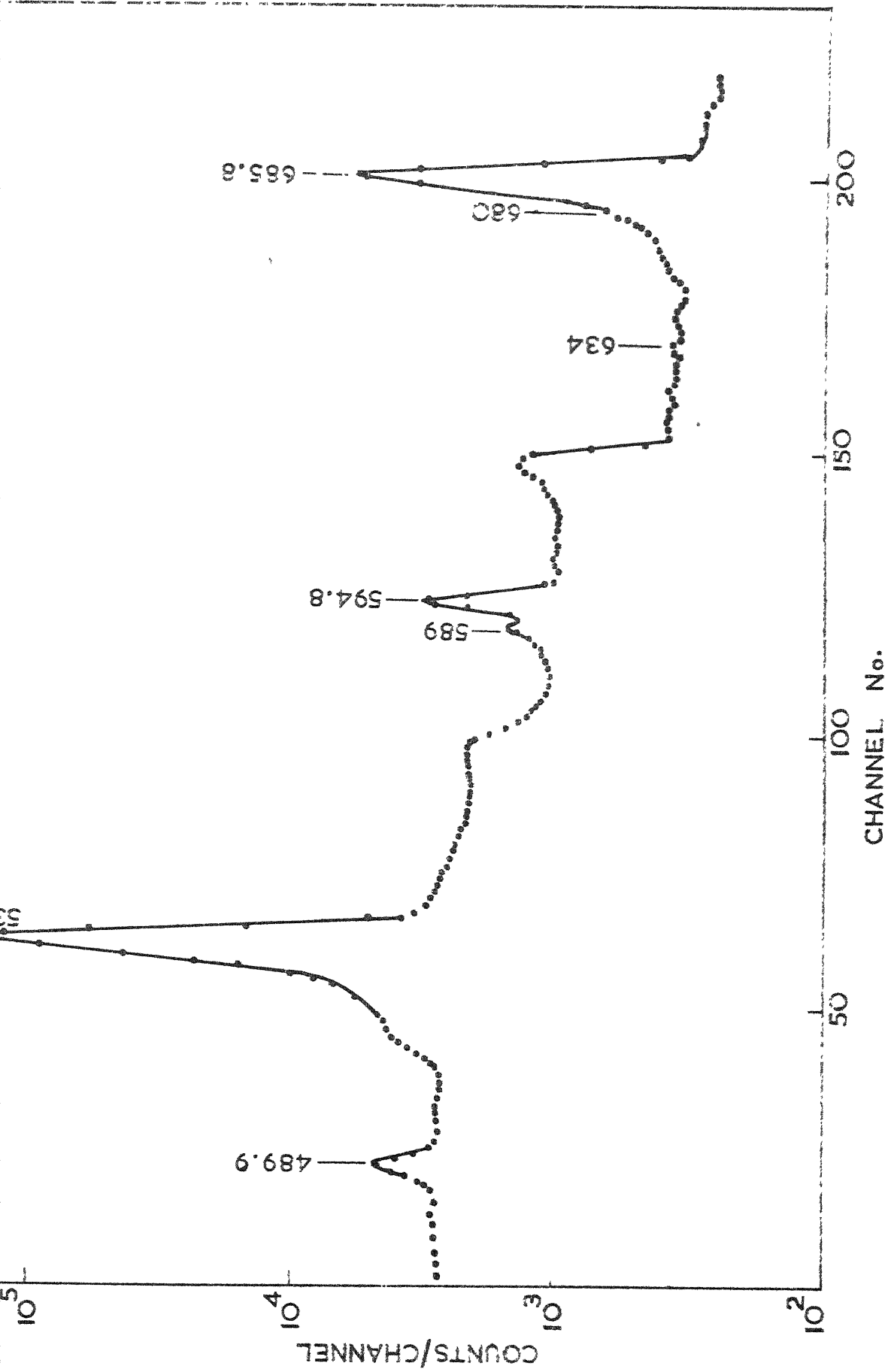


FIG. 4.2 Ge(Li) SPECTRUM OF  $^{147}\text{Nd}$  IN 460-700 KeV ENERGY RANGE

Table 4.1. Gamma Rays Observed in the Decay  $^{147}\text{Nd}^{(a)}$

<u>Bäcklin</u> <u>et al.</u> <sup>14</sup>	<u>Hill</u> <u>et al.</u> <sup>15</sup>	<u>Jacobs</u> <u>et al.</u> <sup>17</sup>	<u>Canty</u> <u>et al.</u> <sup>17</sup>	<u>Dougan</u> <u>et al.</u> <sup>18</sup>	Present
-	-	77	-	-	-
91.0	91.1	91.1	91.0	91	91
120.5	120.49	120.5	120.6	121	120.5
-	-	154.6	-	-	154.8
-	-	-	-	-	184.0
196.6	196.66	197.0	196.6	197	195.9
-	-	-	-	-	228.5
275.4	275.42	275.4	275.1	275	275.0
-	-	-	-	-	307.9
319.2	319.41	319.4	319.3	319	319.5
-	-	-	-	-	349.0
-	-	-	-	-	366.3
398.1	398.22	398.0	397.8	398	398.9
-	-	-	-	-	405.5
410.3	410.3	410.0	409.6	411	410.5
439.8	439.85	439.4	439.4	440	440.0
-	-	-	-	-	450.0
-	-	-	-	-	457.3
489.0	489.3	488.4	488.5	490	489.9
530.9	531.01	530.9	530.7	531	531.0
589.0	589.3	-	-	590	589.0

...Contd.

Table 4.1 (Contd...)

<u>Bäcklin</u> <u>et al.</u> <sup>14</sup>	<u>Hill</u> <u>et al.</u> <sup>15</sup>	<u>Jacobs</u> <u>et al.</u> <sup>16</sup>	<u>Canty</u> <u>et al.</u> <sup>17</sup>	<u>Dougan</u> <u>et al.</u> <sup>18</sup>	Present
595.5	594.7	593.0	594.4	596	594.8
-	-	-	-	-	634.0
-	679.4	-	-	(679)	680.0
686.3	685.8	685.0	686.1	686	685.8

- (a) The results of the earlier workers are also shown for comparison.

Table 4.2. Summary of Sum-coincidence Measurements of  $^{147}\text{Nd}$

Sum coincidence gate energy (keV)		$\gamma$ - $\gamma$ cascades observed	
i)	182	182	$\xrightarrow{91} 91 \xrightarrow{91} 0$
ii)	275	a)	$275 \xrightarrow{184} 91 \xrightarrow{91} 0$
		b)	$685.8 \xrightarrow{154.8} 531 \xrightarrow{120.5} 410.5$
iii)	319.5	a)	$319.5 \xrightarrow{137.5} 182.0 \xrightarrow{182} 0$
		b)	$319.5 \xrightarrow{91} 228.5 \xrightarrow{228.5} 0$
iv)	410.5	a)	$410.5 \xrightarrow{91} 319.5 \xrightarrow{319.5} 0$
		and/or	
			$410.5 \xrightarrow{319.5} 91 \xrightarrow{91} 0$
		b)	$725 \xrightarrow{194} 531 \xrightarrow{211.5} 319.5$
v)	489.9	a)	$489.9 \xrightarrow{398.9} 91 \xrightarrow{91} 0$
		b)	$489.9 \xrightarrow{307.9} 182 \xrightarrow{182} 0$
		c)	$685.8 \xrightarrow{154.8} 531 \xrightarrow{349} 182$
vi)	531	a)	$531 \xrightarrow{440} 91 \xrightarrow{91} 0$
		b)	$531 \xrightarrow{349} 182 \xrightarrow{182} 0$
		c)	$531 \xrightarrow{256} 275 \xrightarrow{275} 0$
		d)	$531 \xrightarrow{211.5} 319.5 \xrightarrow{319.5} 0$
		e)	$531 \xrightarrow{120.5} 410.5 \xrightarrow{410.5} 0$
vii)	594.8	a)	$685.8 \xrightarrow{195.9} 489.9 \xrightarrow{398.9} 91$
		b)	$685.8 \xrightarrow{275.3} 410.5 \xrightarrow{319.5} 91$

...Contd.

Table 4.2 (Contd...)

Sum coincidence gate energy (keV)		$\gamma$ - $\gamma$ cascades observed	
viii)	685	a)	685.8 $\xrightarrow{594.8}$ 91 $\xrightarrow{91}$ 0
		b)	680 $\xrightarrow{589}$ 91 $\xrightarrow{91}$ 0
		c)	685.8 $\xrightarrow{457.3}$ 228.5 $\xrightarrow{228.5}$ 0
		d)	685.8 $\xrightarrow{366.3}$ 319.5 $\xrightarrow{319.5}$ 0
		e)	685.8 $\xrightarrow{275.3}$ 410.5 $\xrightarrow{410.5}$ 0
		f)	685.8 $\xrightarrow{195.9}$ 489.9 $\xrightarrow{489.9}$ 0
		g)	685.8 $\xrightarrow{154.8}$ 531 $\xrightarrow{531}$ 0
ix)	725	a)	725 $\xrightarrow{634}$ 91 $\xrightarrow{91}$ 0
		b)	725 $\xrightarrow{450}$ 275 $\xrightarrow{275}$ 0
		c)	725 $\xrightarrow{405.5}$ 319.5 $\xrightarrow{319.5}$ 0
		d)	725 $\xrightarrow{194}$ 531 $\xrightarrow{531}$ 0

The sum-coincidence spectrum with 275 keV gate has contribution from  $685.8 \rightarrow 410.5$  mode of decay also. The spectrum showed peaks at 91, 120, 155 and 184 keV. The peaks at 91 and 184 can be due to either  $275 \rightarrow 91 \rightarrow 0$  or  $275 \rightarrow 182 \rightarrow 0$  keV mode of decay. It is not possible to decide between these two transitions. The pair of 120 and 155 is due to  $685.8 \rightarrow 531 \rightarrow 410.5$  mode of decay.

The sum-coincidence spectrum with 320 keV gate shows peaks of energies 91, 138, 182 and 228 keV. The pair of 91 and 228 keV arise from the  $319.5 \rightarrow 228.5 \rightarrow 0$  mode of decay, whereas 138 and 182 keV gamma rays are due to  $319.5 \rightarrow 182 \rightarrow 0$  mode of decay.

The spectrum with gate at 410 keV clearly indicated that the primary mode of decay of 410.5 keV level is through the emission of 319.5 and 91 keV gammas. The 489 keV gated sum-coincidence spectrum provides the confirmation of  $489.9 \rightarrow 182$  keV transition. This also provides an additional evidence for the existence of 182 keV level. The spectrum with gate at 531 keV gave a clear indication for the existence of levels at 182, 275 and 319.5 keV.

The sum-coincidence spectra with energy gates at 595, 685 and 725 keV are shown in Figs. 4.3, 4.4 and 4.5. The features of the same spectra are described below.



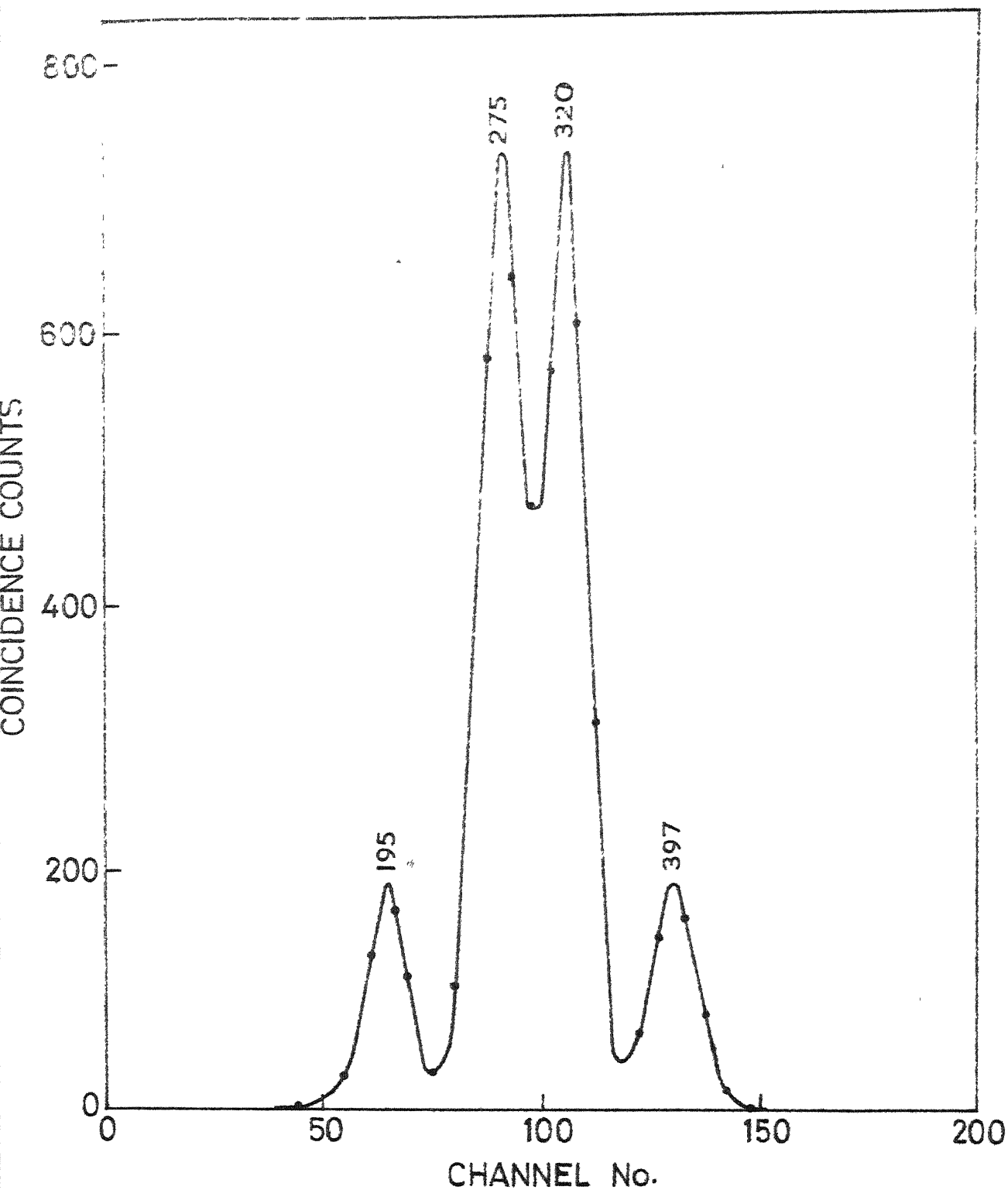


FIG. 4.3 SUM-COINCIDENCE SPECTRUM OF  $^{147}\text{Nd}$  WITH GATE AT 595 KeV

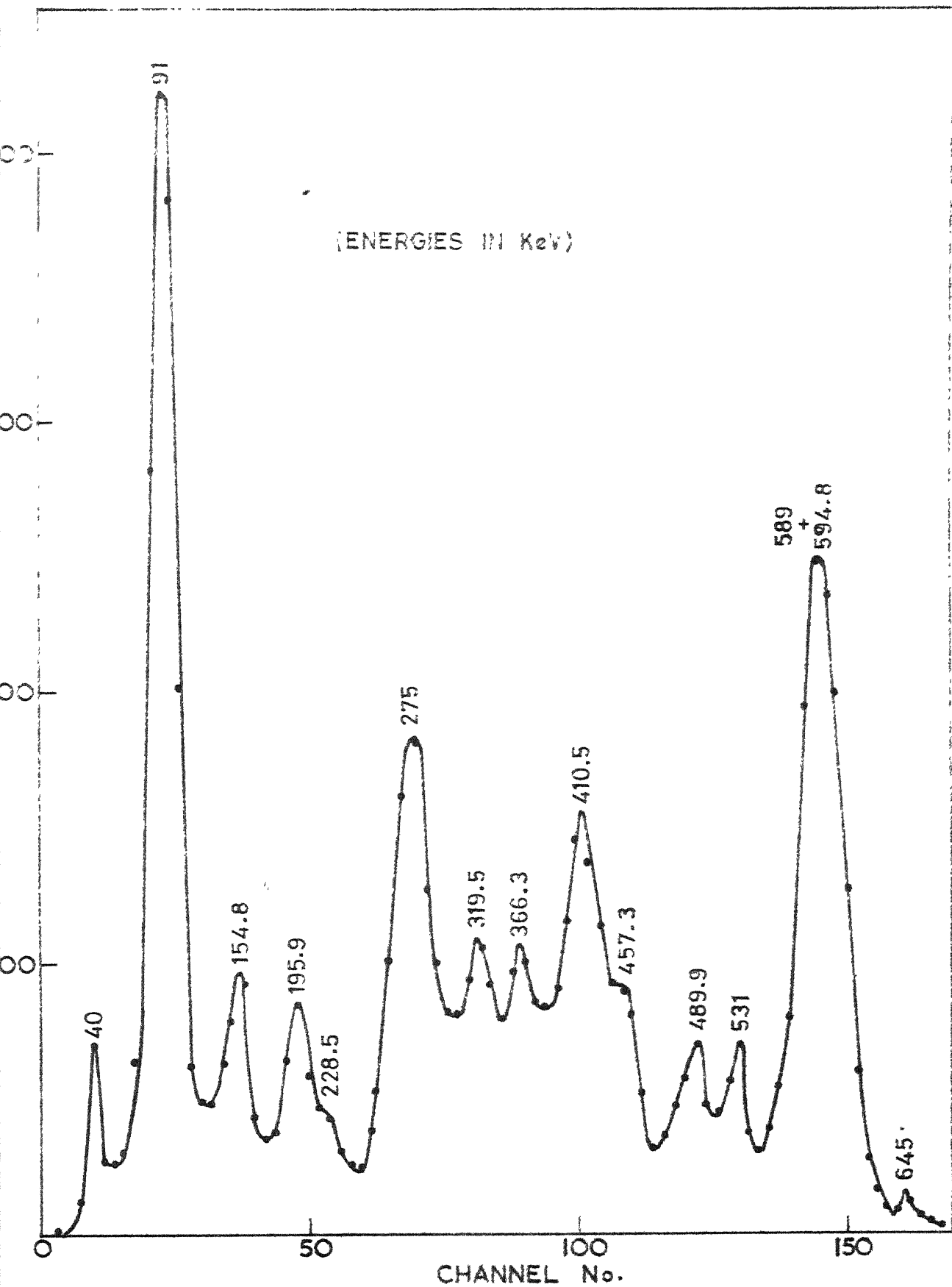


FIG.4.4 SUM COINCIDENCE SPECTRUM OF  $^{147}\text{Nd}$  WITH GATE AT 685 KeV

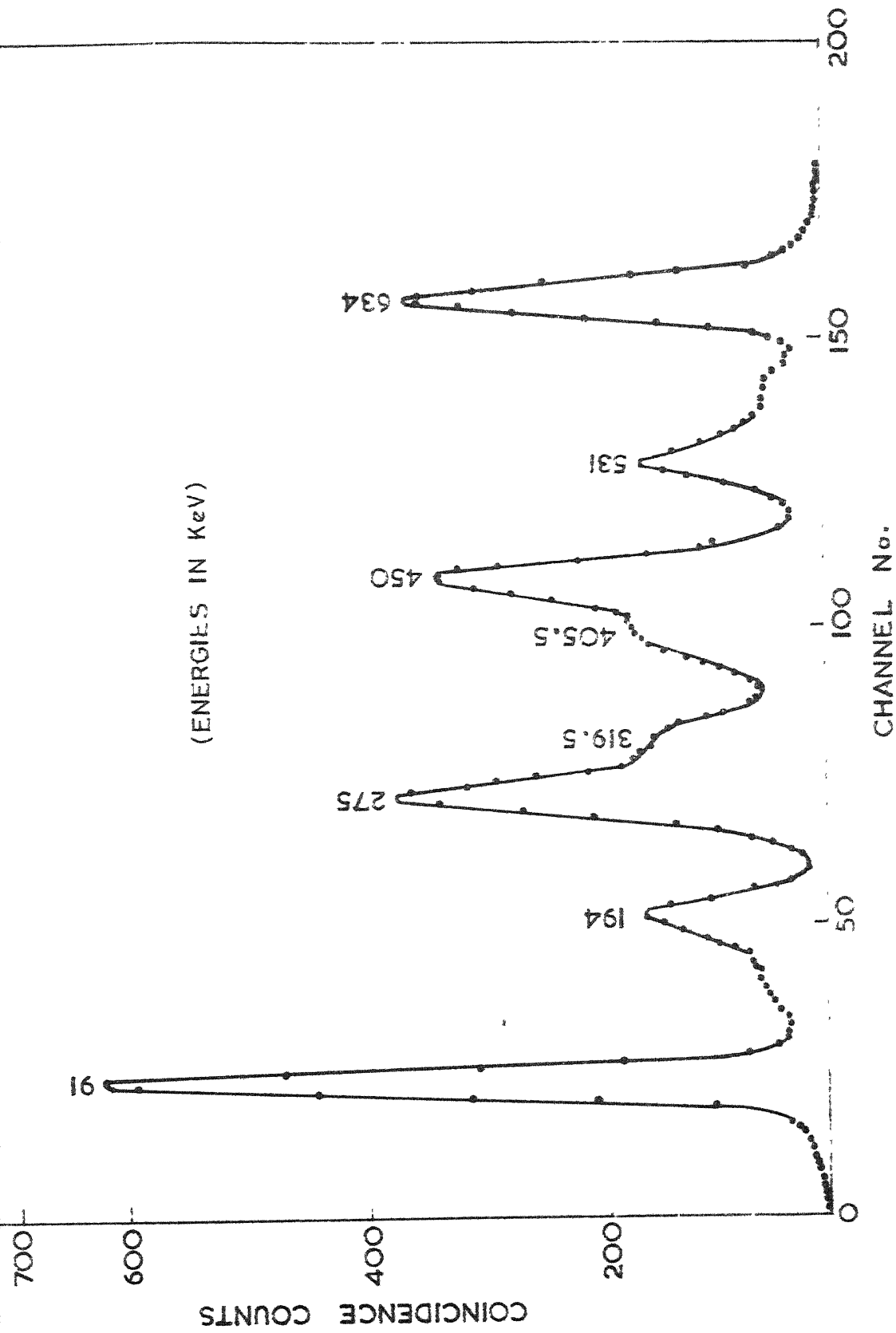


FIG. 4.5 SUM-COINCIDENCE SPECTRUM OF  $^{147}\text{Nd}$  WITH GATE AT 725 KeV

(i) 594.8 keV gate : There is no level assigned at 594.8 keV. However, this sum gate spectrum was explored to examine the transitions resulting from the  $685.8 \rightarrow 91$  keV decay mode. Gamma rays of energies 195.9, 275.3, 319.5 and 398.9 keV were observed. The presence of 195.9 and 398.9 keV gamma pair provides the confirmation of  $685.8 \rightarrow 489.9 \rightarrow 91$  keV decay mode.

(ii) 685.8 keV gate : This sum gate includes both 685.8 and 680 keV levels. The observed gamma transitions are 91, 154.8, 195.9, 228.5, 275, 319.5, 366.3, 410.5, 457.3, 489.9, 531 and  $589 + 594.8$  keV. The occurrence of 228.5 and 457.3 keV gammas in coincidence can only be explained as  $685.8 \rightarrow 228.5 \rightarrow 0$  keV decay mode. It offers evidence for the existence of 228.5 keV level.

(iii) 725 keV gate : The observed clear peaks are at 91, 194, 275, 319, 405, 450, 531 and 634 keV. They are ascribed to the following modes of decay:  $725 \rightarrow 91 \rightarrow 0$ ,  $725 \rightarrow 275 \rightarrow 0$ ,  $725 \rightarrow 319.5 \rightarrow 0$  and  $725 \rightarrow 531 \rightarrow 0$ . The spectrum, thus provides, further evidence for the existence of 275 and 319.5 keV levels.

In addition to the above mentioned sum-coincidence measurements, we have also measured the conventional fast-slow coincidence spectra with gates at 91, 120, 182, 228 and 275 keV. These measurements were done to confirm the energy levels and gamma transitions observed by us in

singles and sum-coincidence spectra. We found that the results of the latter study are consistent with the results mentioned above.

#### IV.4 Discussion

Cork et al.<sup>6</sup> proposed a level at 289 keV. We do not have any indication for the existence of this level. Evans<sup>7</sup> suggested a level at 230 keV to accommodate 230, 260 and 300 keV gamma rays reported originally by Rutledge et al.<sup>4</sup> We observe that 228.5 keV level is populated from 685 and 319.5 keV levels through the 457.3 and 91 keV gamma rays respectively. The 260 and 300 keV gamma rays which were proposed to feed 228.5 keV level were not observed.

We have a definite evidence for the existence of a level at 319.5 keV, reported earlier by Cork et al. and Bashandy et al. This level is populated from 725, 685.8 and 531 keV levels giving 405.5, 366.3 and 211.5 keV gamma transitions. We have indications for the presence of all these three gamma rays in Ge(Li) spectrum. Further evidence is obtained from the sum-coincidence spectra with gates at 725, 685 and 531 keV energies.

Hill et al.<sup>15</sup> reported a level at 680 keV besides the well established level at 685 keV. We also have an indication for the same level in our Ge(Li) spectrum, where an indication exists for the presence of 680 keV gamma ray. Further, a gamma ray of energy 589 keV is also

observed, which can only be explained as from  $680 \rightarrow 91$  keV transition.

Gunye et al.<sup>10</sup>, Spring et al.<sup>11</sup> and Sastry et al.<sup>12</sup> reported a level at 725 keV. We investigated this level in detail and got confirmation of its existence. Our results disagree with these earlier reports in certain details. Gunye et al. and Spring et al. reported a transition  $725 \rightarrow 410.5$  keV for the depopulation of this level. Sastry et al. reported only a crossover transition for the deexcitation of this level. We do not find a crossover transition nor  $725 \rightarrow 410.5$  keV decay mode. Instead, the sum-coincidence spectrum with gate at 725 keV exhibits  $725 \rightarrow 531$ ,  $725 \rightarrow 319.5$ ,  $725 \rightarrow 275$  and  $725 \rightarrow 91$  keV modes of decay. The gamma rays, involved in these transitions, are observed in Ge(Li) spectrum also.

Our measurements confirm the existence of 154.8 keV gamma rays reported by Jacobs et al.<sup>16</sup> and Bashandry et al. We have a conclusive evidence that the gamma ray is due to  $685.8 \rightarrow 531$  keV transition from our sum-coincidence spectrum with a gate at 685 keV. The level scheme constructed, with our results incorporated, is shown in Fig. 4.6.

#### IV.5 Summary

Thirty gamma transitions are observed and levels at 182, 228.5, 275, 319.5 and 725 keV, which were doubtful,

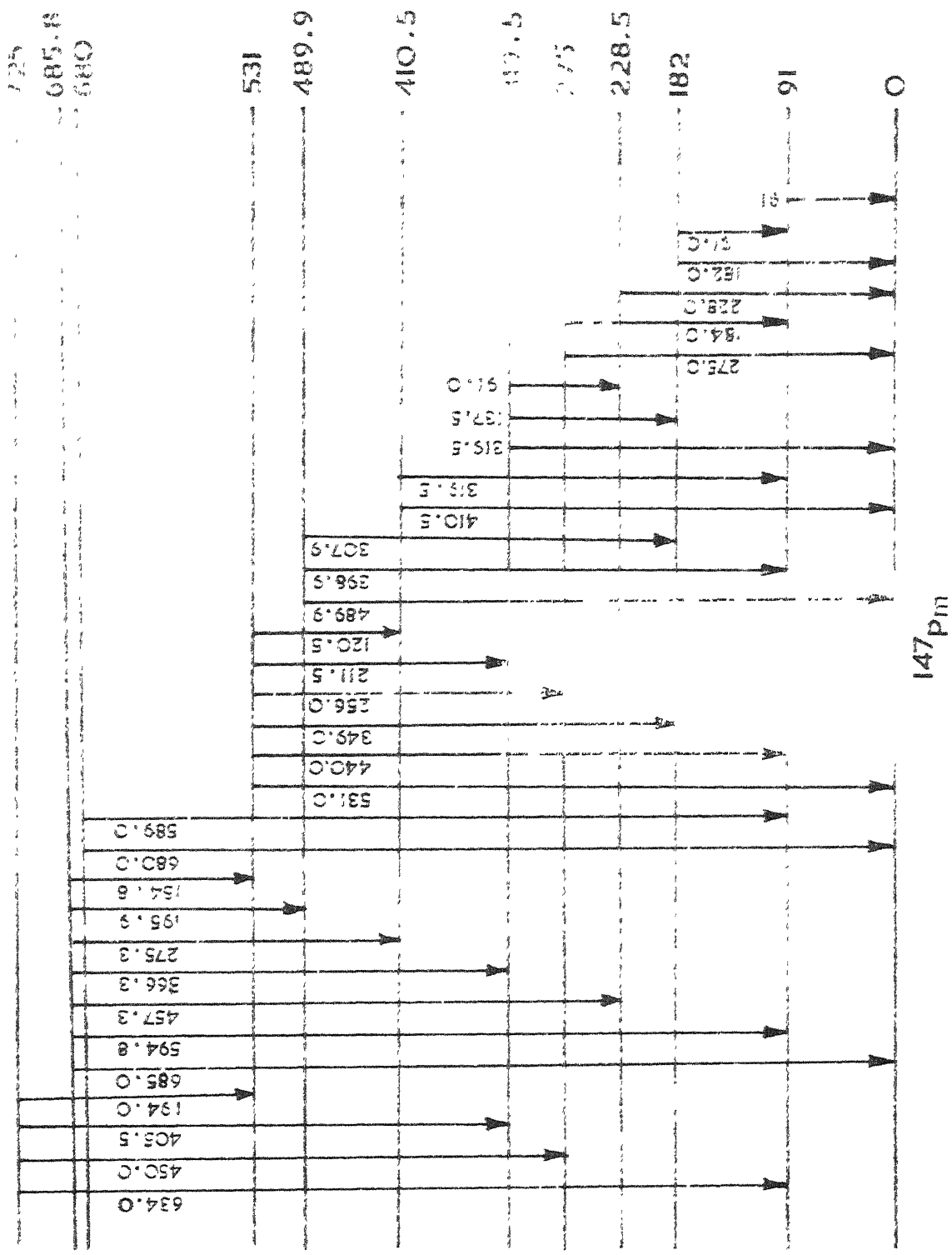


FIG. 4.6 GAMMA DECAY OF  $^{147}\text{Nd}$  AND LEVELS IN  $^{147}\text{Pm}$

are confirmed from our detailed sum-coincidence studies. Our coincidence measurements rule out completely the possibility of levels at 120, 208, 398, 471, 552 and 763 keV proposed by Bashandy et al.



# REFERENCES

1. C.E. Mende ville and E. Shapiro, Phys. Rev. 79 (1950) 391.
2. E. Kondaiah, Phys. Rev. 81 (1951) 1056.
3. W.S. Emmerich and J.D. Kurbatov, Phys. Rev. 83 (1951) 40.
4. W.C. Rutledge, J.M. Cork and S.B. Burson, Phys. Rev. 86 (1952) 775.
5. H.S. Hans, B. Saraf and C.E. Mandeville, Phys. Rev. 97 (1955) 1267.
6. J.M. Cork, M.K. Brice, R.G. Helmer and R.M. Woods, Jr., Phys. Rev. 110 (1958) 526.
7. P.R. Evans, Phil. Mag. 3 (1958) 1061.
8. T.J. Walters, Nuclear Phys. 15 (1960) 653.
9. H.D. Wandt and P. Kleinheinz, Nucl. Phys., 20 (1960) 169.
10. M.R. Gunye, R. Jambunathan and B. Saraf, Phys. Rev. 124 (1961) 172.
11. E. Spring, Phys. Lett. 7 (1963) 218.
12. V.V.G. Sastry, V. Lakshminarayana and S. Jnanananda, Ind. J. Pure and App. Phys. 2 (1964) 207.
13. E. Bashandy and A.A. El-Haliem, Z. Naturf. 22A (1967) 154.
14. A. Bäcklin and S.G. Malmakog, Arkiv Fur Fysik 34 (1967) 459.
15. J.C. Hill and M.L. Wiedenbeck, Nucl. Phys. A98 (1961) 599.
16. E. Jacobs, K. Heyde, M. Dorikens, J. Demuyne and L. Dorikens-Vanpraet, Nucl. Phys. A99 (1967) 411.
17. M.J. Canty and R.D. Connor, Nucl. Phys. A104 (1967) 35.
18. P.W. Dougan and B. Erlandsson, Zeits. Phys. 207 (1967) 105.

## CHAPTER V

### DECAY OF $^{115m}\text{Cd}$

#### V.1 Introduction

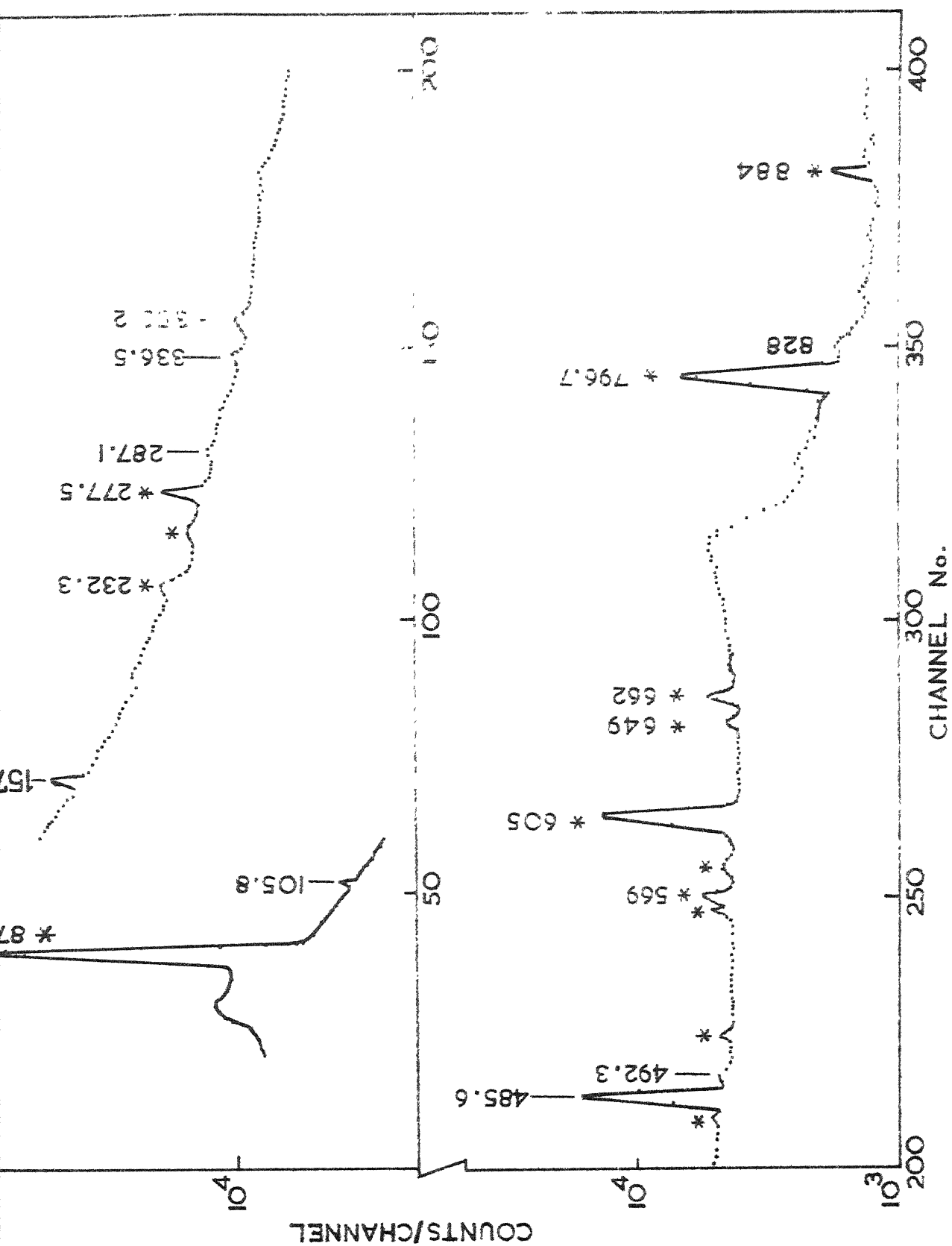
The 43 day decay of  $^{115m}\text{Cd}$  has been the subject of many investigations.<sup>1-6</sup> Visweswara Rao et al.<sup>4</sup> measured the gamma spectra using a sum-coincidence spectrometer. They assigned new levels at 650 and 1560 keV along with several new gamma transitions. Subsequently, Graeffe et al.<sup>6</sup> studied the decay scheme using a Ge(Li)-NaI(Tl) coincidence spectrometer. They did not observe the levels at 650 and 1560 keV. Instead, they reported new levels at 828 and 336 keV. Besides there exist several other inconsistencies in the number of levels and gamma transitions. The present investigation has been carried out to examine the decay scheme in detail.

#### V.2 Details of the Measurements

The  $^{115m}\text{Cd}$  was procured from Bhabha Atomic Research Centre, Bombay, India. Some impurities, including  $^{134}\text{Cs}$ , were found to be present in the source. The radiation due to the impurities was easily identified by recording the Ge(Li) spectra many times over regular periods. Only those gamma rays, showing half life of 43 days have been attributed to the  $^{115m}\text{Cd}$  decay.

The Ge(Li) spectrum was recorded in two energy regions: (i) 0-900 keV, and (ii) 900-1600 keV to cover the entire range of gamma rays. The two spectra are shown in Figs. 5.1 and 5.2. In all 12 gamma rays have been observed. The gamma ray energies are listed in Table 5.1. The results of earlier workers are also given in the table for comparison.

The sum-coincidence spectra were recorded with gates at energies 598, 934, 1133, 1290 and 1420 keV. There is no level at 598 keV, but this spectrum was recorded to see the occurrence of double cascades between 934 and 336 keV levels. This serves to test the  $934 \rightarrow 828 \rightarrow 336$  keV decay mode observed by Graeffe et al. The spectrum recorded with this gate at 598 keV is shown in Fig. 5.3. It clearly establishes the genetic relation between 106 and 492 keV gamma rays, which can only be explained as  $934 \rightarrow 828 \rightarrow 336$  keV cascade decay. It, thus, provides the evidence for the existence of 828 keV level. Further evidence for the existence of this level comes from the sum-coincidence spectrum with gate at 934 keV. The spectrum shows that 934 keV level gets deexcited by emitting a cascade of 106 and 828 keV gamma rays. It is ascribed as  $934 \rightarrow 828 \rightarrow 0$  mode of decay. The results of sum-coincidence measurements at various gate settings are summarized in Table 5.2.



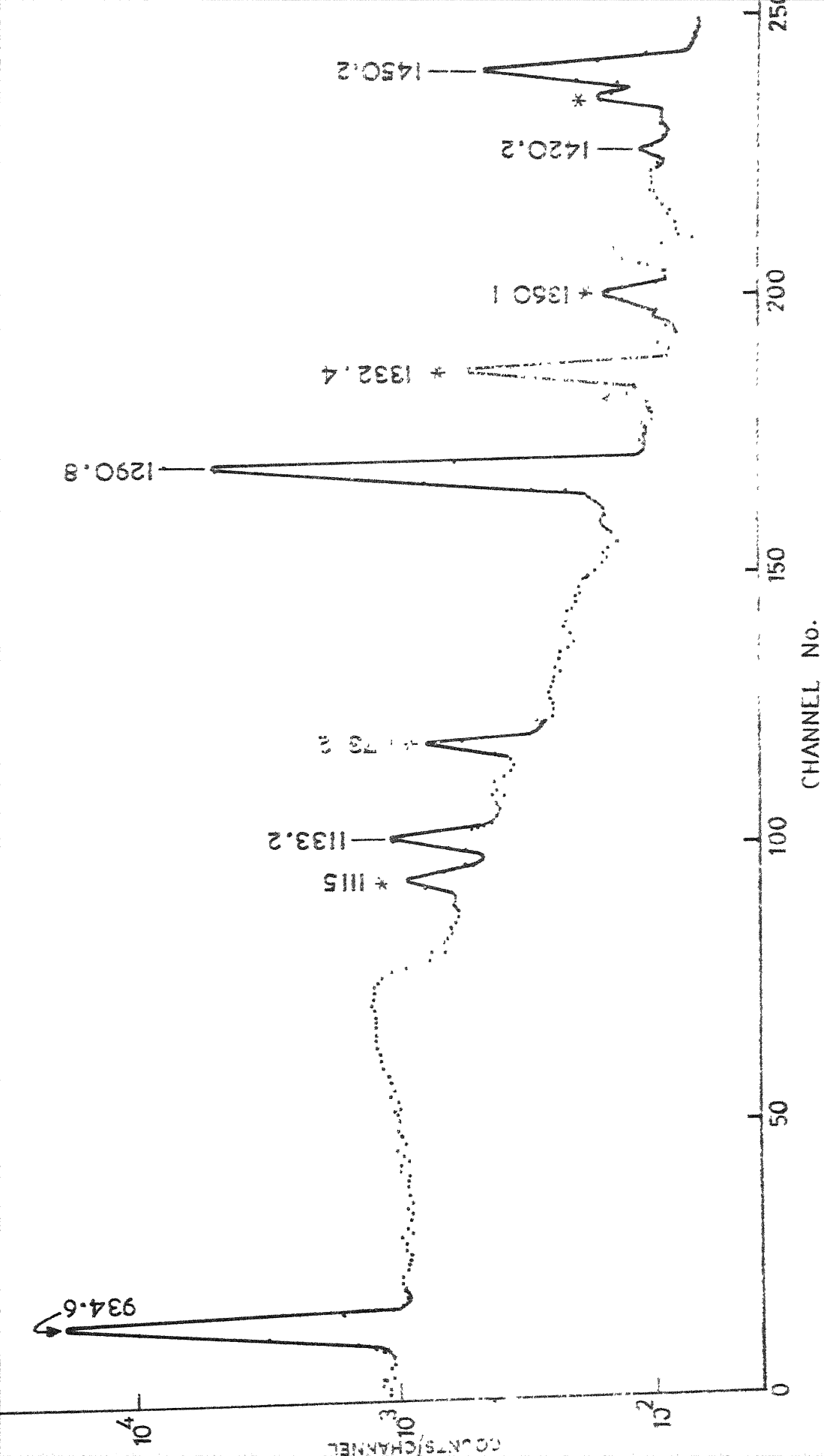


FIG. 5.2 Ge(Li) SPECTRUM OF  $^{115m}\text{Cd}$  IN 900-1500 keV ENERGY RANGE

Table 5.1. Gamma Rays Observed in the Decay of  $^{115m}\text{Cd}$

Rao <u>et al.</u> <sup>4</sup>	Graeffe <u>et al.</u> <sup>6</sup>	Present
-	105,6	105.8
-	(130)	-
165	158.1	157.6
270	-	-
300	(292)	287.1
-	336.3	336.5
485	485.0	485.6
-	492.6	492.3
640	-	-
650	-	-
-	-	828.0
910	-	-
935	934.4	934.6
1125	1133.0	1133.2
1290	1291.2	1290.8
1420	1419.4	1420.2
-	1450.1	1450.2
1560	-	-

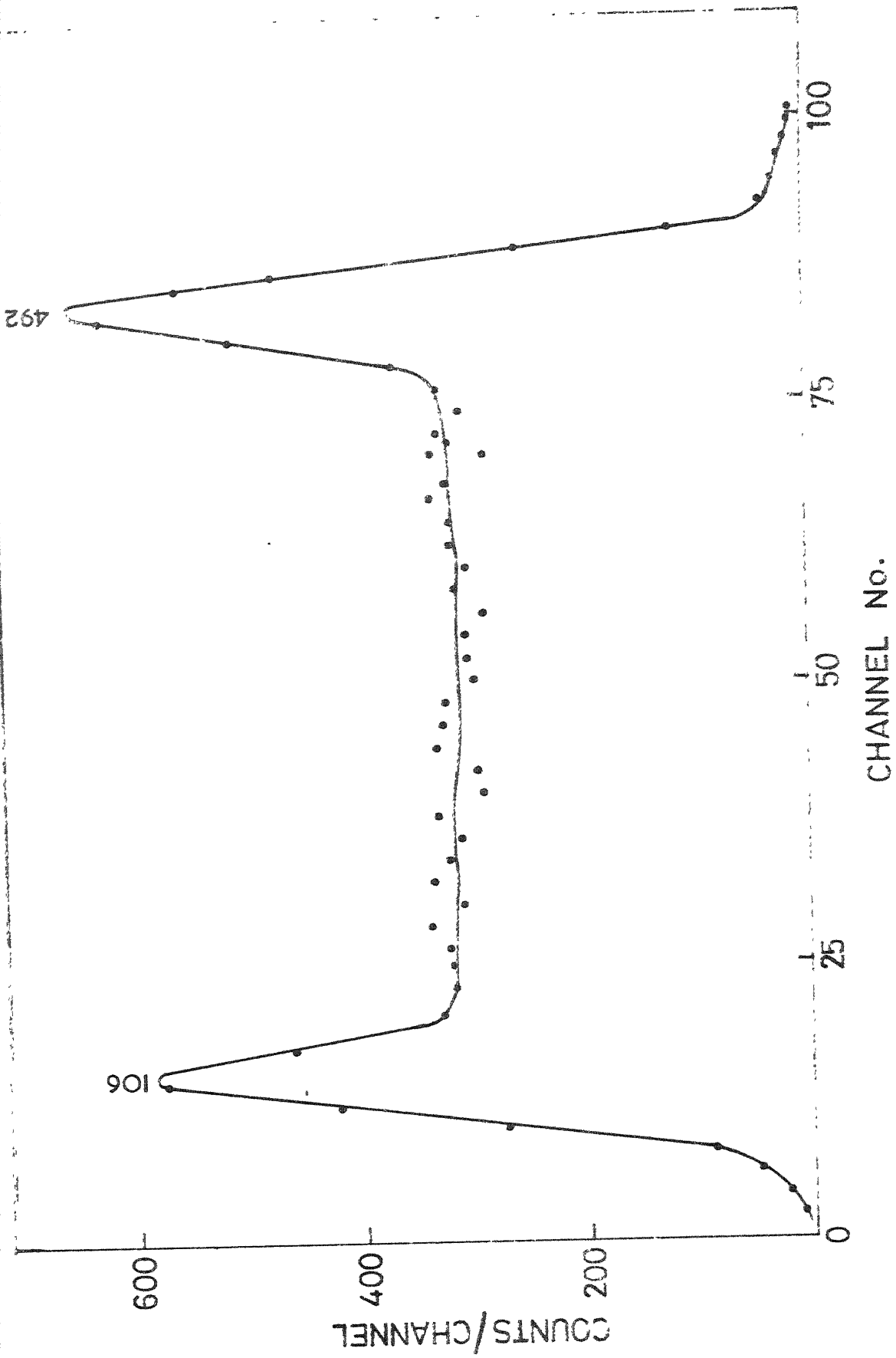


FIG. 5.3 SUM-COINCIDENCE SPECTRUM OF  $^{115m}\text{Cd}$  WITH GATE AT 598 KeV

Table 5.2. Summary of Sum-coincidence Measurements on  $^{115m}\text{Cd}$

Energy gate (keV)		$\gamma$ - $\gamma$ cascades
i)	598	$934 \xrightarrow{106} 828 \xrightarrow{492} 336$
ii)	934	$934 \xrightarrow{106} 828 \xrightarrow{828} 0$
iii)	1133	$1133 \rightarrow 0$
iv)	1290	$1290 \xrightarrow{157} 1133 \xrightarrow{1133} 0$
v)	1420	a) $1420 \xrightarrow{287} 1133 \xrightarrow{1133} 0$
		b) $1420 \xrightarrow{485} 934 \xrightarrow{934} 0$
vi)	1450	$1450 \rightarrow 0$



### V.3 Summary

- (i) The Ge(Li) spectra show that in all only 12 gamma rays originate from the decay of  $^{115m}\text{Cd}$ . The spectra establish that all the levels have a cross-over transition as one of the modes of decay. Graeffe et al. observe the same features except that they did not observe a crossover transition for 828 keV level.
- (ii) In the present measurement, the evidence for the existence of 828 keV level comes from Ge(Li) spectra and also from 598 and 934 keV gated sum-coincidence spectra.
- (iii) Graeffe et al. could not establish the occurrence of 287 keV gamma ray. Both our singles and coincidence measurements confirm the presence of this gamma ray. The coincidence measurements indicate that it arises from  $1420 \rightarrow 1133$  mode of decay.
- (iv) The present investigation does not provide any evidence for levels at 650 and 1560 keV reported by Visweswara Rao et al.

The gamma decay scheme of  $^{115m}\text{Cd}$ , constructed from the results of the present measurements, is shown in Fig.5.4.

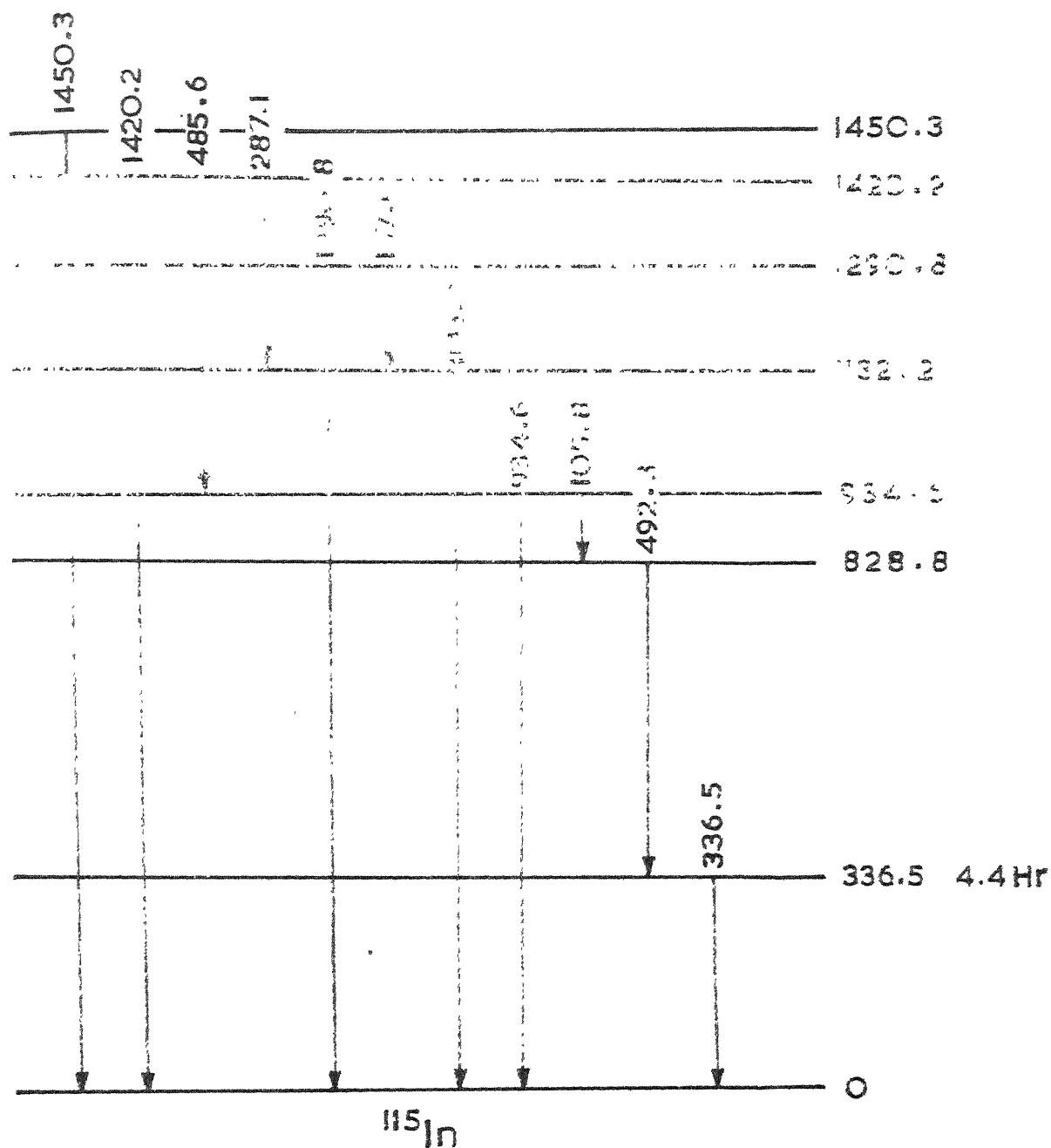


FIG. 5.4 GAMMA DECAY SCHEME OF  $^{115\text{m}}\text{Cd}$  AND LEVELS IN  $^{115}\text{In}$

REFERENCES

1. J.B. Van Der Kooi and C.E. Mandeville, Phys. Rev. 97 (1955) 977.
2. R.P. Sharma and H.G. Devare, Phys. Rev. 131 (1963) 384.
3. J.P. Hurley, R.M. Brown and C.E. Mandeville, Nucl. Phys. 47 (1963) 93.
4. V. Visweswara Rao, V. Lakshminarayana and S. Jnanananda Nucl Phys. 51 (1964) 442.
5. V.R. Pandharipande, R.P. Sharma and G. Chandra Phys. Rev. 136 (1964) B346.
6. G. Graeffe, C.W. Tang, C.D. Coryell and G.E. Gordon Phys. Rev. 149 (1967) 884.

## CHAPTER VI

### NUCLEAR LEVEL. STRUCTURE STUDIES OF $^{99}\text{Ru}$

#### VI.1 Introduction

Levels of  $^{99}\text{Ru}$ , upto the excitation energy of 2.05 MeV are populated in the  $\beta^+$ , EC decay of  $^{99}\text{Rh}$  ground state ( $T_{1/2} = 16.1$  days). The works of Kurbatov et al.<sup>1</sup> and Jha et al.<sup>2</sup> were the main sources of information about this decay till 1965. These investigations were carried out with scintillation detectors. Later studies of Connors<sup>3</sup>, Moss and McDaniels<sup>4</sup> and Antoneva et al.<sup>5</sup> were done with solid state detectors. The work of Connors was, however, restricted to the excited states of energies less than 700 keV. Moss and McDaniels have studied the level structure upto 2.05 MeV and also measured NaI(Tl)-Ge(Li) fast-slow coincidence spectra. They arrived at a decay scheme from the above data and also from a computer programme which searched for excited levels and possible transitions, accepting the gamma ray energies as the input data. Antoneva et al. recorded the singles spectra upto 2.05 MeV using a Ge(Li) spectrometer and assigned the energies and relative intensities of the gamma transitions. It was, therefore, felt that there is insufficient coincidence data to establish the decay scheme. To this end, the sum-coincidence data are recorded at various gate settings and the single spectra are also measured with a Ge(Li) detector.

The source was obtained in solid form from Oak Ridge National Laboratory (USA). The enriched target material (99.95%) was enclosed in an aluminium capsule, and was bombarded with the proton beam of ORNL cyclotron. The 16.1 day  $^{99}\text{Rh}$  activity was produced by (p,n) reaction. The isotope was radiochemically separated to remove the impurities.

The singles spectra were recorded with the Ge(Li) detector and the coincidence spectra were measured with the sum-coincidence set-up described in Chapter II.

## VI.2 Gamma Ray Transitions and Intensities

Typical singles gamma ray spectra recorded with the Ge(Li) detector are shown in Figs. 6.1-6.4. Figure 6.1 shows the gamma rays observed in the energy range of 0-442 keV. We have found no evidence for the existence of the 119.4 keV gamma ray reported by Moss and McDaniels. The spectra recorded with the separated impurity source show the existence of a well defined peak at 119.4 keV. This shows that the 119.4 keV gamma ray does not belong to the decay of  $^{99}\text{Rh}$ . The rest of the gamma ray energies in this region, however, are in agreement with the values of Moss and McDaniels. Gamma ray spectrum in the energy range 400-1200 keV is shown in Fig. 6.2. In addition to the gamma rays reported earlier, we have observed an additional gamma ray at the energy of 910.8 keV. This

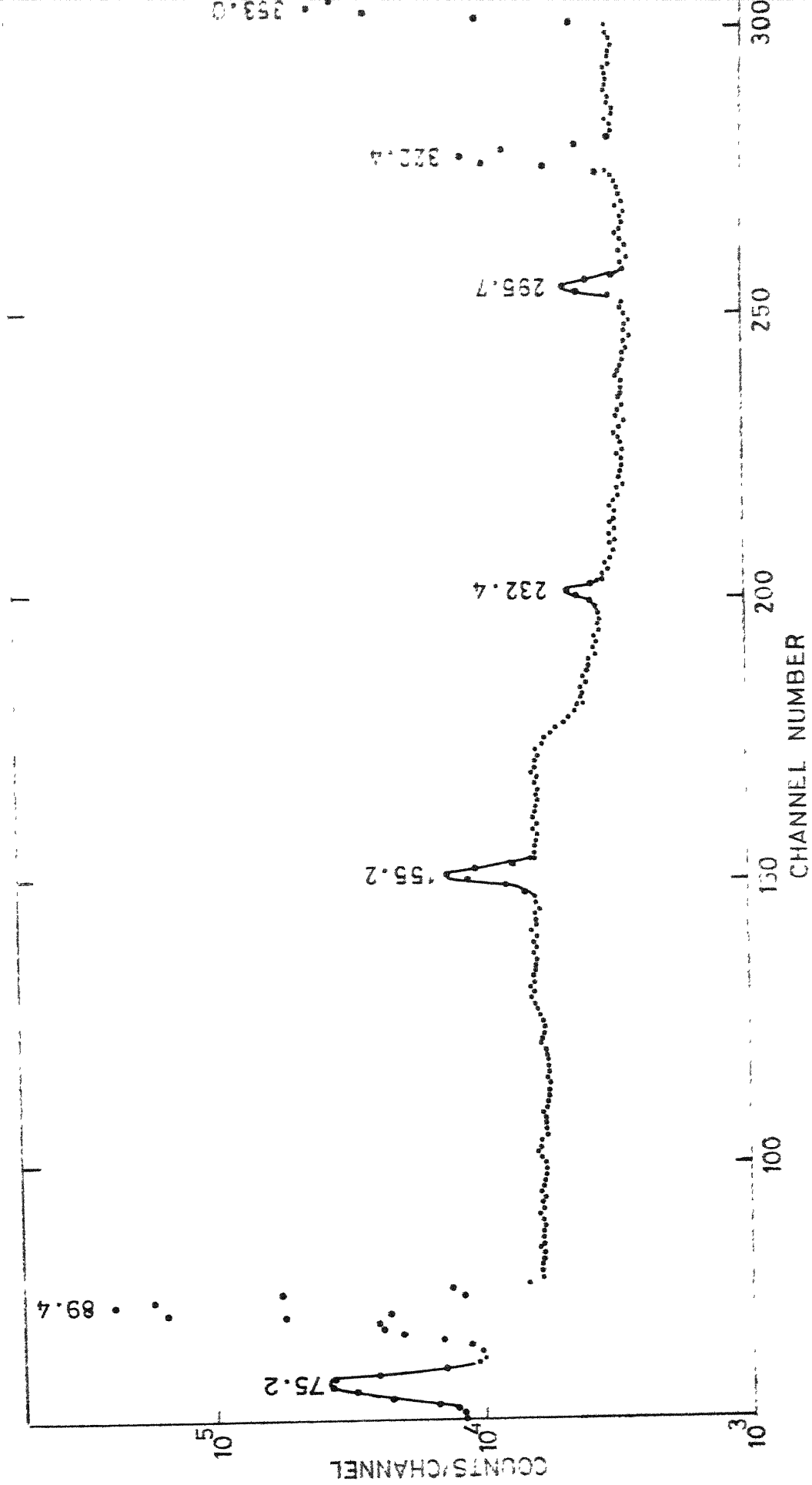


FIG. 6.1 Ge(Li) SPECTRUM OF  $^{99}\text{Rh}$  IN THE ENERGY RANGE OF 70-370 keV

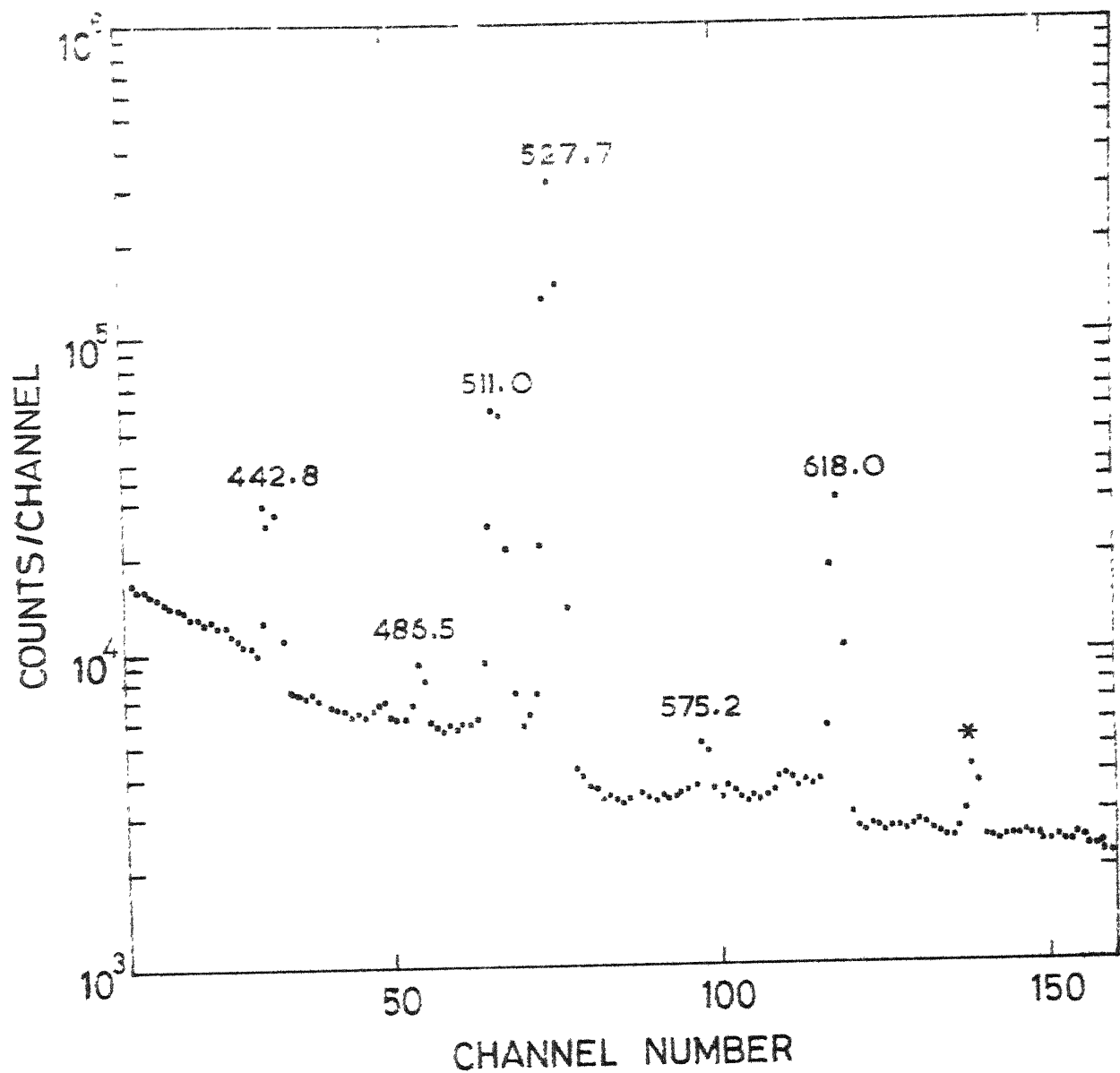


FIG.6.2A Ge(Li) SPECTRUM OF  $^{99}\text{Rh}$  IN THE ENERGY RANGE 400-700 KeV

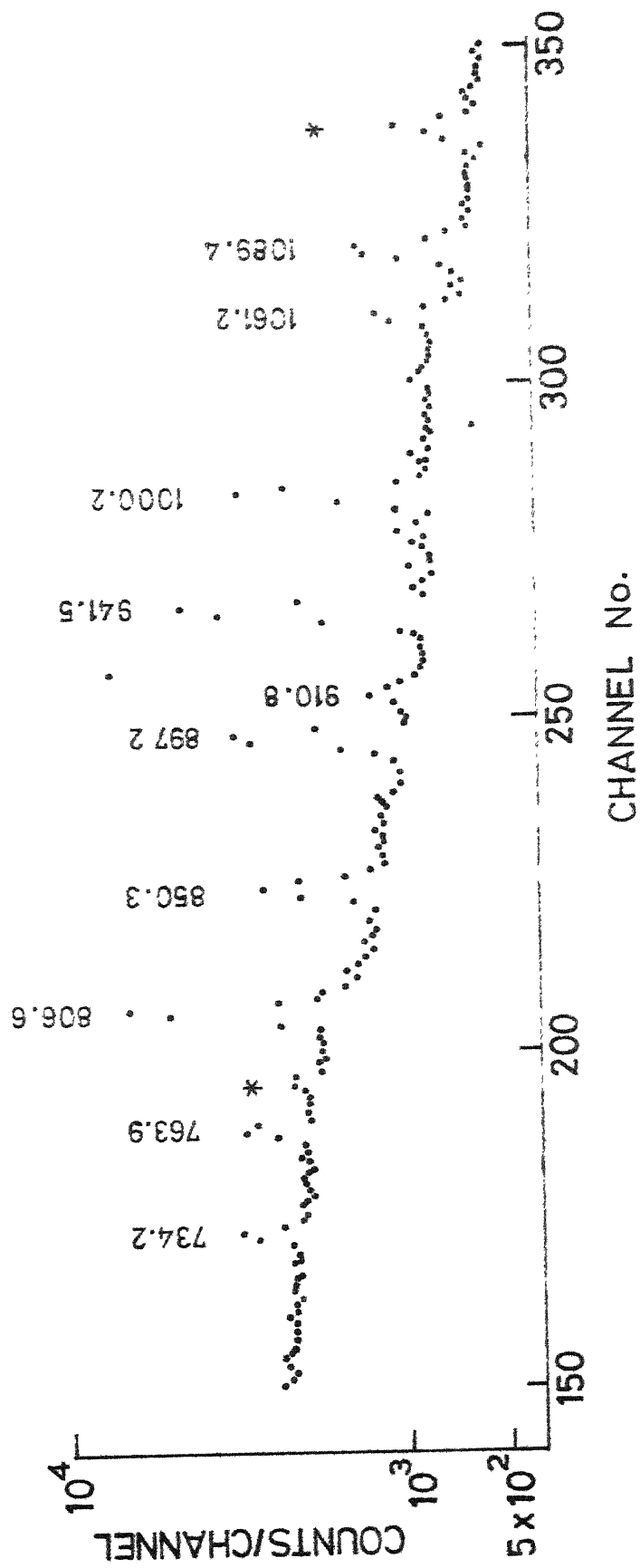


FIG. 6.2b Ge(Li) SPECTRUM OF  $^{99}\text{Rh}$  IN 700-1150 keV ENERGY RANGE



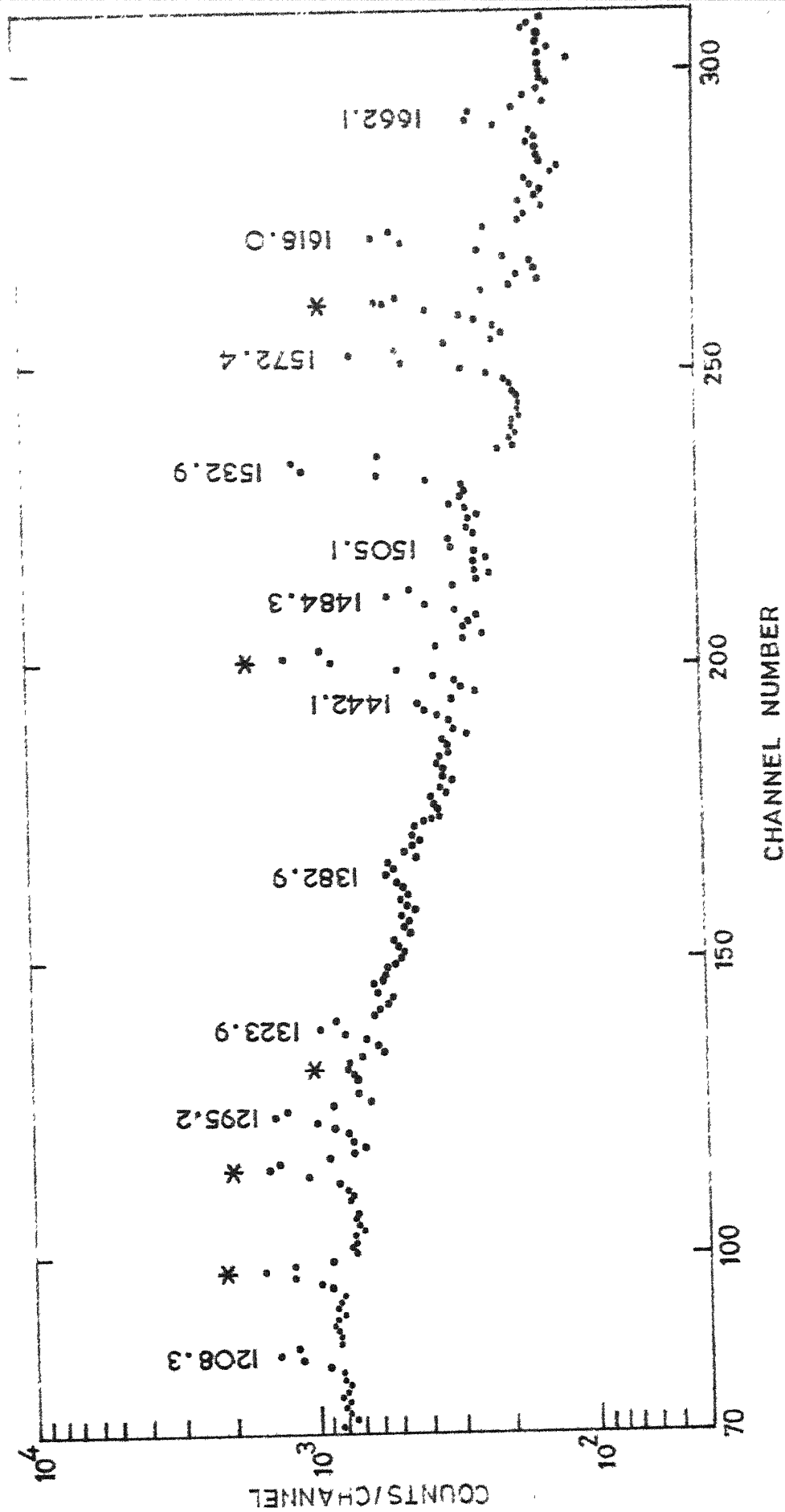


FIG. 6.3 Ge (Li) SPECTRUM OF  $^{99}\text{Rh}$  IN THE ENERGY RANGE OF 1150-1680 KeV

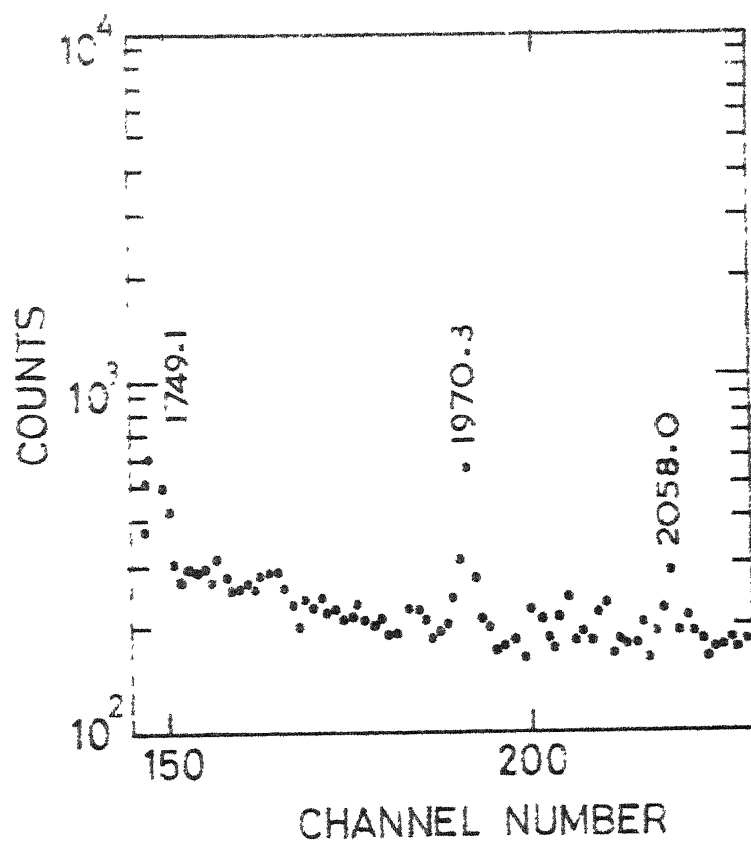


FIG. 6.4 Ge(Li) SPECTRUM OF  $^{99}\text{Rh}$  IN THE ENERGY RANGE 1740-2100 KeV

is found to decay with the half life of 16.1 days. The peak at 778.1 keV does not belong to the 16.1 day decay of  $^{99}\text{Rh}$ . Fig. 6.3 shows the gamma ray spectrum in the range 1200-1750 keV. The gamma ray spectrum in the energy range of above 1960 keV is shown in Fig. 6.4. The gamma rays observed in the singles spectra essentially confirm the results reported by Moss and McDaniels except for minor variations. The energies of the gamma rays observed by us in the 16.1 day decay of  $^{99}\text{Rh}$  are listed in Table 6.1. The energies of the gamma rays in our measurements from our energy calibration are very close to the values reported in ref. 4. We have, therefore, adopted their energy values except in the case of 1295 keV level in  $^{99}\text{Ru}$ . A few gamma ray lines not belonging to the 16.1 day activity of  $^{99}\text{Rh}$  are observed. In the plots, they are marked with asterisk. The origin of these gamma rays has not been explicitly determined.

The areas under the photopeaks of the gamma rays of  $^{99}\text{Ru}$  are determined after subtracting the contribution due to general background radiation. This data, along with the data of full energy peak efficiency of the detector, is used for the evaluation of the relative intensities, which are normalized to the intensity of the annihilation (511 keV) radiation assumed to be of intensity 100. The relative intensities are also listed

Table 6.1. Gamma Rays Observed in the Decay of 16.1 d  $^{99}\text{Rh}$  and Their Relative Intensities

Energy ( $E_\gamma$ ) (keV)	Relative $\gamma$ -ray intensities ( $I_\gamma$ )		
	Moss <u>et al.</u> <sup>4</sup>	Antoneva <u>et al.</u> <sup>5</sup>	Present
89.36	76	100 $\pm$ 10	56.3
119.4	0.13	< 2	-
175.2	5.8	4.5 $\pm$ 1.0	3.8
232.4	1.3	1.5 $\pm$ 0.5	0.72
295.7	2.1	3.5 $\pm$ 0.5	2.6
322.4	16.5	18 $\pm$ 2	9.1
353.0	81.3	100 $\pm$ 10	78.3
442.8	4.3	4.5 $\pm$ 0.5	5.4
486.5	1.5	1.5 $\pm$ 0.5	0.89
annihilation radiation			
527.7	100	100	100
575.2	0.6	0.8 $\pm$ 0.2	0.47
618.0	10.0	11 $\pm$ 1	11.9
734.2	0.8	0.9 $\pm$ 0.2	0.61
763.9	1.0	-	0.88
806.6	3.5	3.6 $\pm$ 0.5	3.5
850.3	0.6	$\leq$ 1	1.1
897.2	1.7	1.7 $\pm$ 0.3	2.1
910.8	-	-	0.13
941.5	3.8	3.3 $\pm$ 0.5	3.4

...Contd.

Table 6.1 (Contd..)

Energy ( $E_\gamma$ ) (keV)	Relative $\gamma$ -ray intensities ( $I_\gamma$ )		
	Moss <u>et al.</u> <sup>4</sup>	Antoneva <u>et al.</u> <sup>5</sup>	Present
1000.2	1.7	$2.0 \pm 0.2$	2.0
1061.2	0.4	$0.6 \pm 0.2$	0.55
1089.4	0.8	$\leq 1$	1.0
1208.3	0.4	$\leq 0.8$	0.66
1295.2	0.9	$1.0 \pm 0.3$	0.72
1323.9	0.4	$\leq 0.5$	0.66
1382.9	0.4	$\leq 0.4$	0.29
1442.1	0.2	$< 0.4$	0.34
1484.3	0.4	$< 0.4$	0.14
1505.1	0.2	$< 0.4$	0.1
1532.9	1.4	$1.9 \pm 0.4$	1.3
1572.4	0.58	$0.7 \pm 0.2$	1.3
1618.0	0.6	$\leq 0.6$	0.9
1662.1	0.15	$< 0.4$	0.23
1749.1	0.15	$< 0.4$	0.6
1970.3	0.4	$\leq 0.4$	0.21
2058.6	0.08	-	0.43

in Table 6.1. The values reported by Moss and McDaniels and that of Antoneva et al. are also included for comparison.

### VI.3 Sum-Coincidence Spectra

The sum-coincidence spectra are measured with the energy gate settings at 575, 618, 734, 850, 897, 941, 1000 and 1295 keV. The spectra, thus recorded, at the different gate settings are shown in Figs. 6.5 to 6.10. In all the spectra intense peaks are observed at 511 keV at the corresponding energy to make up the sum gate. These are due to coincidence between the annihilation quantum and the compton of a gamma ray making up the sum gate. These peaks are duly noted and discarded in the analysis. The results of the measurements are summarized in Table 6.2 and are described below.

- (a) 575 keV gate : The spectrum with gate at 575 keV is shown in Fig. 6.5. This provides evidence for the existence of  $486 \rightarrow 89$  cascade from the level at 575 keV as  $575 \rightarrow 89 \rightarrow 0$  mode of decay.
- (b) 618 keV gate : Figure 6.6 shows the spectrum obtained with the energy gate. Evidence for the existence of  $618 \rightarrow 89 \rightarrow 0$  and  $618 \rightarrow 443 \rightarrow 0$  keV cascades is clearly seen. The observed peak at 305 keV is found to be of half width larger than that expected for a monoenergetic gamma ray of that energy. This broad peak probably comes from the existence of two gamma rays

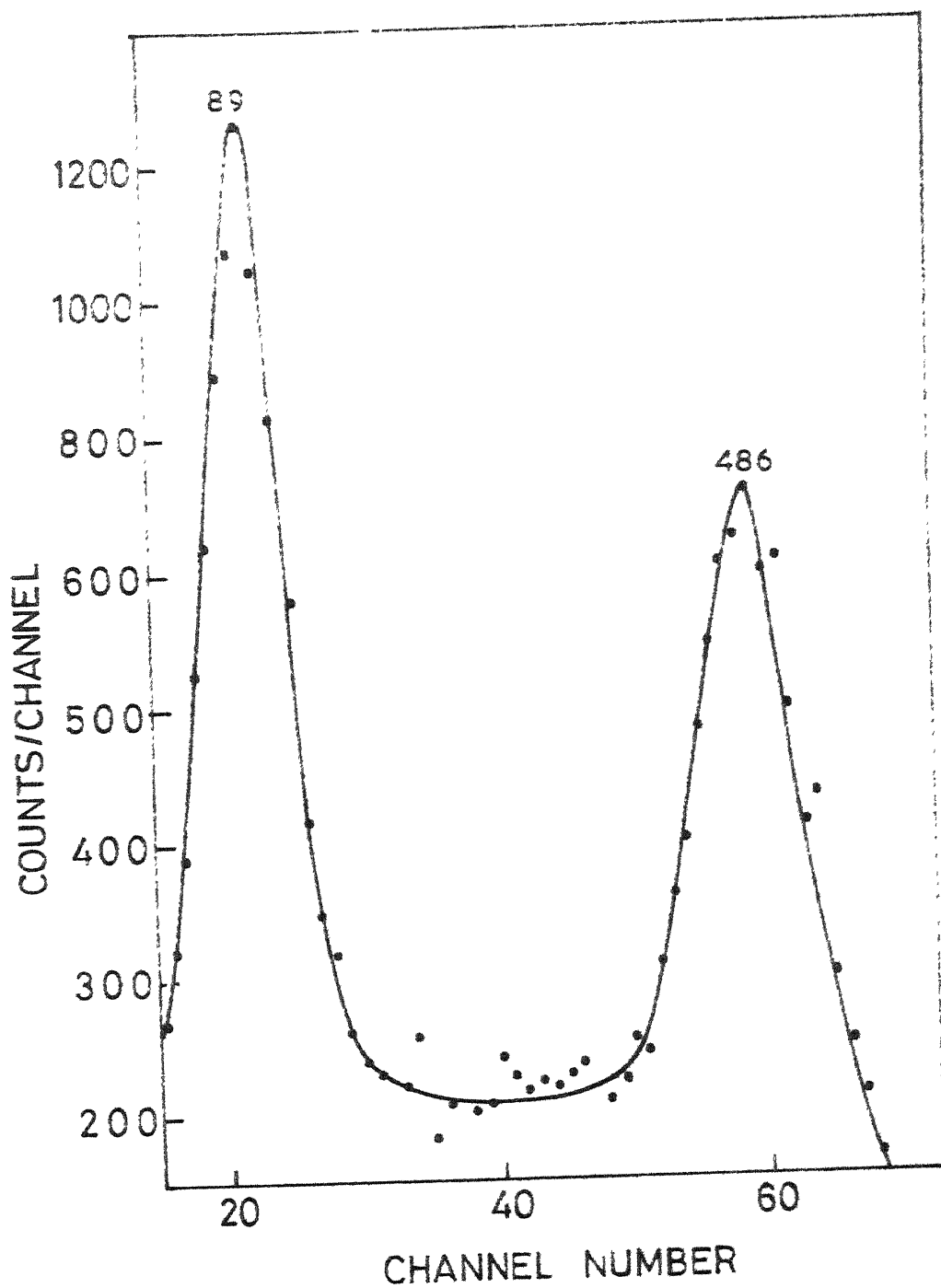


FIG. 6.5 SUM-COINCIDENCE SPECTRUM OF  $^{99}\text{Rh}$  WITH GATE AT 575 KeV

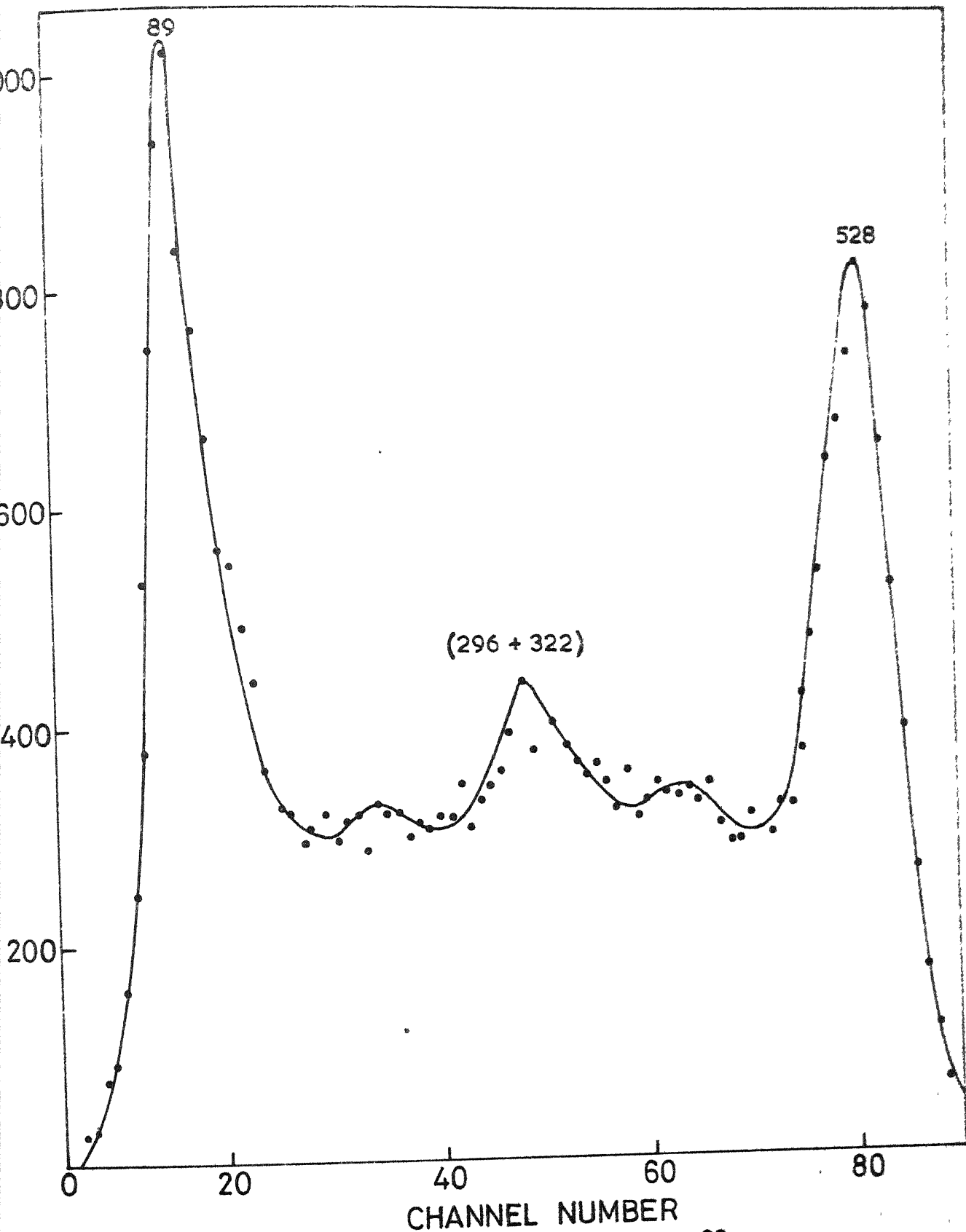


FIG. 6.6 SUM-COINCIDENCE SPECTRUM OF  $^{99}\text{Rh}$  WITH GATE AT 618 KeV



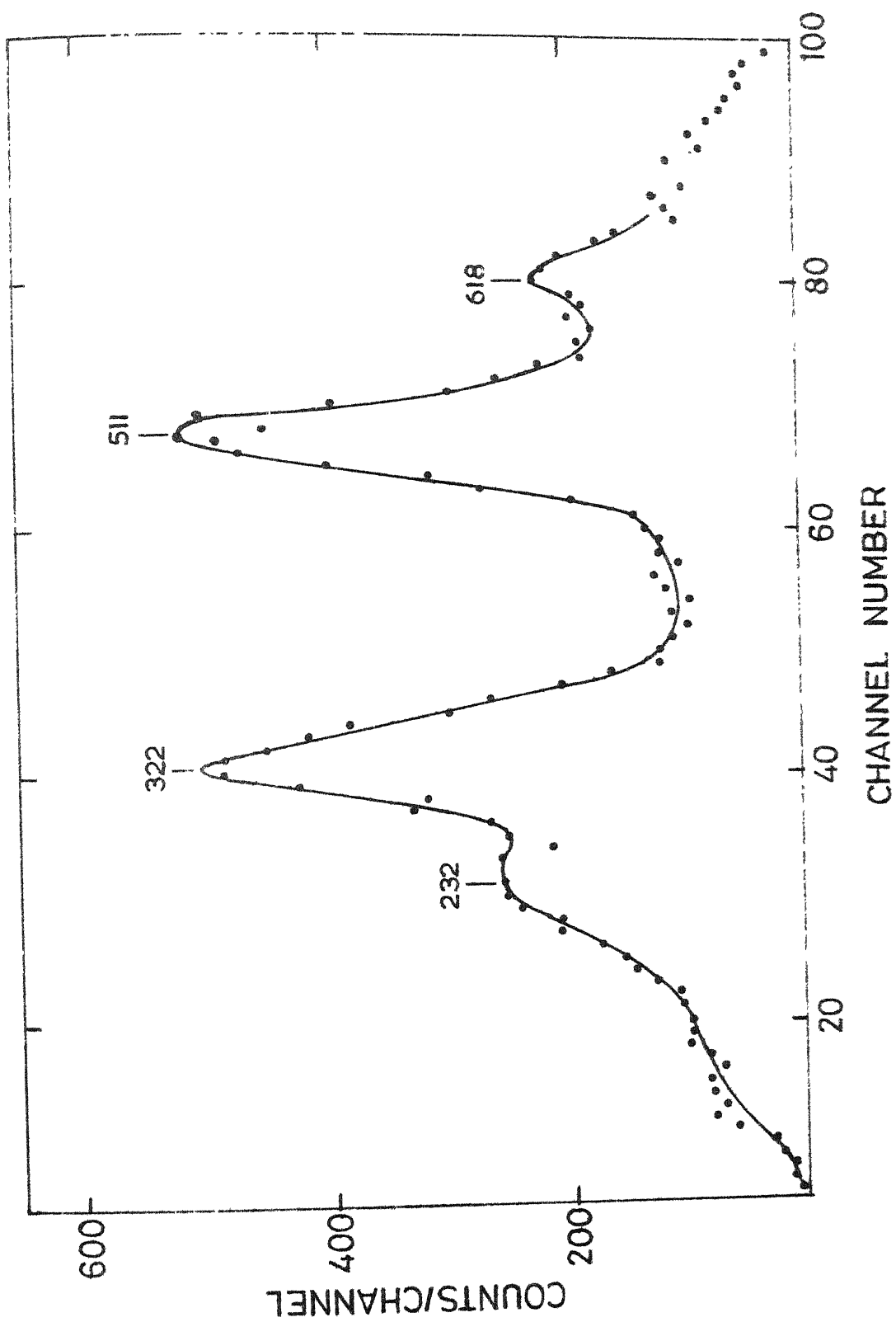


FIG. 6.7 SUM-COINCIDENCE SPECTRUM OF  $^{99}\text{Rh}$  WITH GATE AT 850 KeV

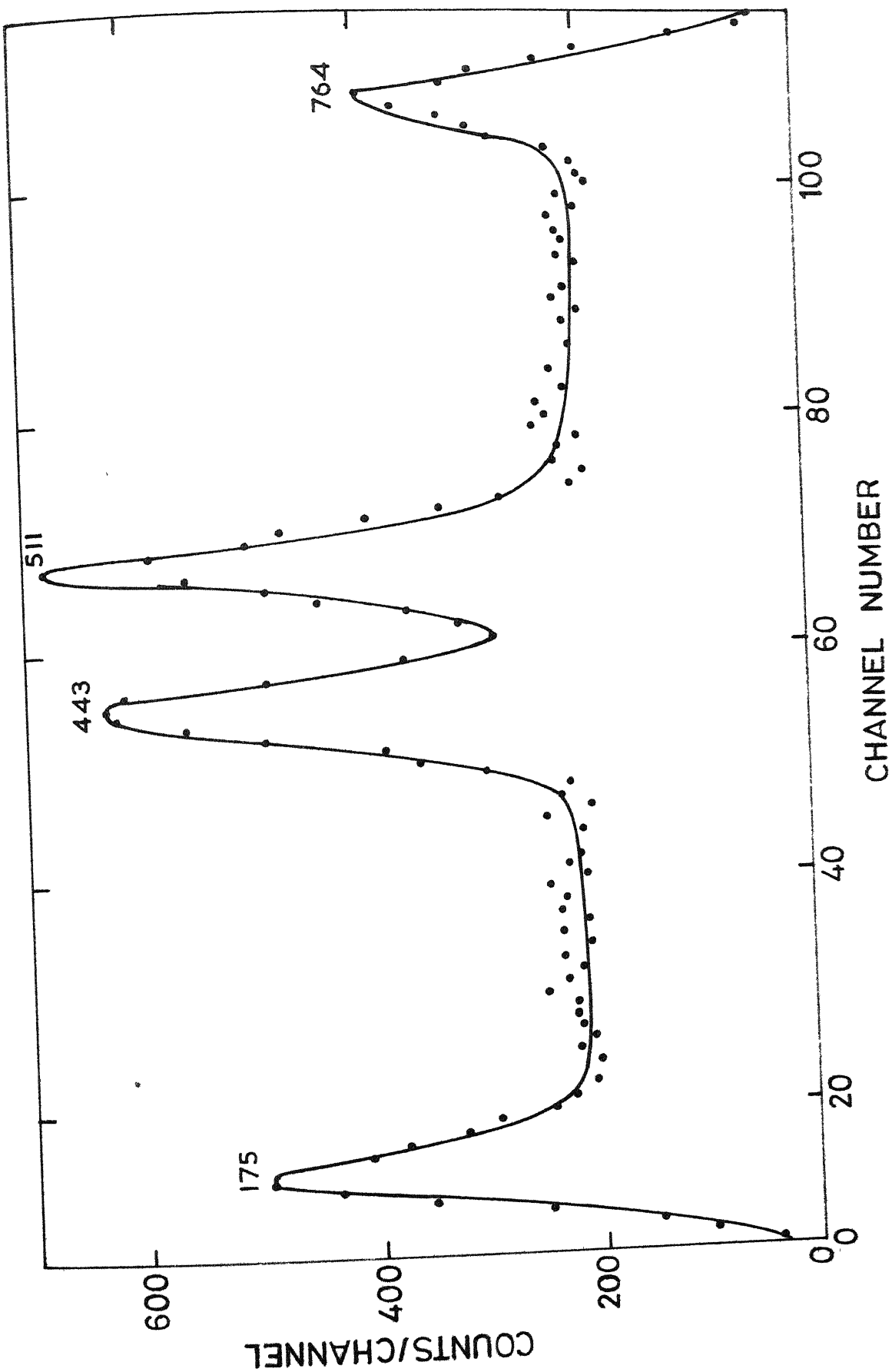


FIG. 6.8 SUM-COINCIDENCE SPECTRUM OF  $^{99}\text{Rh}$  WITH GATE AT 941 KeV

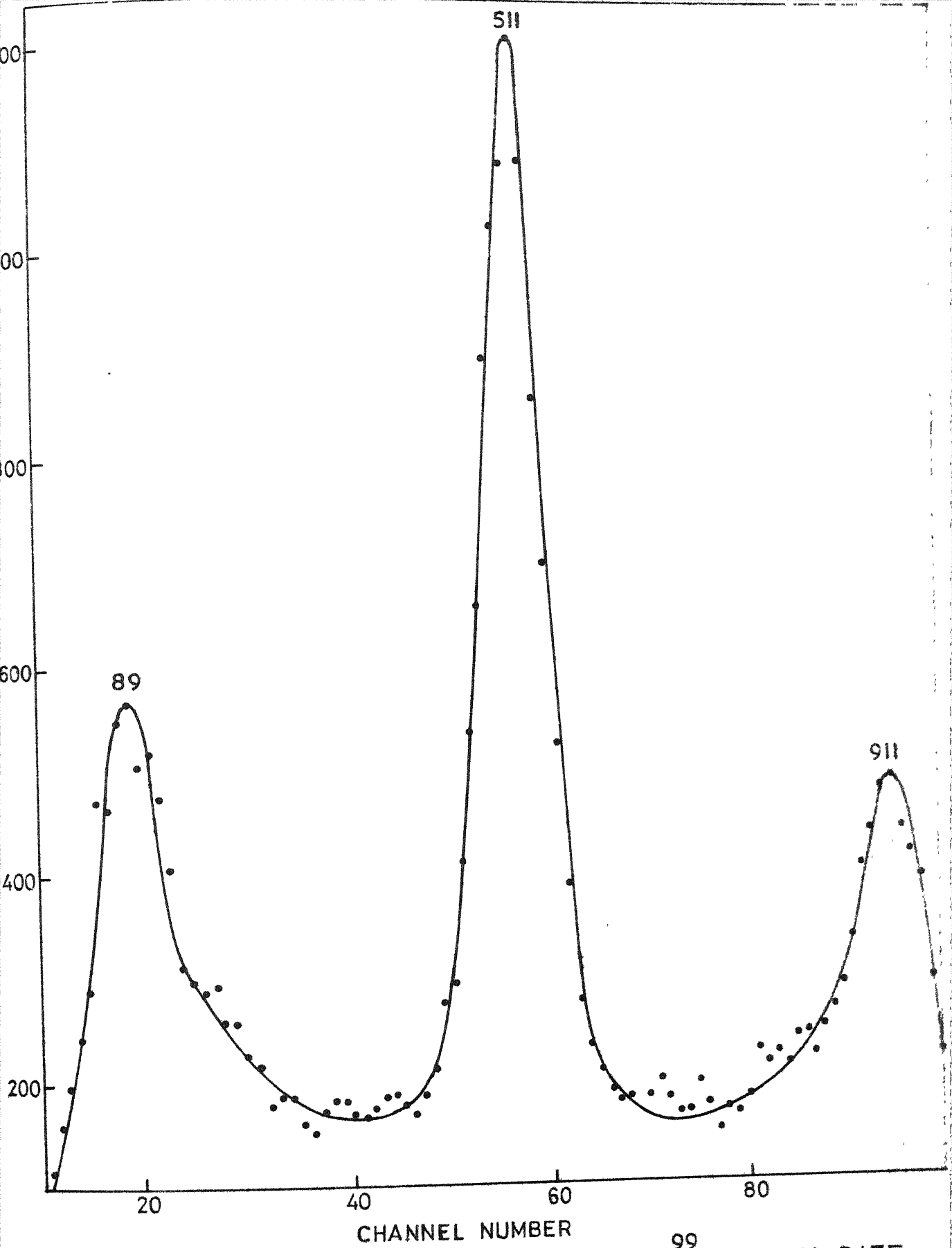


FIG.6.9 SUM-COINCIDENCE SPECTRUM OF  $^{99}\text{Rh}$  WITH GATE AT 1000 KeV

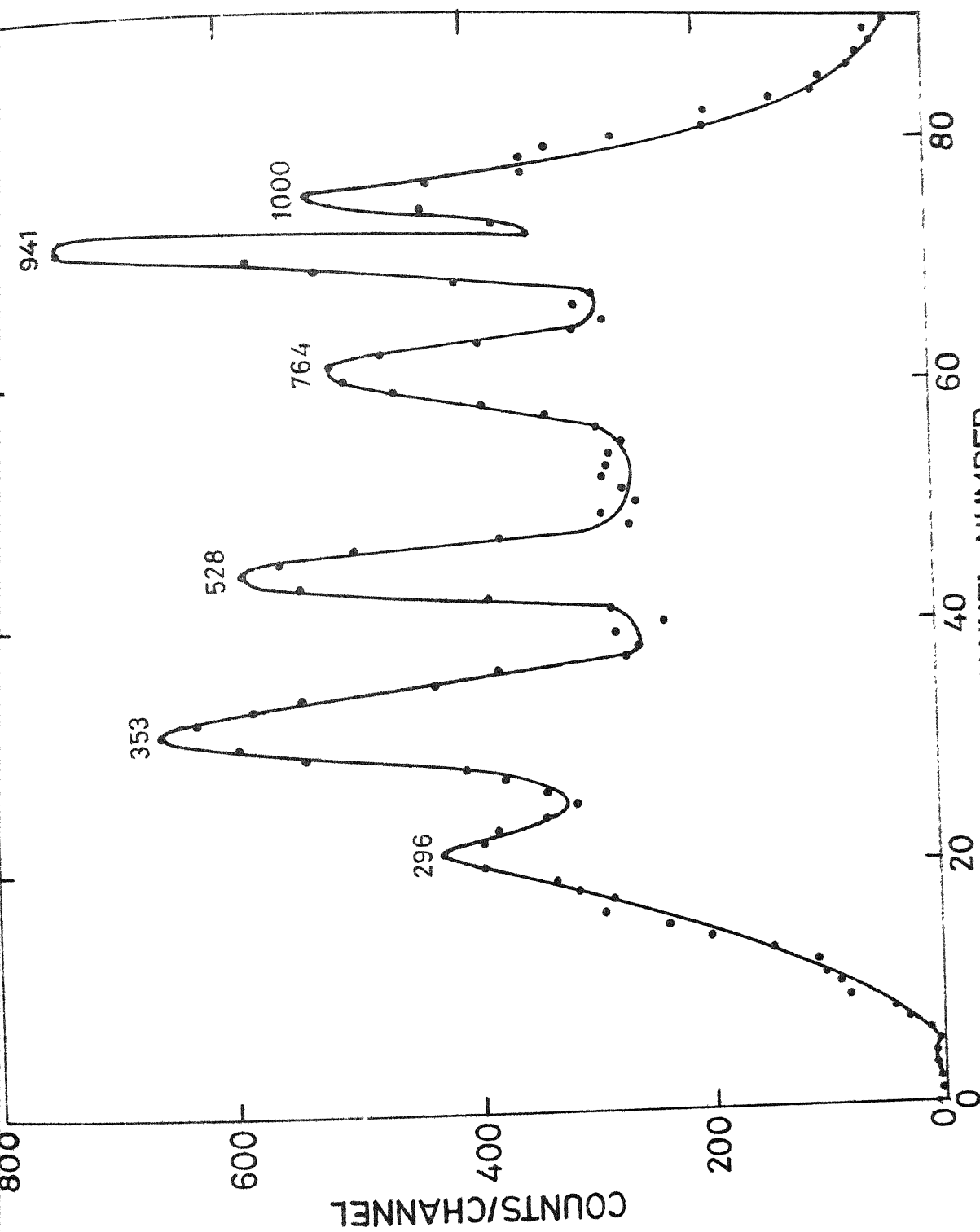


FIG. 6.10 SUM-COINCIDENCE SPECTRUM OF  $^{99}\text{Rh}$  WITH GATE  
AT 1295 KeV

Table 6.2. Summary of the NaI(Tl)-NaI(Tl) sum-coincidence measurements

Sum-coincidence gate energy (keV)		$\gamma$ - $\gamma$ cascades observed			
575		575 $\xrightarrow{486}$	89 $\xrightarrow{89}$	0	
618	(a)	618 $\xrightarrow{528}$	89 $\xrightarrow{89}$	0	
	(b)	618 $\xrightarrow{296}$	322 $\xrightarrow{322}$	0	
	(c)	618 $\xrightarrow{175}$	443 $\xrightarrow{443}$	0	
734		734 $\xrightarrow{734}$	0		
850	(a)	850 $\xrightarrow{232}$	618 $\xrightarrow{618}$	0	
	(b)	850 $\xrightarrow{850}$	0		
897		897 $\xrightarrow{808}$	89 $\xrightarrow{89}$	0	
941		941 $\xrightarrow{763}$	175		
1000		1000 $\xrightarrow{911}$	89 $\xrightarrow{89}$	0	
1295	(a)	1295 $\xrightarrow{295}$	1000 $\xrightarrow{1000}$	0	
	(b)	1383 $\xrightarrow{940}$	443 $\xrightarrow{344}$	89	
	(c)	1383 $\xrightarrow{765}$	618 $\xrightarrow{528}$	89	

with energies 296 and 322 keV as due to the  $618 \rightarrow 322 \rightarrow 0$  cascade mode of decay. Thus, this spectrum clearly shows that 618 keV level has branchings to 89, 322 and 443 keV levels.

- (c) 734 keV gate : The spectrum at this gate setting shows that there is only a crossover transition for this level with no cascade mode of decay.
- (d) 850 keV gate : The spectrum at this gate setting is shown in Fig. 6.7. The spectrum gives a clear indication for the existence of a 232 and 618 keV pair of coincident gamma rays. This is noted as  $850 \rightarrow 618 \rightarrow 0$  cascade mode of decay. The 232 keV gamma ray is explained by Moss and McDaniels as a transition between 322 and 89 keV levels, whereas the present results show that it is resulting from the branching of 850 keV level to the 618 keV level.
- (e) 897 keV gate : The spectrum recorded with this gate setting gives a clear indication of 808-89 keV gamma pair, which is accounted for as  $897 \rightarrow 89 \rightarrow 0$  keV transition mode.
- (f) 941 keV gate : Figure 6.8 shows the spectrum recorded with this gate setting. There is a clear evidence for a cascade of 763 and 175 keV gamma pair, which can be included as due to  $1383 \rightarrow 618 \rightarrow 443$  modes of decay. This further confirms the  $618 \rightarrow 443$  keV

transition as observed in the spectrum gated at 618 keV. This spectrum shows the presence of a new transition between 1383 and 618 keV levels.

- (g) 1000 keV gate : The spectrum with the energy gate at 1000 keV is shown in Fig. 6.9. Besides, the peaks due to the coincidences of annihilation radiation, a coincident gamma ray pair of 89 and 911 keV is observed. This is fitted as due to  $1000 \rightarrow 89 \rightarrow 0$  transition. This cascade pair is not reported by earlier workers.
- (h) 1295 keV gate : Figure 6.10 shows the spectrum recorded with gate at 1295 keV. Three gamma pairs are observed. They are fitted as due to the following transitions.

295 and 1000 keV       $1295 \rightarrow 1000 \rightarrow 0$

941 and 353 keV       $1383 \rightarrow 443 \rightarrow 89$

765 and 528 keV       $1383 \rightarrow 618 \rightarrow 89$

This spectrum provides further confirmation of the  $1383 \rightarrow 618$  keV transition observed in the spectrum with gate at 941 keV. Another new cascade mode observed here is the  $1295 \rightarrow 1000 \rightarrow 0$  transition.

#### VI.4 Summary

The results of the present investigation agree reasonably well with the results of Moss and McDaniels except for the following findings:

- (i) There is no evidence for the presence of a 119.4 keV gamma ray. The fact that an intense 119.4 keV gamma ray is observed in the spectrum of chemically separated impurity, leads to the conclusion that the 119.4 keV gamma ray does not belong to the 16.1 day decay of  $^{99}\text{Rh}$ .
- (ii) The 232 keV gamma ray was reported to be due to a transition between 322 and 89 keV levels.<sup>4</sup> But the sum coincidence results with energy gate at 850 keV demonstrate that it is due to a transition between 850 and 618 keV levels.
- (iii) Moss and McDaniels suggested that the 764 keV gamma ray arises due to a transition between 1662 and 897 keV levels. The present investigation indicates that it arises from the transition between 1383 and 618 keV levels. Our results, however, do not rule out the possibility that 765 keV gamma ray might also arise as the transition between 1662 and 897 keV levels.
- (iv) The sum-coincidence spectrum with gate at 1000 keV gives evidence for a new transition of 911 keV energy. The transition is probably between 1000 and 89 keV levels. A gamma ray of 910.8 keV energy is also observed in the Ge(Li) spectrum.



- (v) The sum-coincidence spectrum with gate at 1295 keV provides evidence for a new gamma ray of 295 keV energy as a transition between 1295 and 1000 keV energy levels.

From the intensity balance consideration of the gamma rays, the percentage population of the different levels in the  $\beta^+$ , EC decay is calculated and log ft values for each  $\beta^+$ , EC transition is deduced using the available nomograms.<sup>11</sup> Except for that of the transition to 2058 keV level, the log ft values for the transitions to the other levels are consistent for the transitions to be first forbidden. So it is most likely that all the levels except the 2058 keV level, populated in the decay are of even parity and of spin assignments  $\frac{1}{2}$ ,  $\frac{3}{2}$  and  $\frac{5}{2}$  since the ground state of  $^{99}\text{Rh}$  is of  $J^\pi = \frac{1}{2}^-$ . It is also likely that 2058 keV level is of  $J^\pi = \frac{1}{2}^-$  or  $\frac{3}{2}^-$ . These conclusions are in agreement with the observations of Antoneva et al. The level scheme indicating the gamma cascades of the various levels in  $^{99}\text{Ru}$ , along with the log ft values, is shown in Fig. 6.11.

#### VI.5 Comments on the Level Structure of $^{99}\text{Ru}$

Nuclei with partially filled  $g_{9/2}$  proton shell configuration are of much theoretical interest, due to their complicated level structure. For nuclei, with a few protons in  $g_{9/2}$  shell, the few particle excitations

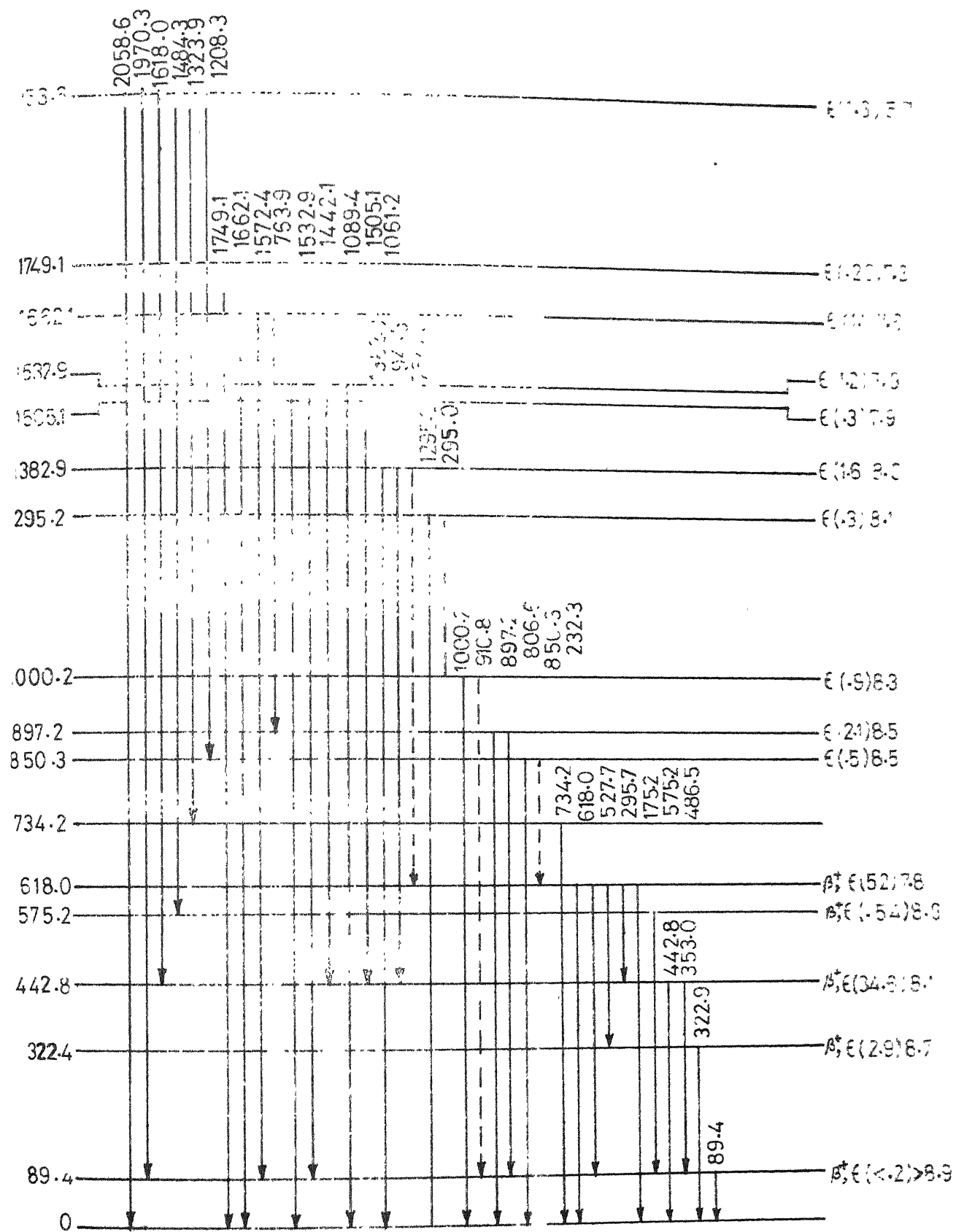


FIG. 6.11 GAMMA DECAY SCHEME OF  $^{99}\text{Rh}$  (16.1 DAYS)  
AND LEVELS OF  $^{99}\text{Ru}$

treating Zr [ $Z=40$ ,  $38 \pi (p_{\frac{1}{2}})^2$ ] as the core, have been attempted. But as the proton number increases, these calculations become unmanageable. For such nuclei, one has to verify whether the few particle interaction models are still valid. However, such detailed calculations are not available for  $^{99}\text{Ru}$ . Kistner et al.<sup>10</sup> performed the coulomb excitation experiments and attempted to compare their results with the core-excitation model. Moss and McDaniels attempted to explain the structure by three different nuclear models and they felt that the core-excitation model is the most plausible one. But this model could not explain the observed magnetic moments. Besides, Antoneva et al. discussed the structure of individual levels separately and concluded that core-excitation model may not be applicable here and according to them it can only be said that these levels exhibit many particle nature. Recently, Lederer et al.<sup>6</sup> have measured the properties of odd and even Ru isotopes and discussed the structure of these nuclei to some extent. We make an attempt to present a qualitative discussion of the structure of  $^{99}\text{Ru}$  levels, with the help of experimental data available for Mo and Ru nuclei. It is hoped that such comments may prove helpful for further quantitative calculations.

It is interesting to study the systematics of level schemes as we proceed from Mo to Ru isotopes and also for different odd A isotopes in ruthenium, in order to get some insight into the nuclear structure of  $^{99}\text{Ru}$ . In this study of systematics, we observe that even parity states exhibit a different nature, when compared to the systematics of odd parity states. So we discuss them separately. The energy level spectra for even and odd parity states of odd A, Mo and Ru isotopes are shown in Figs. 6.12 and 6.13. The level structure are taken from Lederer et al., Antoneva et al.<sup>7</sup>, Dzhelepov et al.<sup>8</sup> and Table of isotopes compiled by Lederer et al.<sup>9</sup>

(i) Even parity states : As can be seen from the energy level spectra of  $^{97}\text{Ru}$ ,  $^{99}\text{Ru}$  and  $^{101}\text{Ru}$ , the positions of even parity states are not much affected by the addition or removal of even number of neutrons. But, the comparison with the corresponding levels in molybdenum isotopes shows that the levels in ruthenium isotopes are much lower in energy. It, thus, appears that these levels might be mainly of proton seniority number 2 and neutron seniority 1. In other words, these are the many particle configuration states with  $(\pi g_{9/2})^2_{2^+, 4^+, 6^+, 8^+}$  coupling to a neutron of  $(d_{5/2})^1_{5/2}$  with seniority 1.

Moss and McDaniels suggested that the first excited state in  $^{99}\text{Ru}$  is a member of the quintet of one phonon in

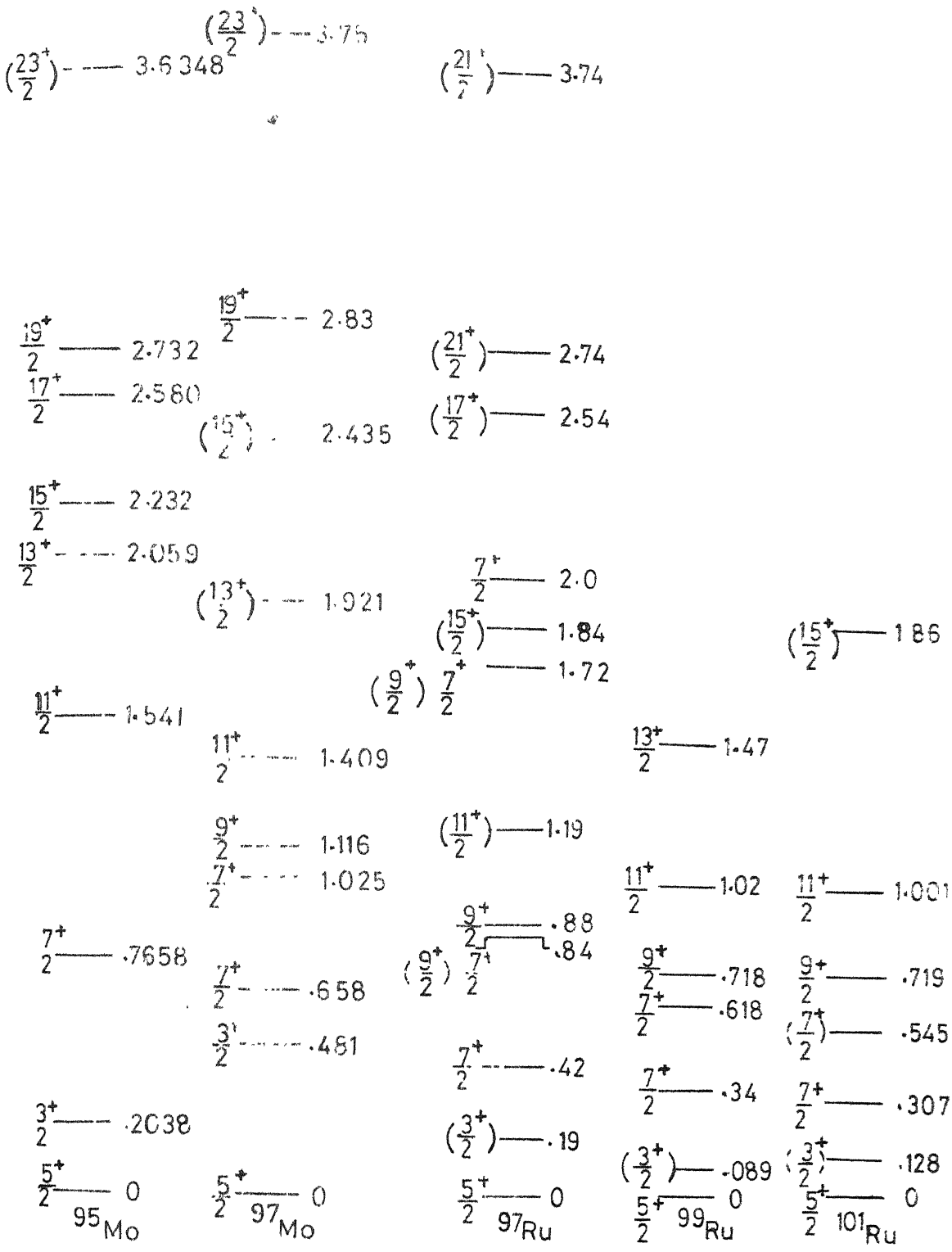


FIG. 6.12 SYSTEMATICS OF EVEN PARITY STATES OF ODD A Mo AND Ru ISOTOPES.

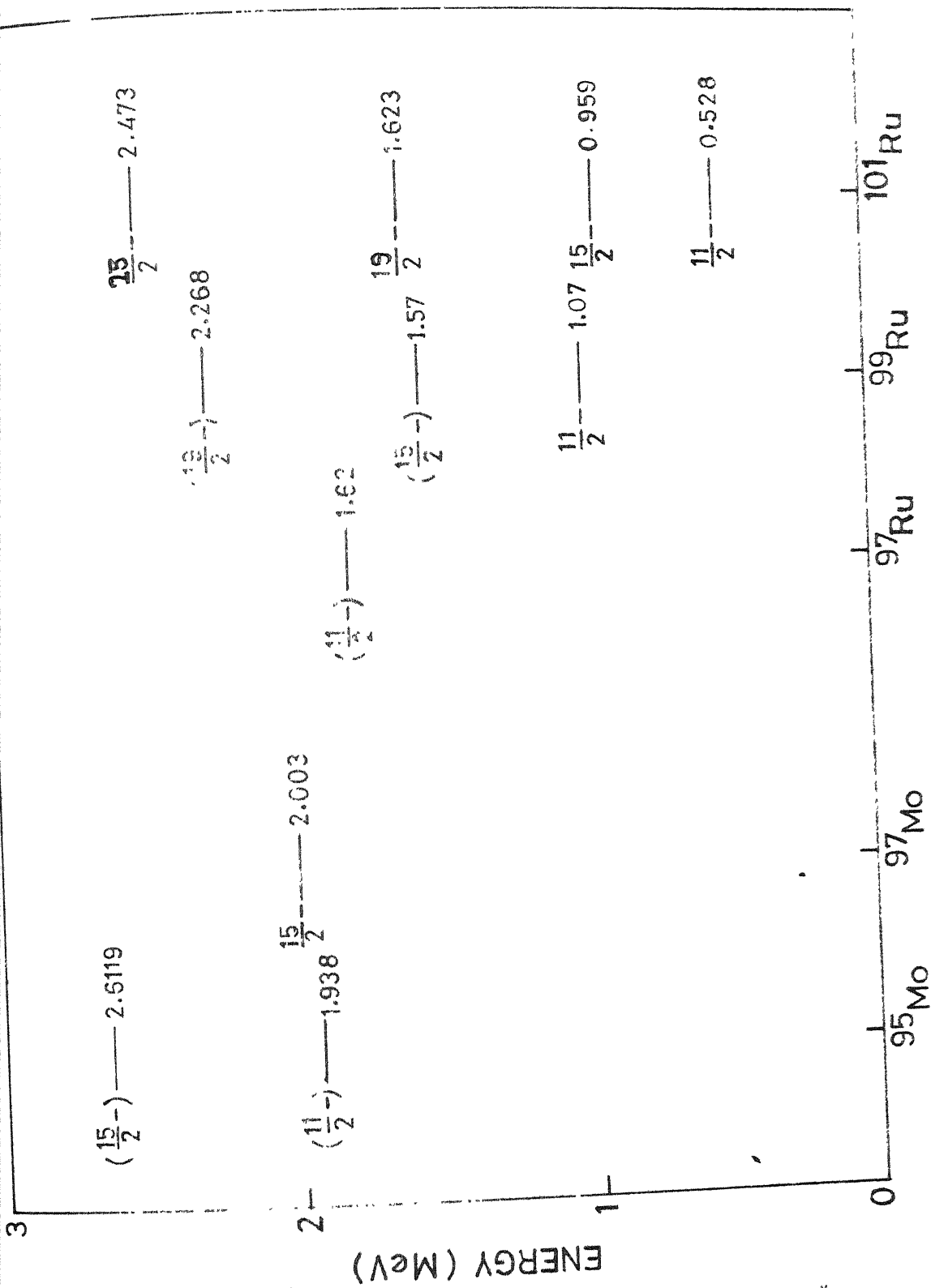


FIG. 6.13 SYSTEMATICS OF ODD PARITY STATES OF ODD A MO AND RU

$^{98}\text{Ru}$  coupled to the  $(d_{5/2})_{5/2}^1$  neutron. But this could not satisfactorily explain the observed magnetic moment of the state. It seems that the only plausible comment one can make is that the first excited state of many particle configuration.

Antoñeva et al. considered the 340 keV level  $(7/2^+)$  to be of single particle nature. It is very doubtful if this could be a single particle state. The gradual change of the position of the lowest  $7/2^+$  states in Mo and Ru isotopes --- suggests that these are of many particle nature. The relatively large change in the position with the change of proton number by two, when compared to the change as the neutron number is altered, is also in favour of the above arguments. However, the admixture of different configurations cannot be ruled out.

(ii) Odd-parity states : Unlike the even parity states, the odd parity states are much affected in their position with the change of neutron number. From the energy spectra of Mo and Ru isotopes, it can be seen that for neutron rich isotopes the odd parity states with high spin values lie at low energies. It is also observed that the positions are not much affected with the change of proton number. The systematic change with the increase of the number of neutrons is consistent with the explanation of quasi-particle excitations suggested by Lederer et al.

According to Lederer et al. these odd parity high spin states arise due to the coupling of the odd neutron in  $h_{11/2}$  state with the core of  $0^+$ ,  $2^+$ ,  $4^+$  and  $6^+$  to give the spins of  $11/2^-$ ,  $15/2^-$ ,  $19/2^-$  and  $23/2^-$ . The energy-wise lowering down of these states, as the neutron number is increased, is understandable within the framework of quasiparticle excitations.

To summarise, it appears that the levels of  $^{99}\text{Ru}$  exhibit complicated structure, so that a few nuclear interaction models may not satisfactorily explain them. The structure suggests that the even parity states are due to proton excitations and neutron excitations affect the odd parity states. It means that the possible neutron excitations in g, s, d shells have very little effect on the even parity states and no proton holes in f-p shell result in the odd parity states.



REFERENCES

1. J.B. Kurbatov, C.W. Townley, B. Feilgley and M.H. Kurbatov, Bull. Amer. Phys. Soc. 5 (1960) 240.
2. S. Jha, S. Johnston and T.D. Nainan, Bull. Amer. Phys. Soc. 8 (1963) 524.
3. P.I. Connors, Thesis, Pennsylvania State Univ. (USA) 1966.
4. G.A. Moss and D.K. McDaniéls, Phys. Rev. 162 (1967) 1087.
5. N.M. Antoneva, E.P. Grigoreva and L.F. Protasova, Bull. Acad. Sci. USSR (Phys. Ser.) 34 (1971) 771.
6. C.M. Lederer, J.M. Jaklevic and J.M. Hollander, Nucl. Phys. A169 (1971) 489.
7. N.M. Antoneva, E.P. Grigoreva, G.S. Katykhin, L.F. Protasova, E.J. Ryndina and V.G. Tishin, Bull. Acad. Sci. USSR (Phys. Ser.) 33 (1970) 1209.
8. B.S. Zhelepov, N.M. Antoneva, M.K. Nikitin and V.B. Smirnov, Sov. Phys. Doklady, 10 (1965) 20.
9. Table of Isotopes (6th Edition, 1967; John Wiley Publications), Compiled by C.M. Lederer, J.M. Hollander and I. Perlman.
10. O.C. Kistner and A. Schwarzschild, Phys. Rev. 154 (1967) 1182.
11. Nuclear Spectroscopy Tables (1959, North Holland Publ. Co.) Compiled by A.H. Wapstra, G.J. Nijgh and P. Van Lieshort.

CHAPTER VII  
DECAY OF  $^{63}\text{Zn}$

VII.1 Introduction

The 38.4 min decay of  $^{63}\text{Zn}$  has been the subject of several investigations. Two recent investigations<sup>1,2</sup> have indicated the presence of several new gamma transitions. However, the results of these measurements are not in agreement. Thus, at present, there is no unambiguous decay scheme available for this isotope. We attempted to identify all the gamma rays with a Ge(Li) detector and to confirm that they are emanated from  $^{63}\text{Zn}$  decay by examining their half lives. Fast-slow coincidence measurements were also done.

VII.2 Details of Measurements

The activity of  $^{63}\text{Zn}$  was produced by  $^{64}\text{Zn}(n,2n)^{63}\text{Zn}$  reaction using the 2 MV Van de Graaff accelerator as the neutron generator. The 14 MeV neutrons, required for the experiment, were produced by  $^3\text{H}(d,n)^4\text{He}$  reaction. A natural zinc target (>99% purity) was employed. The gamma ray spectra were measured with the Ge(Li) detector, described earlier, in expanded energy scales to achieve precise energy assignments. The half life of each gamma ray was determined to make sure that the decay rate is 38.4 minutes. Some long lived gamma components were also

observed and they were taken into account during analysis.

The measurements of coincidence spectra were carried out with the Ge(Li)-NaI(Tl) fast-slow assembly. The spectra were recorded with gates at 511, 670 and 962 keV energy.

### VII.3 Results

The Ge(Li) spectra are shown in Figs. 7.1-7.6. The spectra shows are the superpositions of measurements from several bombardments. The energies of gamma rays are listed in Table 7.1. The results of earlier workers are also shown for comparison. We do not get any evidence for the existence of gamma rays of 684, 923.5, 1087, 1150, 1168, 1189 and 2048.6 keV energies reported by Borchert<sup>1</sup>. We also did not observe the 1573.3, 2082.1 and 3101 keV gamma rays reported by Kiuru and Holmberg<sup>2</sup> and also by Borchert. Also, the 1340.0 keV gamma ray observed by Kiuru and Holmberg was not observed in the present study. However, the 2103 keV gamma ray, reported by Borchert, but not observed by Kiuru and Holmberg was observed in our measurements and additional new gamma rays of 1716 and 1734 keV energies were also observed. As shown in Fig. 7.7, all these gamma rays exhibit the 38.4 minute half life, thus showing that they belong to the  $^{63}\text{Zn}$  decay. Instead of a 2780 keV gamma ray, reported by the earlier workers, a gamma ray of 2773 keV was observed, requiring the level populated to be of 2773 keV energy. Fast-slow coincidence

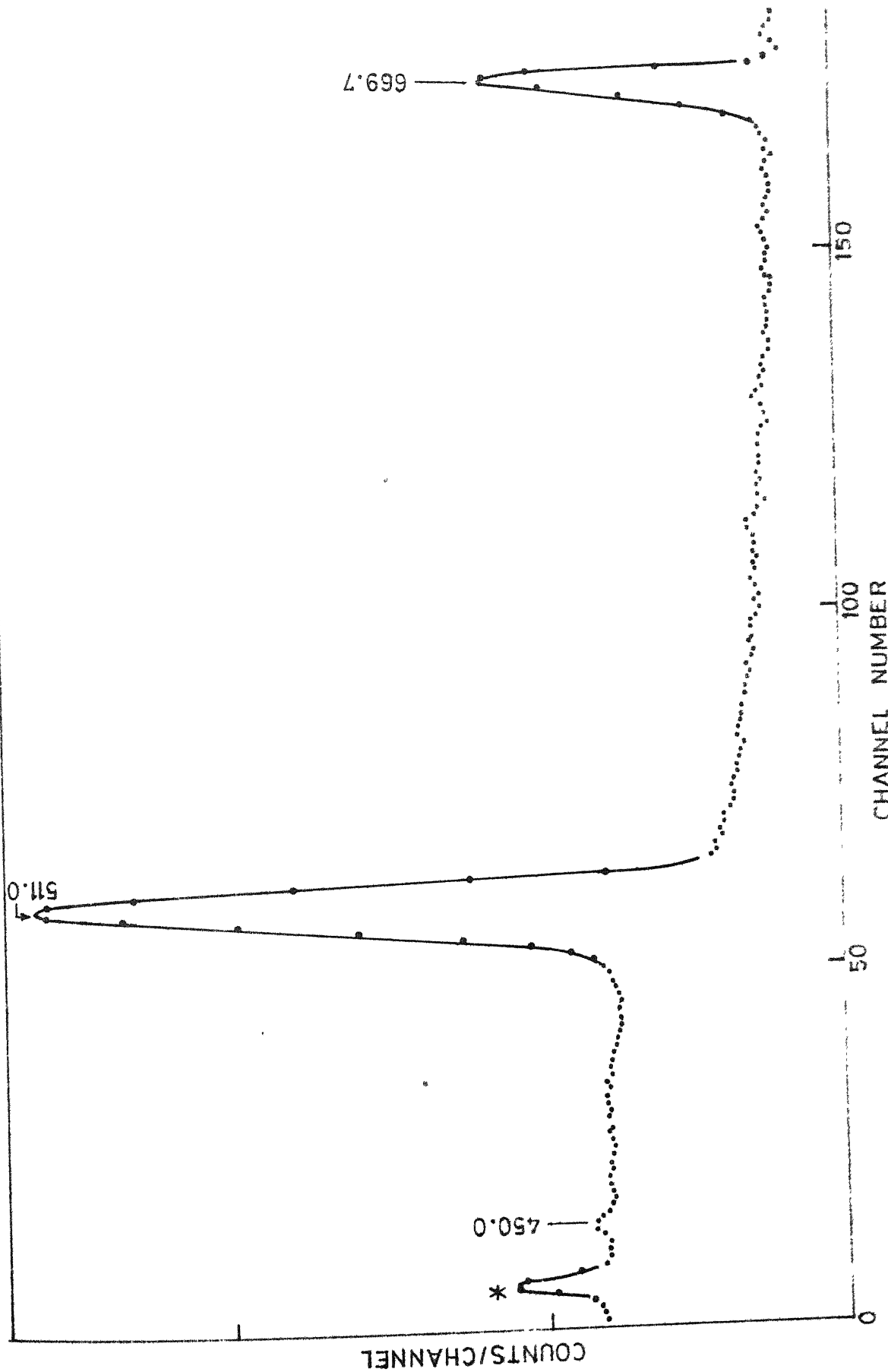


FIG. 7.1 Ge(Li) SPECTRUM OF  $^{63}\text{Zn}$  IN THE ENERGY REGION 400-700 keV

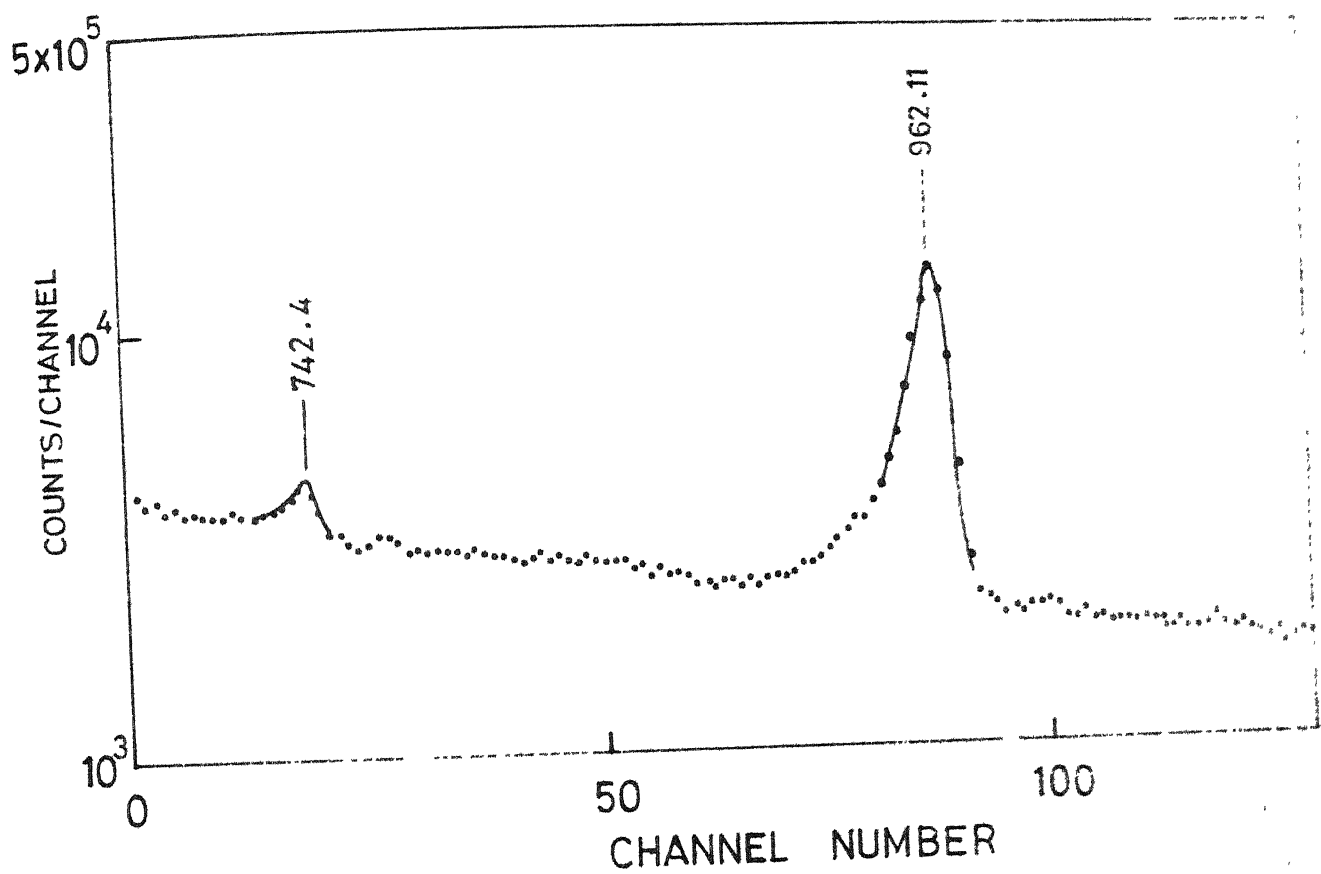


FIG.7.2 Ge(Li) SPECTRUM OF  $^{63}\text{Zn}$  IN THE ENERGY REGION 700 - 1050 KeV

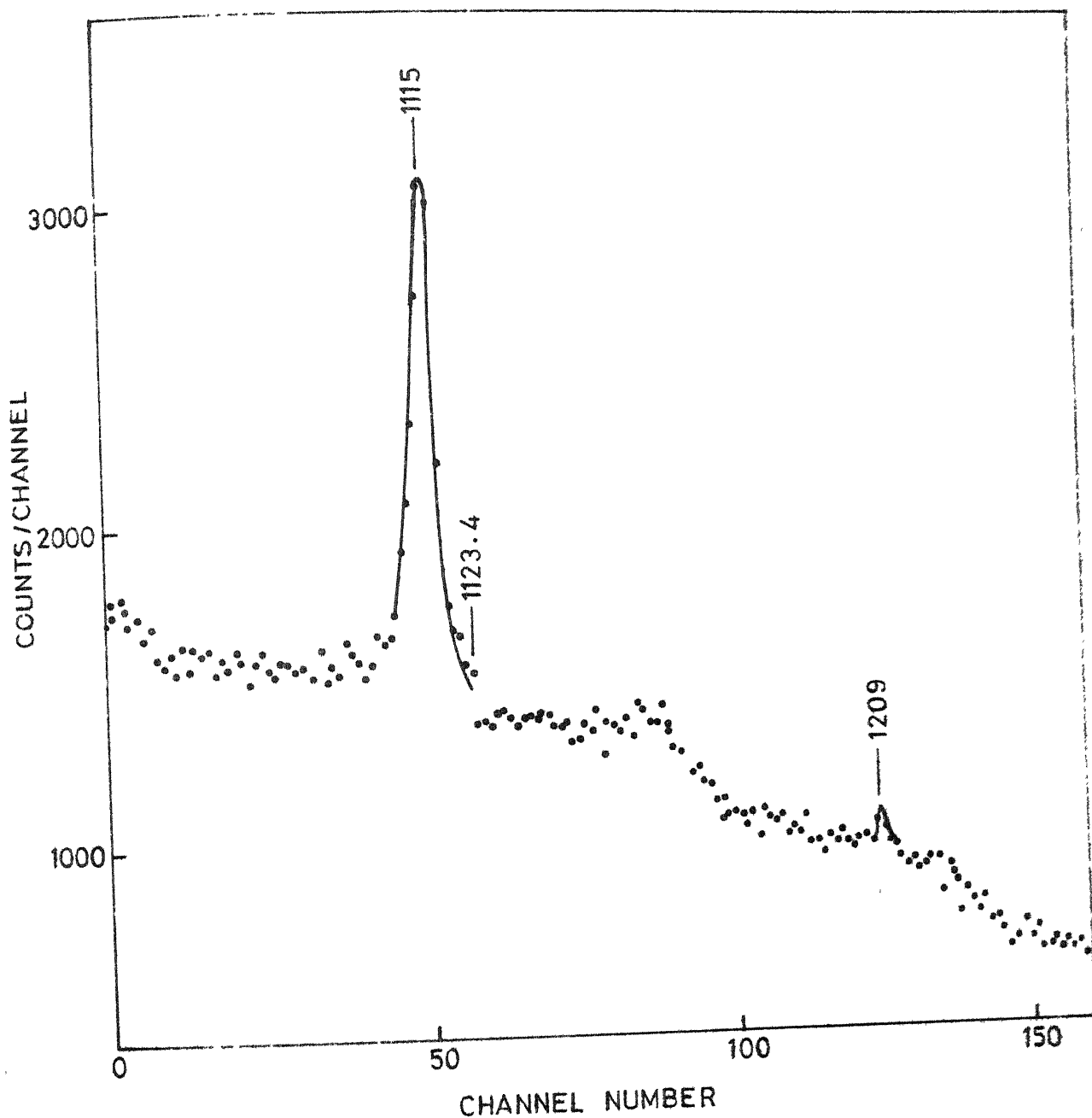


FIG. 7.3 Ge(Li) SPECTRUM OF  $^{63}\text{Zn}$  IN THE ENERGY REGION 1050-1250 KeV

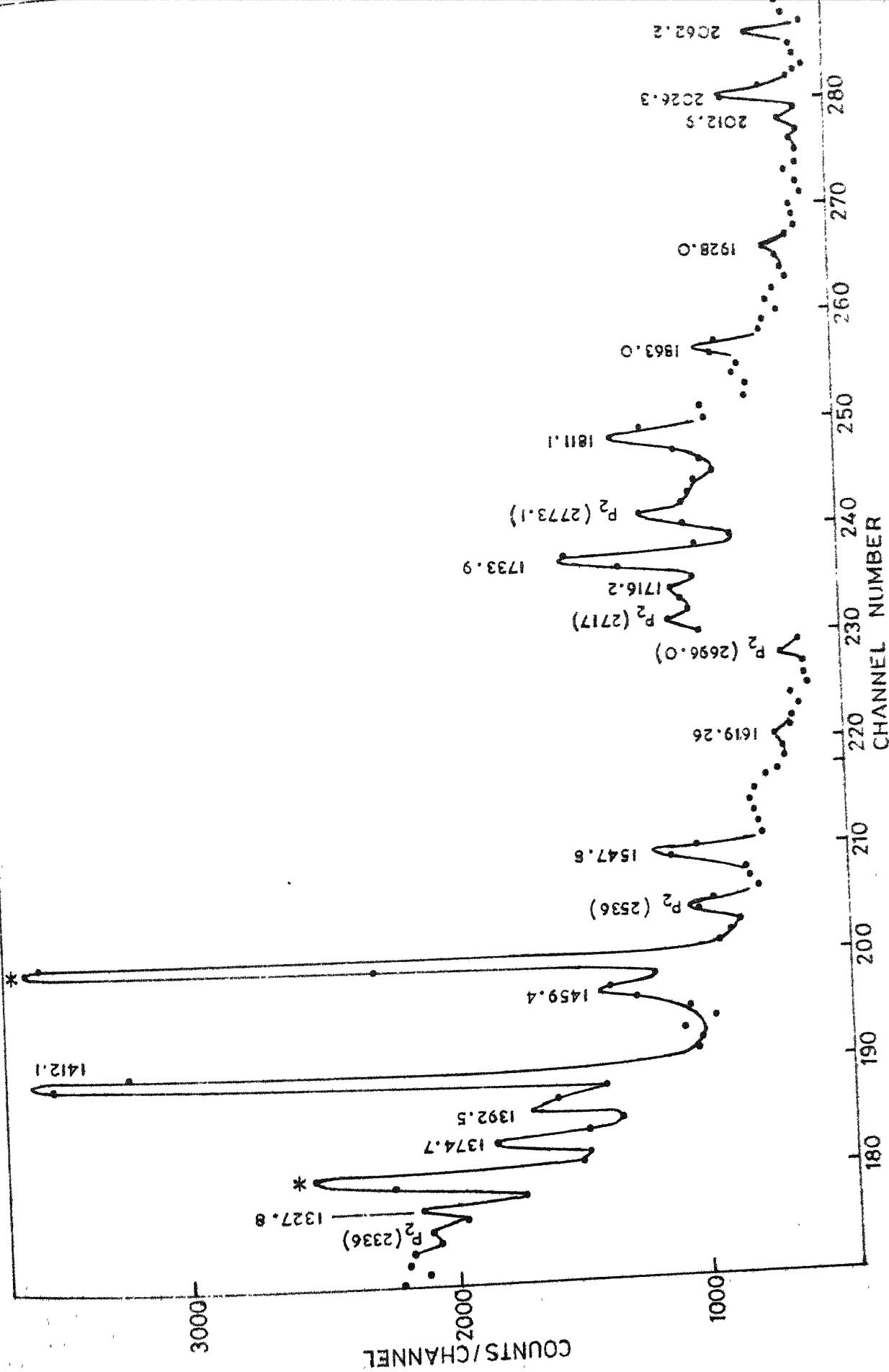
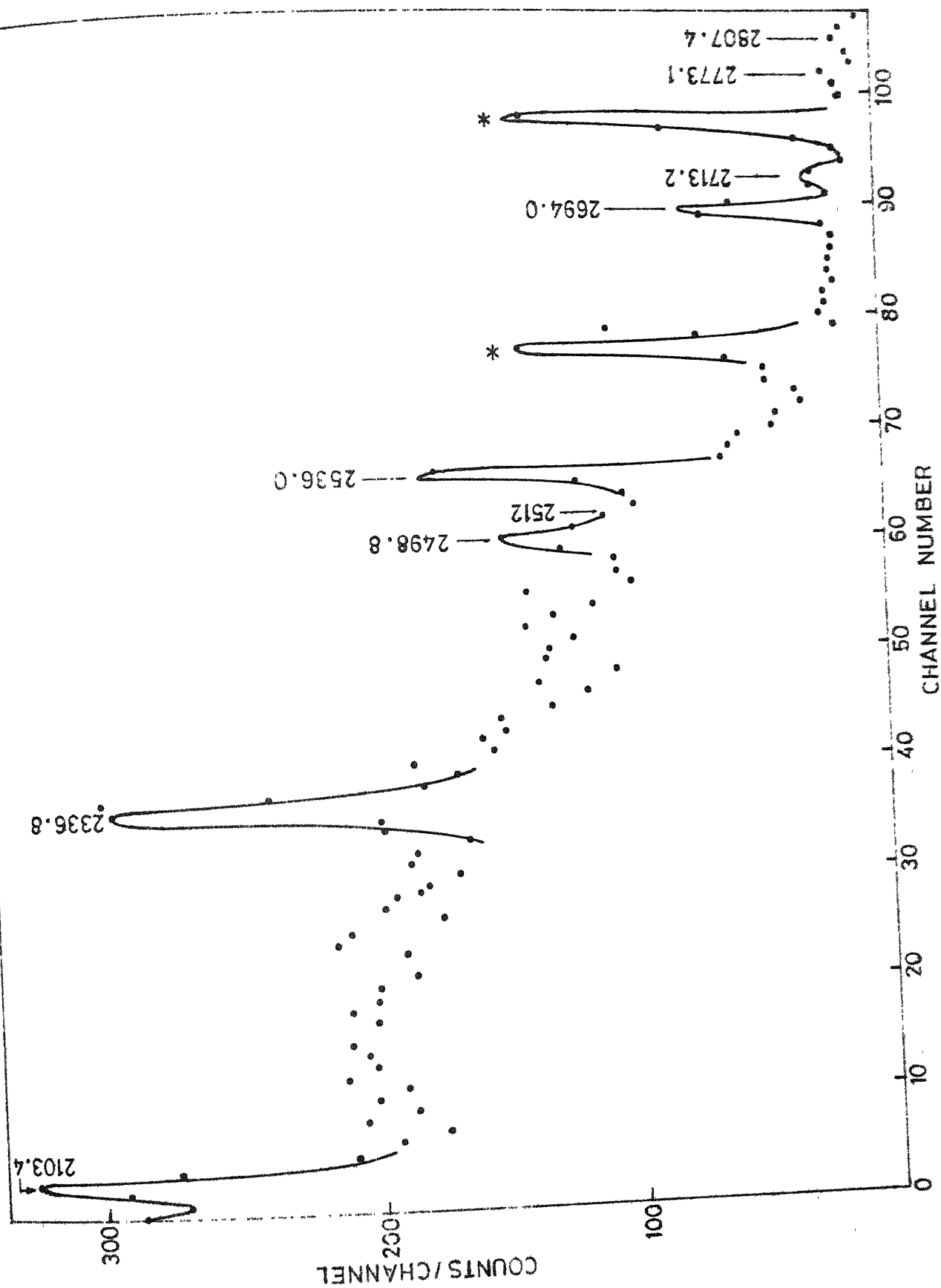


FIG. 7.4 Ge(Li) SPECTRUM OF  $^{63}\text{Zn}$  IN THE ENERGY REGION 1300-2100 KeV





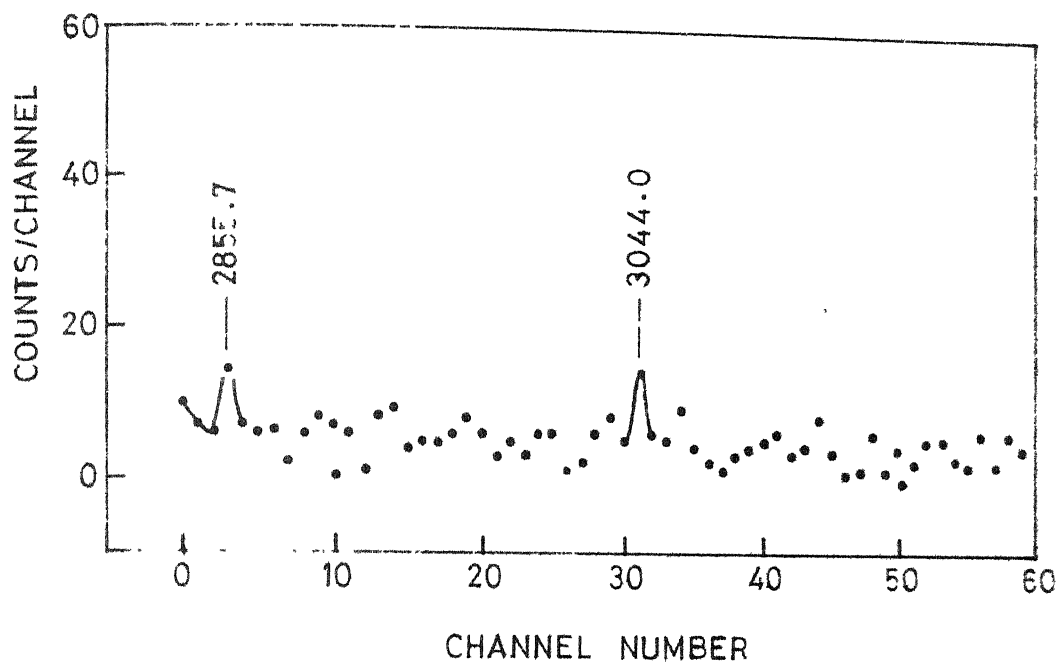


FIG. 7.6 Ge(Li) SPECTRUM OF  $^{63}\text{Zn}$  IN THE ENERGY REGION 2820-3300 KeV

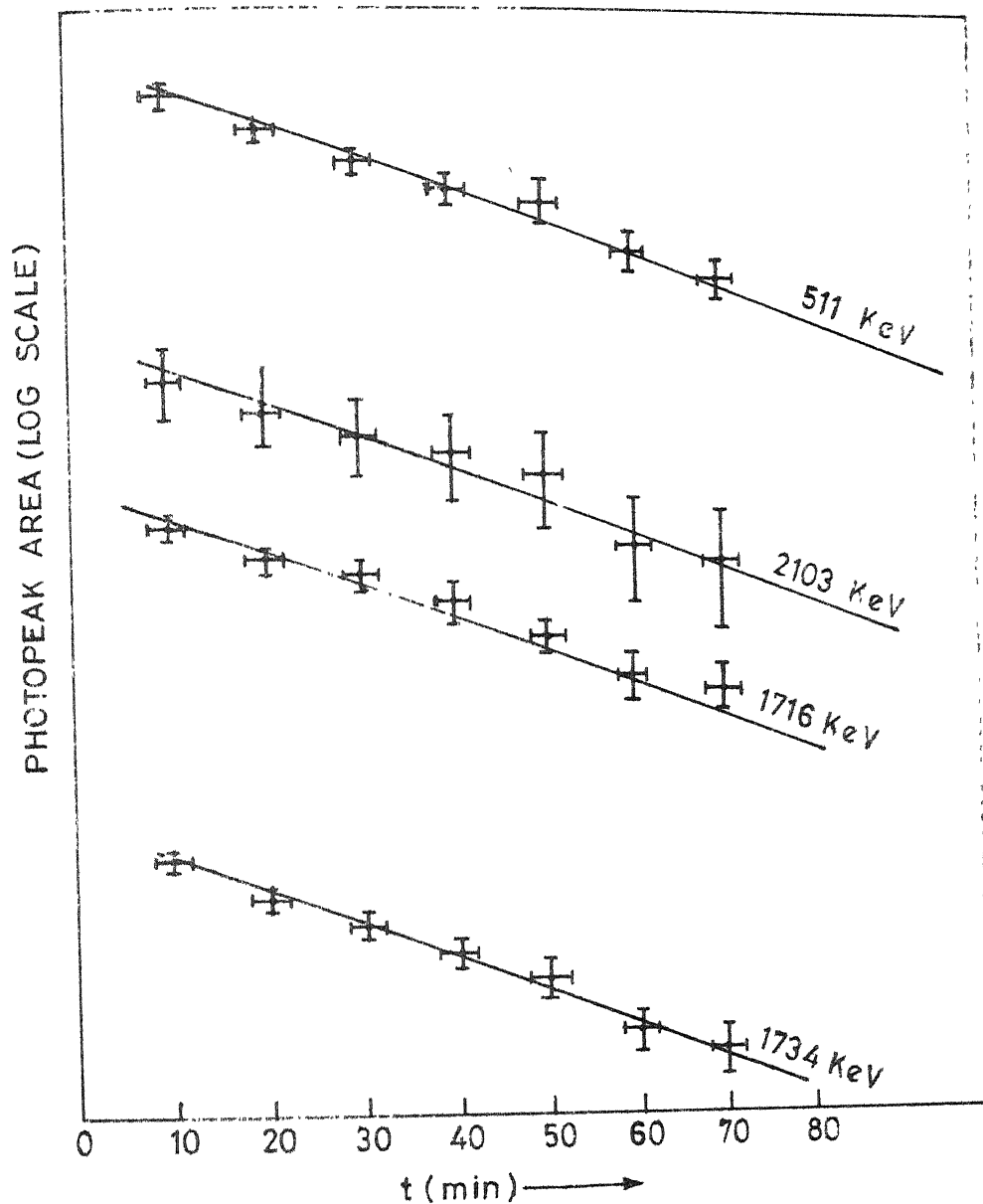


FIG. 7.7 HALF LIFE PLOTS OF ANNIHILATION QUANTUM (511 KeV) AND 1716, 1734 AND 2103 KeV GAMMA RAYS OF  $^{63}\text{Zn}$

Table 7.1. Gamma Ray Energies from the 38.4 m decay of  $^{63}\text{Zn}$ 

Borchert <sup>1</sup>	Kiuru <u>et al.</u> <sup>2</sup>	Present
364.5 $\pm$ 2.0	-	?
450.0 $\pm$ .5	449.8 $\pm$ 1.0	450.0
511	511	511
669.6 $\pm$ .2	669.75 $\pm$ .2	669.7
684.7	-	-
742.5 $\pm$ .5	742.0 $\pm$ 1.0	742.4
923.5	-	-
961.9 $\pm$ .2	962.1	962.1
1087 $\pm$ 2	-	-
1123.7 $\pm$ .3	1123.6 $\pm$ 1.0	1123.4
1150 $\pm$ 2	-	-
1168 $\pm$ 3	-	-
1189 $\pm$ 3	-	-
1208 $\pm$ 2	1209.1 $\pm$ 1.0	1208.2
1326.4 $\pm$ .3	1327.1 $\pm$ 1.0	1327.8
-	1340.0	-
1374.3 $\pm$ .3	1374.4 $\pm$ 1.0	1374.7
1391.5 $\pm$ .4	1392.1 $\pm$ 1.0	1392.5
1411.9 $\pm$ .2	1412.1 $\pm$ 1.0	1412.1
1546.9 $\pm$ .2	1546.6 $\pm$ 1.0	1547.8
1574.0 $\pm$ 2	1573.3 $\pm$ 1.0	-

...Contd.

Table 7.1 (Contd...)

Borchert <sup>1</sup>	Kiuru <u>et al.</u> <sup>2</sup>	Present
-	-	1716.2
-	-	1733.9
1816.9	1825.6	1811.0
1865.3	1863.4	1863.0
2010.9	2012.0	2012.3
2027.2	2026.7	2026.3
2048.6	-	-
2062.0	2062.7	2062.2
2082.0	2082.1	-
2103.2	-	2103.4
2336.5	2336.7	2336.8
2497.7	2497.1	2498.8
2512.0	2512.1	2512.0
2535.9	2536.2	2536.0
2696.7	2696.7	2696.0
2717.0	2716.8	2713.1
2780.1	2780.1	2773.1
2806.5	2807	2807.4
2857.4	2856	2855.7
2882	-	-
-	2890	2890.1
3044.9	3044	3044
3100.9	3101	-

measurements were done with each gate setting for several bombarded samples. The spectra were superposed. Even after 10-15 bombardments for each spectrum, reasonable statistics were not obtained. It is because the cascade branchings of  $^{63}\text{Cu}$  are very weak and much prolonged data collection times are necessary.

A level scheme constructed with the present results shown in Fig. 7.8. Spins and parities of the levels are as shown by Borchert, adopted from the reports of the earlier workers.

#### VII.4 Discussion

There have been various attempts to explain the structure of the low lying levels on the basis of core-excitation model, treating  $^{63}\text{Cu}$  levels as due to a  $p_{3/2}$  proton coupled to the even-even core of  $^{62}\text{Ni}$ . A quartet of levels is expected to arise due to the  $p_{3/2}$  proton coupling to the excited  $2^+$  core of  $^{62}\text{Ni}$ . For sometime, the 1412.1 keV level has been considered as the  $3/2^-$  member of the multiplet. Later experiments showed it to be a  $5/2^-$  state. Thankappan and True<sup>3</sup> showed that the 2012 keV excited state of  $^{63}\text{Cu}$  can be the  $3/2^-$  member. But they could not explain the occurrence of levels at 1547 and 1863 keV.

The 670 ( $1/2^-$ ) and 962 ( $5/2^-$ ) keV levels are populated in the ground state decay of  $^{63}\text{Zn}$  ( $3/2^-$ ). The



transitions are allowed, Gamow-Teller transitions. In the Appendix, we show that there should exist a simple geometrical ratio independent of nuclear matrix elements between the ft values of the two transitions if these two are the members of the multiplet. In the calculation it is necessary to assume that both the parent and daughter ( $^{63}\text{Zn}$  and  $^{63}\text{Cu}$ ) are a single particle coupled to the same core. If the description of  $^{63}\text{Cu}$  quartet as due to a particle coupled to the excited  $2^+$  core of  $^{62}\text{Ni}$  is valid, then the description that it is due to a particle coupled to the analog  $2^+$  state in  $^{62}\text{Cu}$  is also equally valid. For simplicity of evaluation, we assumed the parent  $^{63}\text{Zn}$  nucleus as a particle coupled to the ground state of  $^{62}\text{Cu}$ . These assumptions give the calculated ratio

$$\frac{(ft)_{3/2 \rightarrow 1/2}}{(ft)_{3/2 \rightarrow 5/2}} = 2.6$$

whereas the experimental value is 1.05.

Needless to say that the assumption made regarding the configuration of  $^{63}\text{Zn}$  is open to questions and thus this ratio is not expected to yield any reliable information about the quartet states. Nevertheless, it may be emphasized that a more realistic calculation of the decay of  $^{63}\text{Zn}$  to these four quartet states can provide a reasonable test of the hypothesis that the  $^{63}\text{Cu}$  excited states can be represented as coupling of  $2^+$  vibrational state of  $^{62}\text{Ni}$  and a proton.

# APPENDIX

The core-excitation multiplet satisfy the centre of gravity theorem due to Lawson and Uretsky<sup>4</sup>, i.e.,

$$\sum_j (2j + 1) (E_j - E_c) = 0$$

where  $j$  takes the possible total angular momentum values of the core-multiplet members,  $E_j$  is the respective excitation energy values and  $E_c$  is the excitation energy of the corresponding core state. Also the  $B(E2)$  values for the transitions of the members of the multiplet to the ground state are separately equal to the  $B(E2)$  value for the transition from the excited state to the ground state of the even-even core as shown by de Shalit.<sup>5</sup> Here we provide another test for the core-excitation model if two members of the multiplet are populated in the  $\beta$  decay from the same parent nuclear state.

The members of the multiplet are of wave functions  $|j_c \ j \ j_f\rangle$  with  $j_f$  taking different values for different states and the parent nuclear state is described by  $|j'_c \ j' \ j_i\rangle$  wave function.

The square of the transition matrix element

$$|M|^2 = \frac{1}{(2j_i+1)} \sum_{m_i, m_f} |\langle \Psi_f | \Gamma_\lambda | \Psi_i \rangle|^2 \quad (7.1)$$

Taking  $|\Psi_f\rangle = |j_f\rangle$ ;  $|\Psi_i\rangle = |j_i\rangle$



$$|M|^2 = \frac{1}{(2j_i+1)} \sum_{m_i, m_f} |\langle j_f || \Gamma_\lambda || j_i \rangle|^2 \quad (7.2)$$

Applying Wigner-Eckart theorem

$$|\langle j_f || \Gamma_\lambda || j_i \rangle|^2 = \left[ (-)^{j_f - m_f} \begin{Bmatrix} j_f & \lambda & j_i \\ -m_f & \mu & m_i \end{Bmatrix} \right]^2 \times |\langle j_f || \Gamma_\lambda || j_i \rangle|^2 \quad (7.3)$$

Thus

$$|M|^2 = \frac{1}{(2j_i+1)} \left[ \sum_{m_i, m_f} (-)^{j_f - m_f} \begin{Bmatrix} j_f & \lambda & j_i \\ -m_f & \mu & m_i \end{Bmatrix} \right]^2 \times |\langle j_f || \Gamma_\lambda || j_i \rangle|^2 \quad (7.4)$$

As mentioned earlier

$$|j_f\rangle = |j_c \ j \ j_f\rangle$$

$$\text{and } |j_i\rangle = |j'_c \ j' \ j_i\rangle$$

$$\text{So } |\langle j_f || \Gamma_\lambda || j_i \rangle|^2 = |\langle j_c \ j \ j_f || \Gamma_\lambda || j'_c \ j' \ j_i \rangle|^2$$

$$= (2j_f+1)(2\lambda+1)(2j_i+1) \begin{Bmatrix} j_c & j & j_f \\ j'_c & j' & j_i \\ \lambda_1 & \lambda_2 & \lambda \end{Bmatrix}^2 \times$$

$$|\langle j_c || \Gamma_{\lambda_1} || j'_c \rangle|^2 |\langle j || \Gamma_{\lambda_2} || j' \rangle|^2 \quad (7.5)$$

$$\text{Thus, } |M|^2 = \frac{1}{(2j_i+1)} \left[ \sum_{m_i, m_f} (-)^{j_f - m_f} \begin{Bmatrix} j_f & \lambda & j_i \\ -m_f & \mu & m_i \end{Bmatrix} \right]^2 \times$$

$$(2j_f+1)(2\lambda+1)(2j_i+1) \begin{Bmatrix} j_c & j & j_f \\ j'_c & j' & j_i \\ \lambda_1 & \lambda_2 & \lambda \end{Bmatrix}^2 \times$$

$$|\langle j_c || \Gamma_{\lambda_1} || j'_c \rangle|^2 |\langle j || \Gamma_{\lambda_2} || j' \rangle|^2 \quad (7.6)$$

If two members of the multiplet are populated by the same type of interaction resulting in same  $\Gamma_{\lambda_1}$  and  $\Gamma_{\lambda_2}$  for both the transitions, then the ratio of ft values for the final states 1 and 2 is given by

$$\frac{(ft)_2}{(ft)_1} = \frac{|M|_1^2}{|M|_2^2} = \frac{(2j_1+1)}{(2j_2+1)} \frac{\left\{ \begin{matrix} j_c & j & j_1 \\ j'_c & j' & j'_i \\ \lambda_1 & \lambda_2 & \lambda \end{matrix} \right\}^2}{\left\{ \begin{matrix} j_c & j & j_2 \\ j'_c & j' & j'_i \\ \lambda_1 & \lambda_2 & \lambda \end{matrix} \right\}^2} \quad (7.7)$$

and is independent of the actual values of the matrix elements. The conditions under which this relation is satisfied are:

- (i) The two final states are of same configuration, i.e., a core coupled to a particle (hole) of a  $j$  value resulting in the members of the multiplet.
- (ii) The two members being considered should be populated by the same kind of interaction, i.e., the transition is either pure Fermi or Gamow-Teller transition.

REFERENCES

1. I. Borchert, Z. Phys. 223 (1969) 473. —
2. A. Kiuru and P. Holmberg, Z. Phys. 233 (1970) 146.
3. V.K. Thankappan and W.W. True, Phys. Rev. 137 (1965) B793.
4. R.D. Lawson and J.L. Uretsky, Phys. Rev. 108 (1957) 1300.
5. A. de-Shalit, Phys. Rev. 122 (1961) 1530.

CHAPTER VIII  
STUDY OF  $^{27}\text{Al}(p,\gamma)^{28}\text{Si}$  RESONANCE DECAYS

VIII.1 Introduction

The measurements described in this Chapter were performed with a 2 MV Van de Graaff accelerator procured from High Voltage Engineering Corporation, U.S.A. It is a horizontal machine with a radio frequency ion-source. Since this was the first experiment on this newly installed machine, it was necessary to do various preliminary tests to check the feasibility of such experiments under the present conditions.

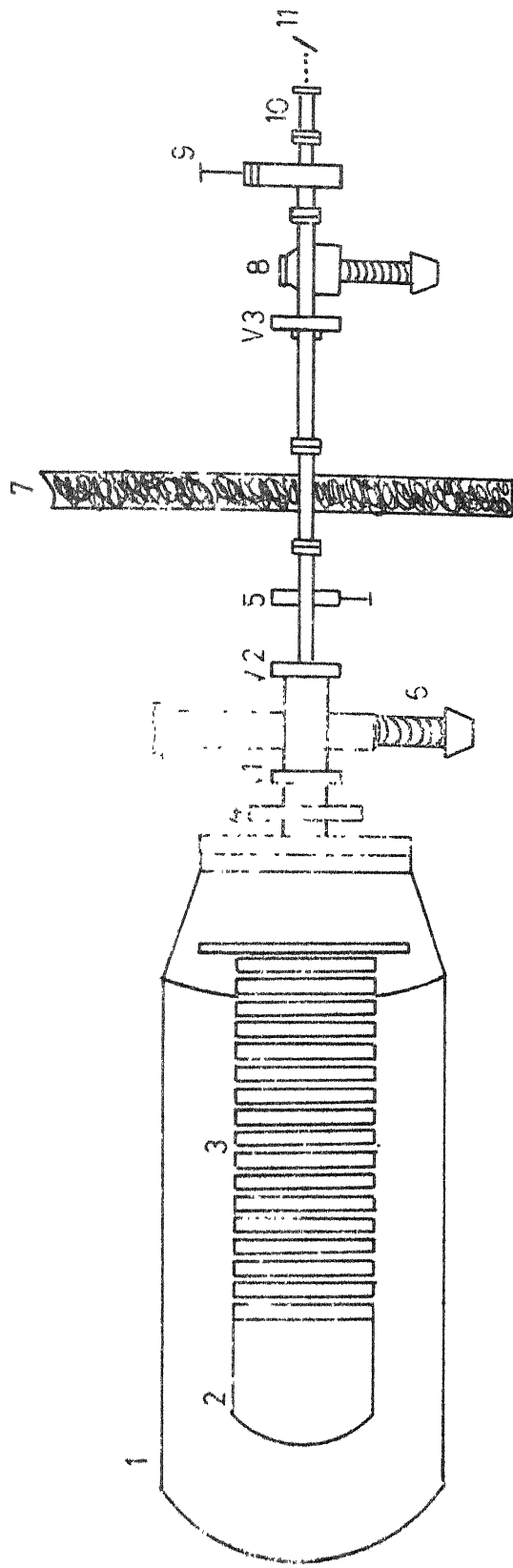
The accelerator voltage is presently measured with a digital voltmeter using the signal from the generating voltmeter provided in the machine. At present, there is no switching and stabilizing magnet and thus better energy definition is not possible. In the absence of these stabilizing units, the machine voltage is found to be stable within  $\pm 2$  KV over periods of a few hours. Sufficiently large proton beam currents are available with a beam spot size of the order of 5 mm diameter at a distance of 6 meters from the tank base. A large number of diverse measurements were made to test the quality of the beam and the ones relevant to this experiment are described below:

- a) Stability and reproducibility of the beam
- b) Energy resolution of the beam
- c) Calibration cum linearity checks.

## VIII.2 Stability etc. of the Proton Beam

The experimental layout is shown in Fig. 8.1. The collimator system described in Chapter 2, was used with slits of diameters 2 cm and 1 cm. This was followed by the target holder, also described in Chapter 2. A  $^{10}\text{BF}_3$  proportional counter was used for neutron detection and a 12.5 x 12.5 cm NaI(Tl) scintillation detector was used for gamma yield measurements.

A sensitive test for estimating the stability of the beam energy is from the measurement of the yield of a reaction threshold spectrum. When we measure the yield from such a reaction for a fixed beam charge, with the high voltage fixed to correspond to the middle portion of the steep rising part of the threshold spectrum, the factors that affect the change of yield are : (a) fluctuations in the beam energy value, (b) fluctuations in the concentrations of atomic and molecular beam components, and (c) target deterioration effects. Of these, the effect of target deterioration is easy to estimate as it would result only in the continuous decrease in the yield as a function of time, whereas the other two effects appear as the fluctuations over a mean value of the yield. In our experiment, the yield of neutrons



- |                                |   |                         |
|--------------------------------|---|-------------------------|
| 1) ACCELERATOR TANK            | 5) BEAM VIEWER AND STOPPER                      | 9) THREE TARGET CHAMBER |
| 2) HIGH VOLTAGE TERMINAL SHELL | 6) MACHINE VACUUM SYSTEM                        | 10) BEAM COLLIMATOR     |
| 3) SUPPORTING COLUMN           | 7) CONCRETE WALL                                | 11) EXPERIMENTAL TARGET |
| 4) BEAM STREERERS              | 8) OIL DIFFUSION PUMP WITH LN <sub>2</sub> TRAP |                         |

V1 V2 V3 ARE GATE VALVES

FIG.8.1 VAN DE GRAAFF ACCELERATOR ASSEMBLY

from  ${}^3\text{H} (p,n) {}^3\text{He}$  reaction was measured. A thick target was used and it was found to withstand beam currents of 10  $\mu\text{A}$  for several hours without appreciable deterioration. It was, therefore, assumed that the change of yield due to the target deterioration during the present experimental period was negligibly small. From the experimental data, the fluctuations in countrate were found to correspond to a maximum of  $\pm 2$  keV fluctuation in the mean particle beam energy. It results in the upper limit of  $\pm 2$  keV fluctuations for the particle beam energy at 1 MeV.

Another important feature is a test of reproducibility of the beam energy, i.e., to what accuracy one can reproduce the same energy at different times. This aspect was tested by locating the 992 keV resonance of  ${}^{27}\text{Al}(p,\gamma) {}^{28}\text{Si}$  reaction thrice, each measurement being made after 10 hours of the earlier measurement. The yield curves recorded on the three occasions are shown in Fig. 8.2. The curves 2 and 3 were measured on the same day when the machine had been continuously operating and the curve 1 was recorded on a different day. The difference in the yields of the curves was, due to the different amounts of charge collected. The figure shows that the resonance energy can be reproduced to within  $\pm 1$  keV.

A knowledge of the beam energy spread is essential to estimate the minimum separation needed between two

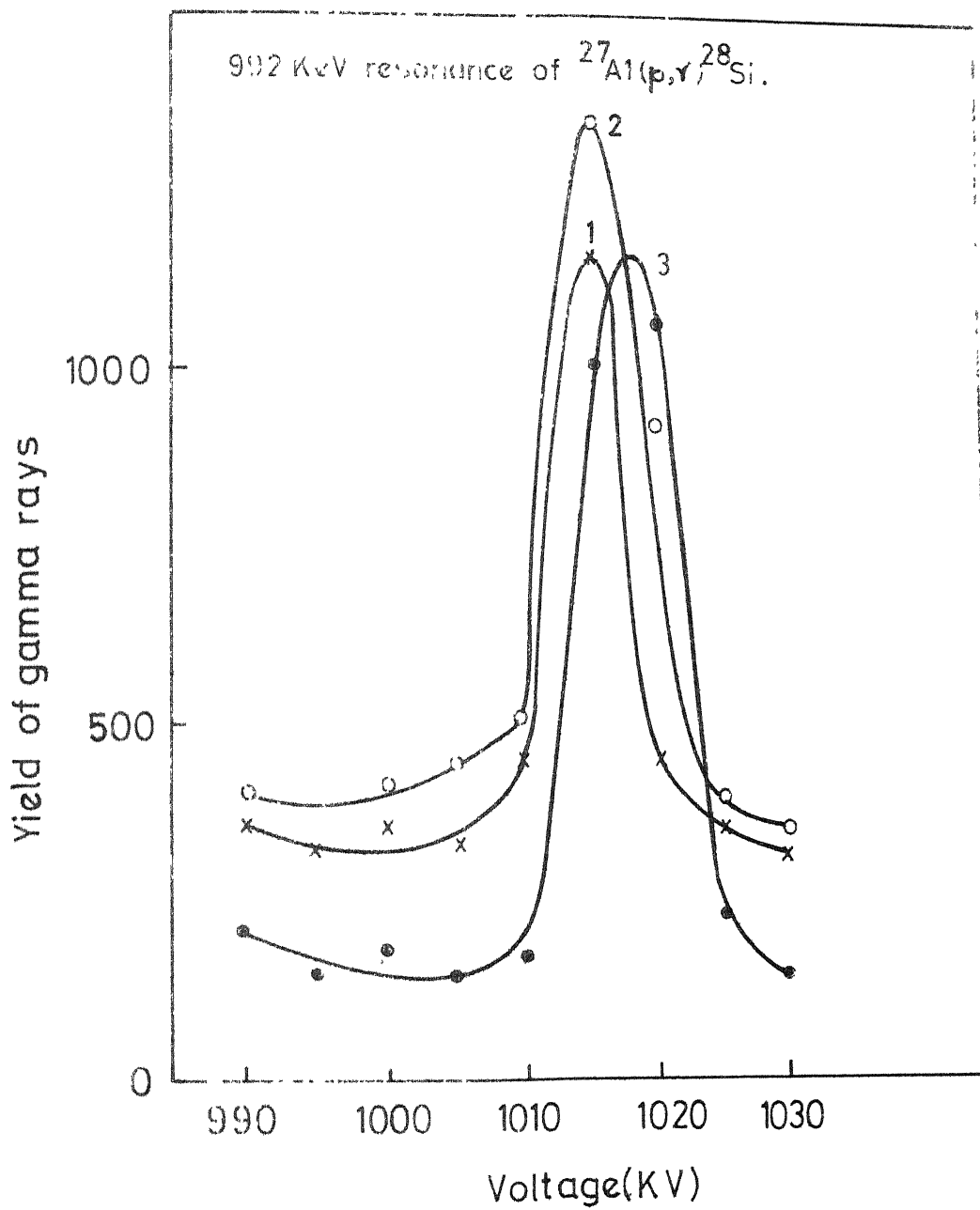


FIG.8.2 REPRODUCIBILITY TEST OF BEAM ENERGY



neighbouring resonances for them to be resolved with the present system. An attempt was, therefore, made to estimate the beam energy resolution. To this end, the width of the narrow resonance at proton energy  $E_p = 992$  keV in  $^{27}\text{Al}(p,\gamma)^{28}\text{Si}$  reaction was measured using a target of 2 keV thickness for 1 MeV protons. From the experiment, the beam spread was found to be of the order of 6 keV, the contributions due to the finite target thickness and natural width of the resonance having been taken into account. —

The knowledge of the energy of a charged particle beam from an accelerator is necessary in the measurement of nuclear reaction  $Q$  values or in the measurement of the energies of excited nuclear states from the resonance reactions. The energies of several resonance and threshold reactions have been determined by absolute measurements such as by electrostatic and magnetic deflection methods. Marion<sup>1</sup> has examined the data from different measurements and arrived at adopted values. The measurement of these resonance and threshold reactions serve as the energy calibration of the accelerator. In the calibration of the present accelerator, the 992, 1381, 1388 and 1588 keV resonances in  $^{27}\text{Al}(p,\gamma)^{28}\text{Si}$  and the 872 keV resonance in  $^{19}\text{F}(p,\alpha\gamma)^{16}\text{O}$  reactions and also the yield of the threshold reaction  $^3\text{H}(p,n)^3\text{He}$  reaction were used. As the beam energy spread is 6 keV the resonance energies known even

to an accuracy of about 1 keV, could be used for calibration. The resonances at 1381, 1388 and 1588 keV in  $^{27}\text{Al}(p,\gamma)^{28}\text{Si}$  were, therefore, used in the present experiment.

Neutron threshold experiment was done with a tritium target. The total yield of the neutrons (Y) emitted, when a target of finite thickness is employed, is given by

$$Y \propto (\delta E)^{3/2} \quad (\text{VIII.1})$$

where  $\delta E$  is the bombarding energy above the threshold value. The threshold is determined by extrapolation to zero yield in the plot of  $Y^{2/3}$  against the bombarding beam energy value. The neutron yield is measured as a function of the bombarding proton energy. (Yield) $^{2/3}$  is plotted against the digital voltmeter reading. Threshold value is obtained by extrapolating to the zero yield. The curve is shown in Fig. 8.3.

The resonances in aluminium were located by using an aluminium target of 2 keV thickness for 1 MeV protons. The 12.5 x 12.5 cm NaI (Tl) detector was employed for the detection of gamma rays. The yield of the gamma radiation ( $E_\gamma > 1$  MeV) was measured as a function of the accelerator voltage as read on the digital voltmeter. The resonances were located and the corresponding digital voltmeter readings were noted. The 872 keV resonance in  $^{19}\text{F}(p,\alpha\gamma)^{16}\text{O}$  reaction was also observed in the same yield spectrum, due to the fluorine contamination, which generally occurs. The yield curve of these resonances is shown in Fig. 8.4.

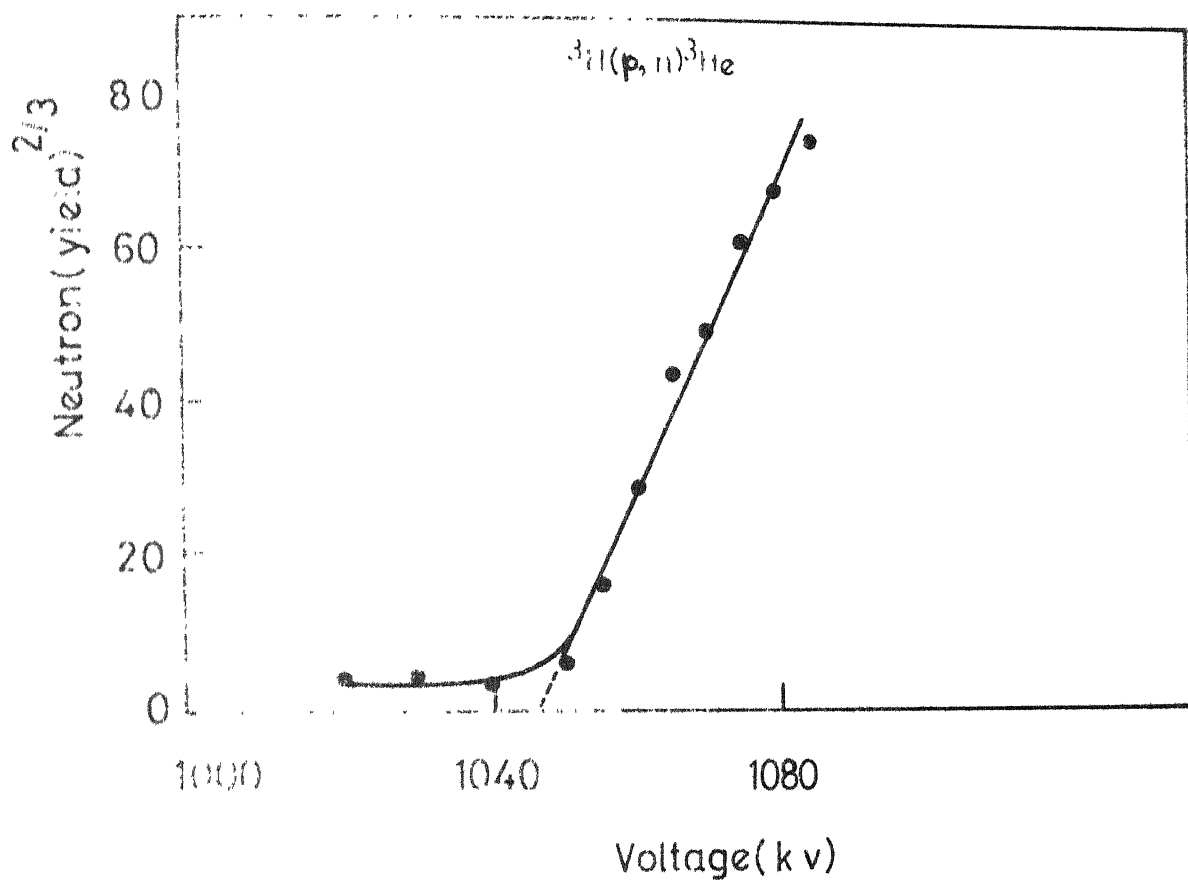


FIG. 8.3 THRESHOLD SPECTRUM OF  ${}^3\text{H}(p,n){}^3\text{He}$  REACTION

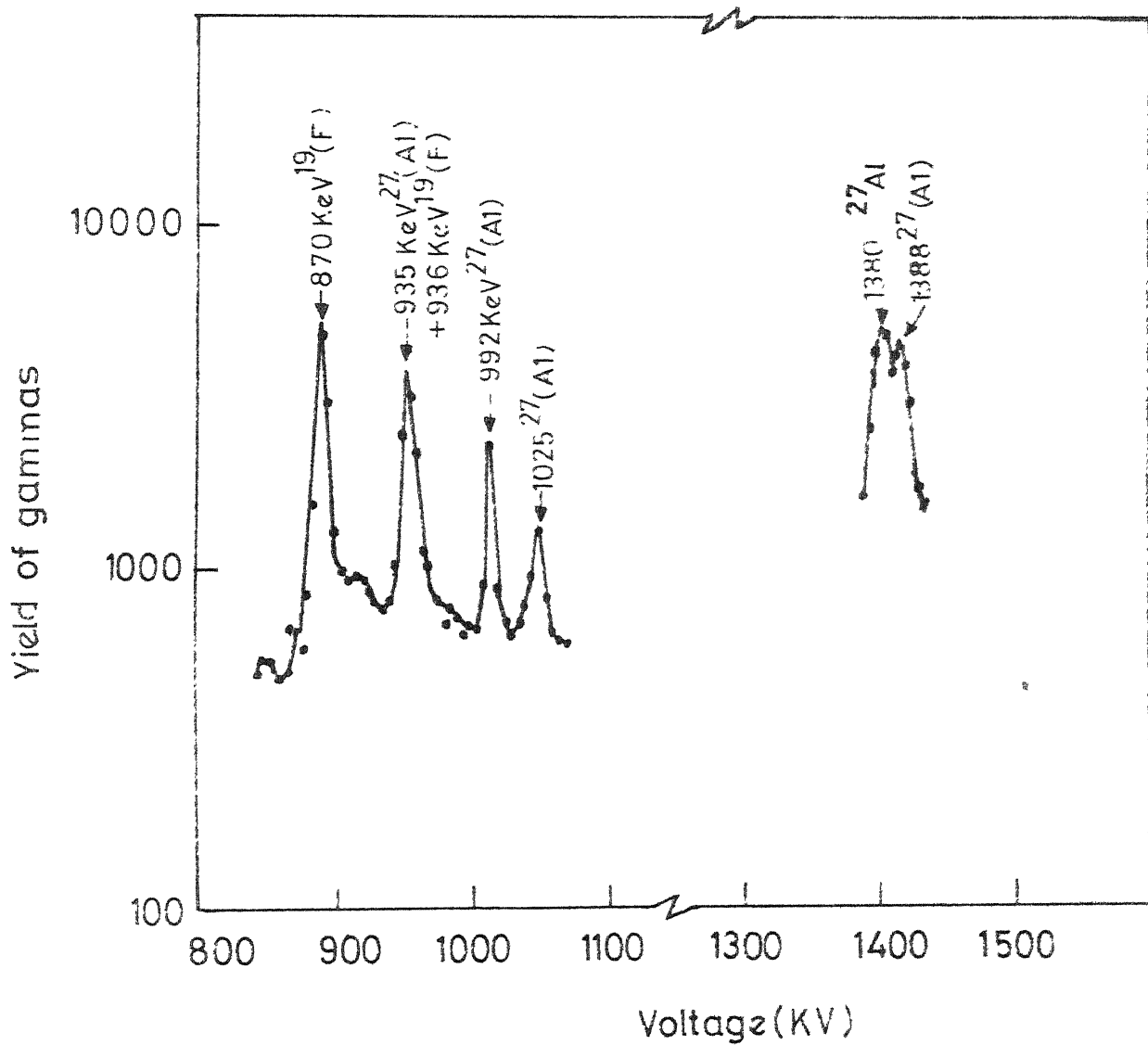


FIG.8.4 RESONANCE IN  $^{27}\text{Al}(p,\gamma)^{28}\text{Si}$  AND  $^{19}\text{F}(p,\alpha\gamma)^{16}\text{O}$  REACTION FOR CALIBRATION

The results of the above reaction measurements are summarized in the calibration plot shown in Fig. 8.5, where the recommended energies of the reactions are plotted against the digital voltmeter readings. The above tests indicate that the decay studies of resonances separated from the neighbouring ones, by about 6 keV are feasible.

### VIII.3 Study of the Gamma Decay of 992 and 1261 keV Resonances in $^{27}\text{Al}(p,\gamma)^{28}\text{Si}$ Reaction

The resonances in  $^{28}\text{Si}$  have been the subject of many investigations. Gibson et al.<sup>6</sup> studied the gamma decay of a few resonances in 1.2-2.4 MeV proton energy region with a 20 c.c. Ge(Li) detector to determine the gamma energies. Recently, Meyer et al.<sup>4,5</sup> studied the gamma decay of resonances upto 2 MeV proton energy. However, the results of Meyer et al. differ from the results of Gibson et al. and that of earlier workers. For example, the 10.27 MeV level reported by Ophel and Osgood<sup>2</sup> and Azuma et al.<sup>3</sup> in the decay of 992 keV resonance was not observed by Meyer et al. Further, about 37% decays of 9.42 MeV and 21% decays of 7.93 MeV levels, populated in the decay of 992 keV resonance, were also not identified. Besides, the levels at 11.08, 10.91, 7.9 and 6.89 MeV energies, reported by Gibson et al. to have been populated in the decay of 1261 keV resonance, were not observed by Meyer et al. It may be pointed that the results obtained in these

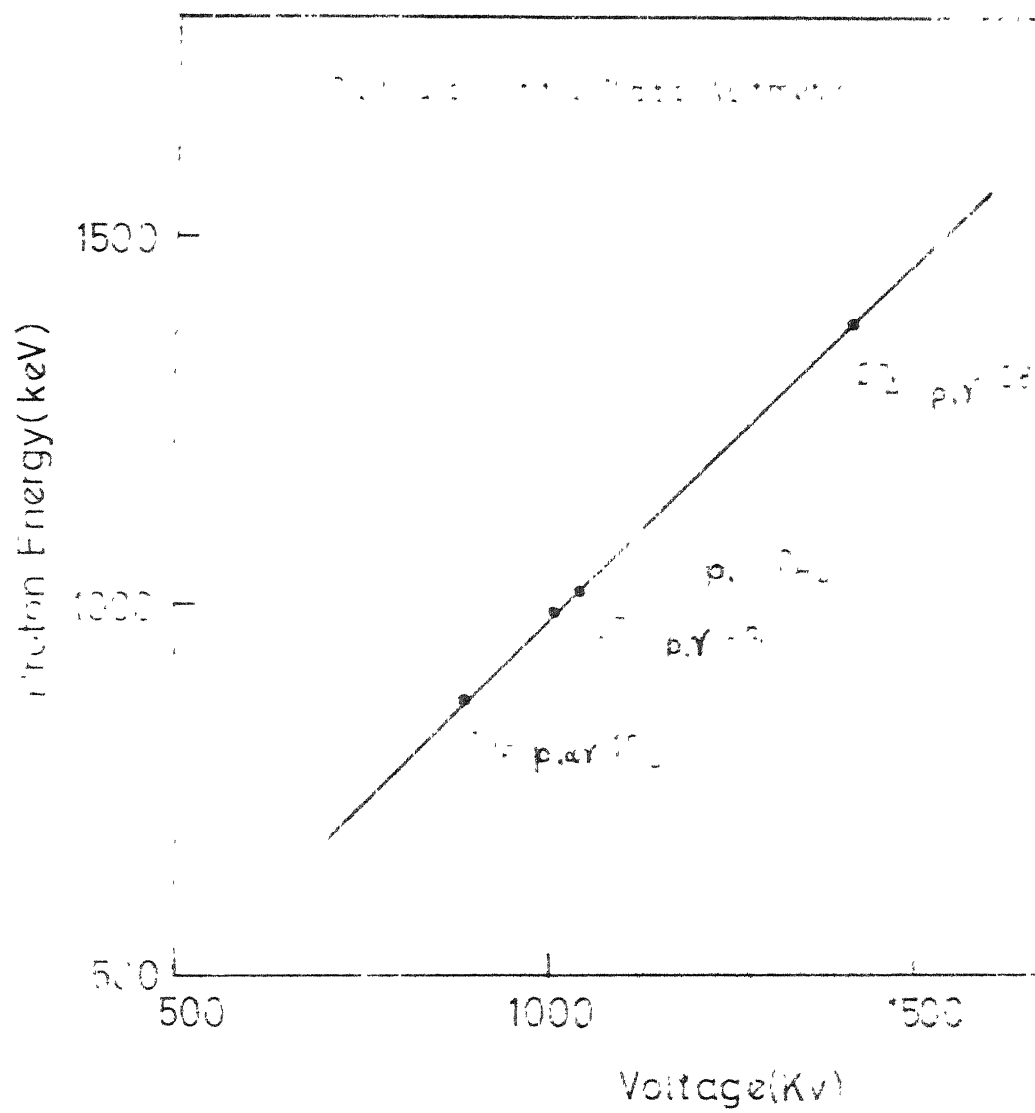


FIG. 8.5

measurements were only from singles spectra with Ge(Li) detector. Earlier measurements of sum-coincidence spectra at these resonances were by Antoufiev et al.<sup>7</sup> They measured spectra with gates at 10.76 and 11.02 MeV respectively for 992 and 1261 keV resonances. However, their measurements were not aimed at these discrepancies. The present investigation was undertaken to measure Ge(Li) spectra as well as sum-coincidence spectra at these resonances to get better idea of the genetic relations of the gamma transitions. We present here only those results which help in resolving the above mentioned discrepancies.

The first stage of the study was the measurement of excitation function. An aluminium target of 2 keV thickness for 1 MeV protons was used for this purpose. The target holding systems are described in Chapter II. The target was cooled by running water. A proton beam current of 2  $\mu$ A was used in the measurement. The gamma yield, for  $E_\gamma > 1$  MeV, was measured as a function of proton energy. The excitation function, thus obtained, is shown in Fig. 8.6.

An aluminium target of 15 keV thickness for 1 MeV protons was used for the gamma decay study of 992 and 1261 keV resonances. Proton beam currents of 7  $\mu$ A and 15  $\mu$ A were used for Ge(Li) spectra and coincidence measurements respectively. The 12.5 x 12.5 cm NaI(Tl) detector, kept at an angle of  $90^\circ$  with respect to the proton beam was used as

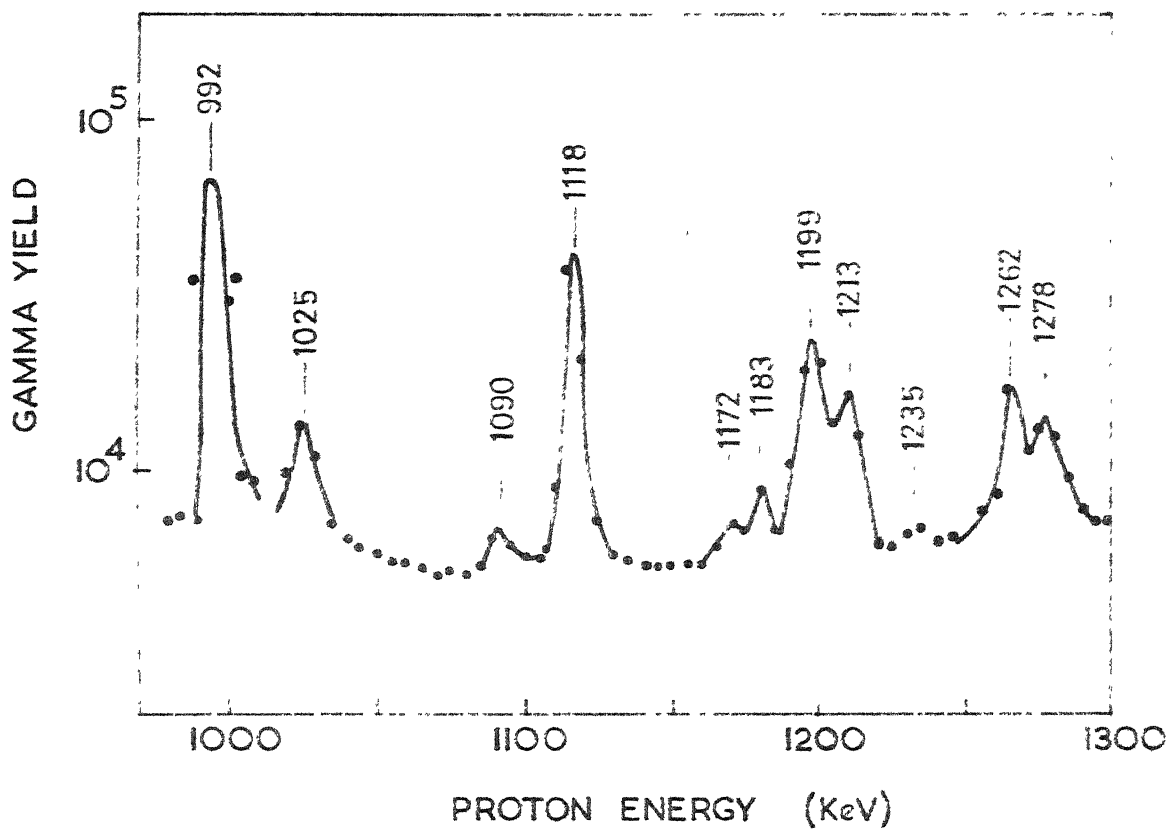


FIG. 8.6 EXCITATION FUNCTION FOR  $^{27}\text{Al}(p, \gamma)^{28}\text{Si}$  REACTION IN 950-1300 KeV ENERGY RANGE



the monitor counter to account for the target deterioration. No appreciable target deterioration was observed over periods of 24 hours.

The Ge(Li) detector of 4.2 c.c. effective volume was used in the measurement of singles spectra. The sum-coincidence spectrometer, described earlier, was used for coincidence measurements.

#### VIII.4 Gamma Decay of 992 keV Resonance

The singles spectra were recorded using the Ge(Li) detector. First, the spectrum was measured in 0-12 MeV gamma energy range to cover the entire region of interest. Another expanded spectrum of 1-3 MeV was also recorded to achieve precise energy values. The spectra are shown in Figs. 8.7(a), 8.7(b) and 8.8. In the second stage, sum-coincidence spectra with gates at 10.76 MeV and 6.28 MeV were recorded to study the double cascades in  $12.54 \rightarrow 1.78$  and  $12.54 \rightarrow 6.26$  MeV decays. The two spectra are shown in Figs. 8.9 and 8.10 and the results are summarized in Table 8.1.

An inherent difficulty exists in the detection of 10.27 MeV gamma ray, because its photopeak falls under the intense first escape peak of 10.76 MeV gamma ray arising due to  $12.54 \rightarrow 1.78$  MeV transition. Similarly, the first escape peak of 10.27 MeV gamma ray falls under the second escape peak of 10.78 MeV gamma ray. In our spectrum, there is an indication of the second escape peak of 10.27 MeV



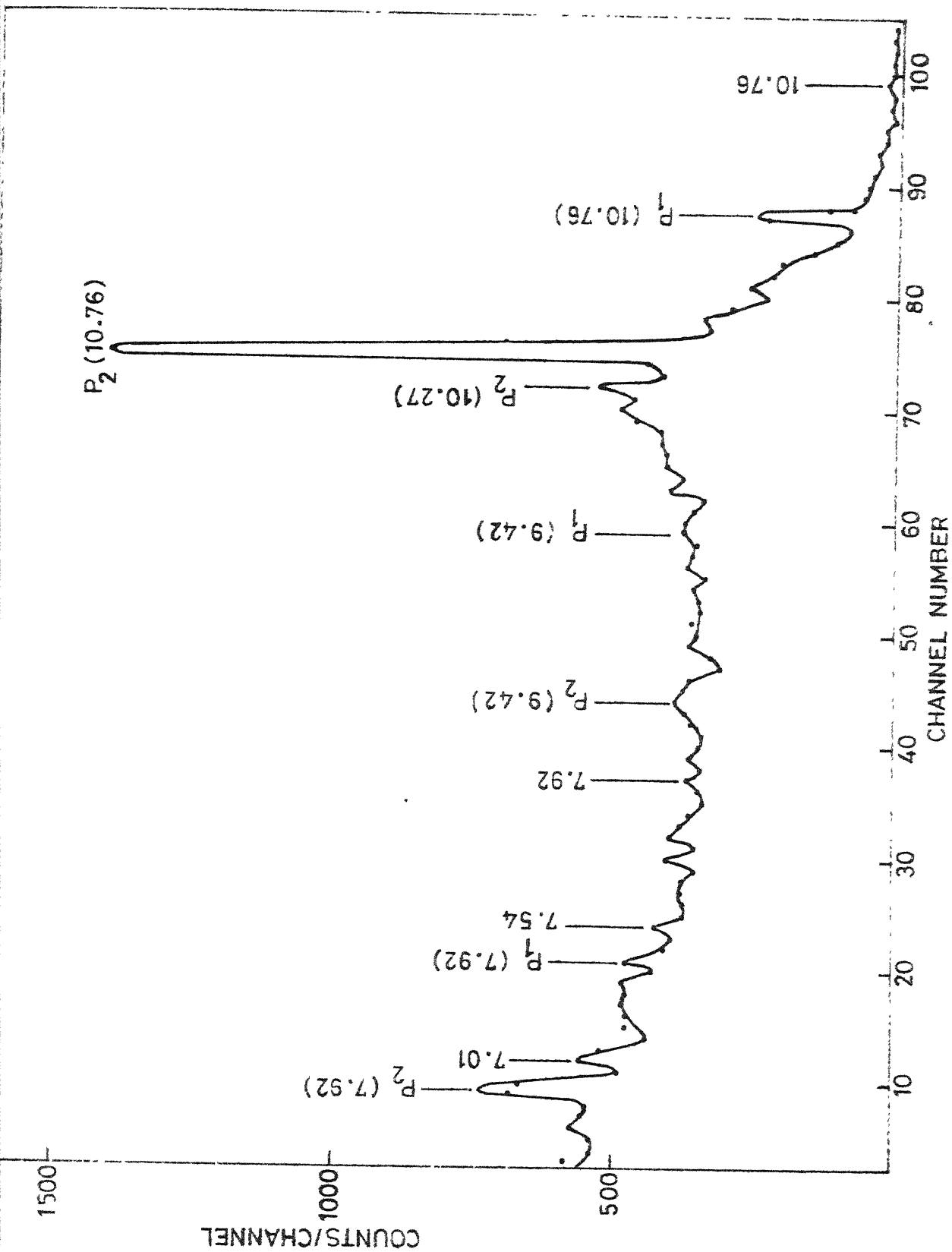


FIG. 8.7 b Ge(Li) SPECTRUM OF GAMMA RAYS FROM  $E_p = 992$  KeV  
 RESONANCE IN  $^{27}\text{Al}(p, \gamma)^{28}\text{Si}$  REACTION IN THE ENERGY REGION  
 6.5 - 11.0 MeV

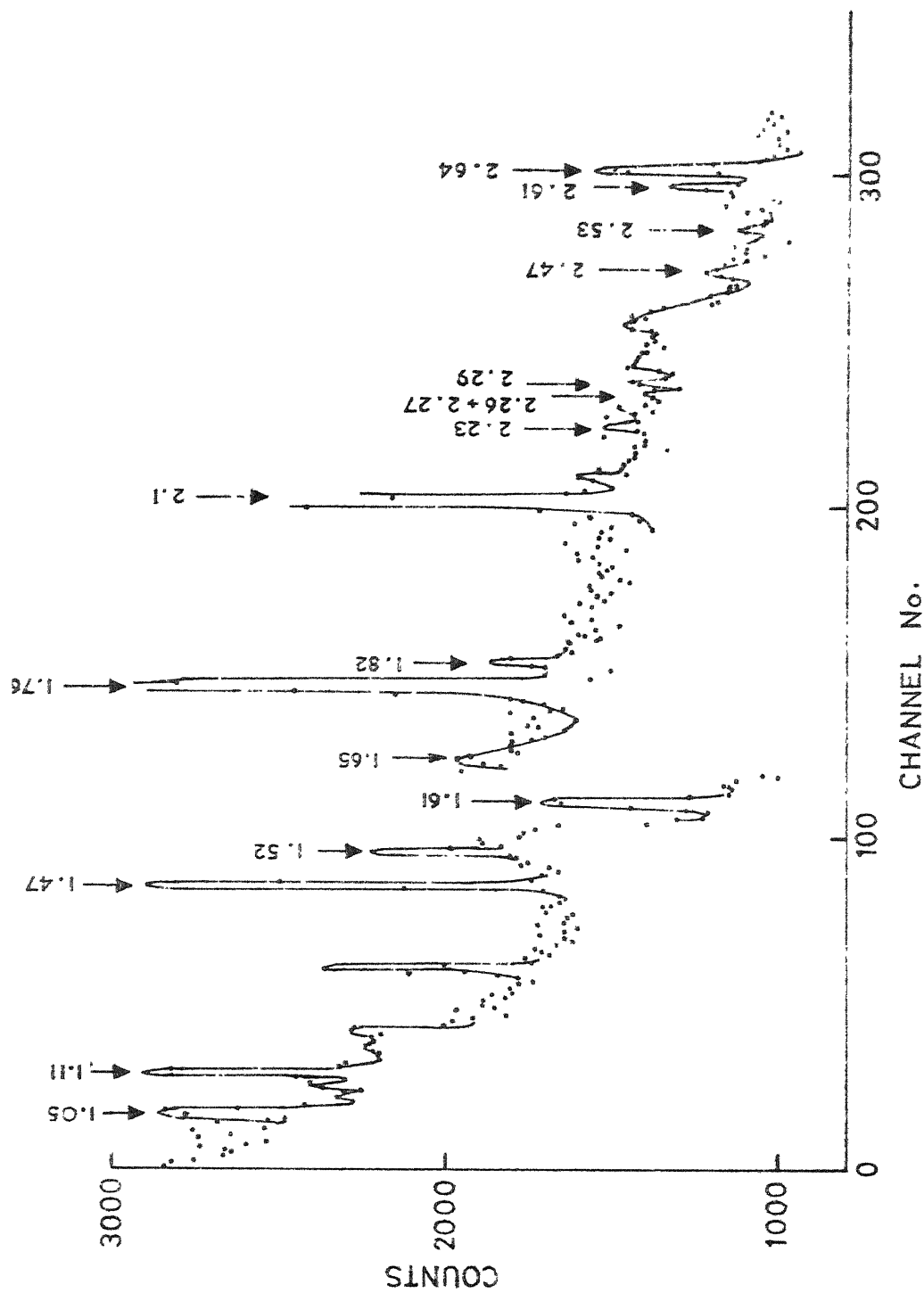


FIG.8.8 1-3 MeV GAMMA RAY SPECTRUM OF  $^{27}\text{Al}(p,\gamma)^{28}\text{Si}$   
WITH  $E_p = 992 \text{ KeV}$

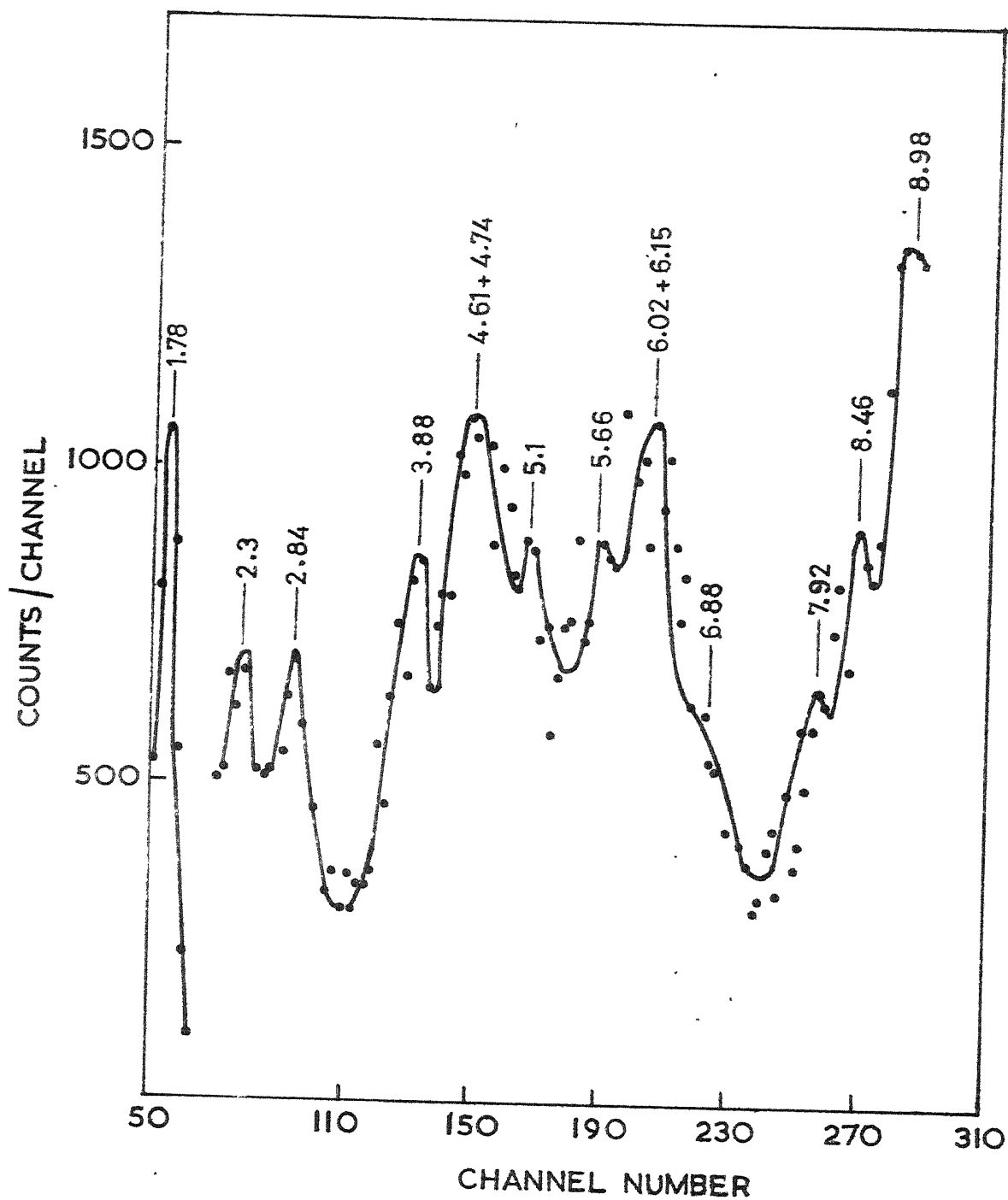


FIG. 8.9 SUM COINCIDENCE SPECTRUM OF 992 KeV RESONANCE IN  $^{27}\text{Al}(p,\gamma)^{28}\text{Si}$  WITH GATE AT 10.76 MeV

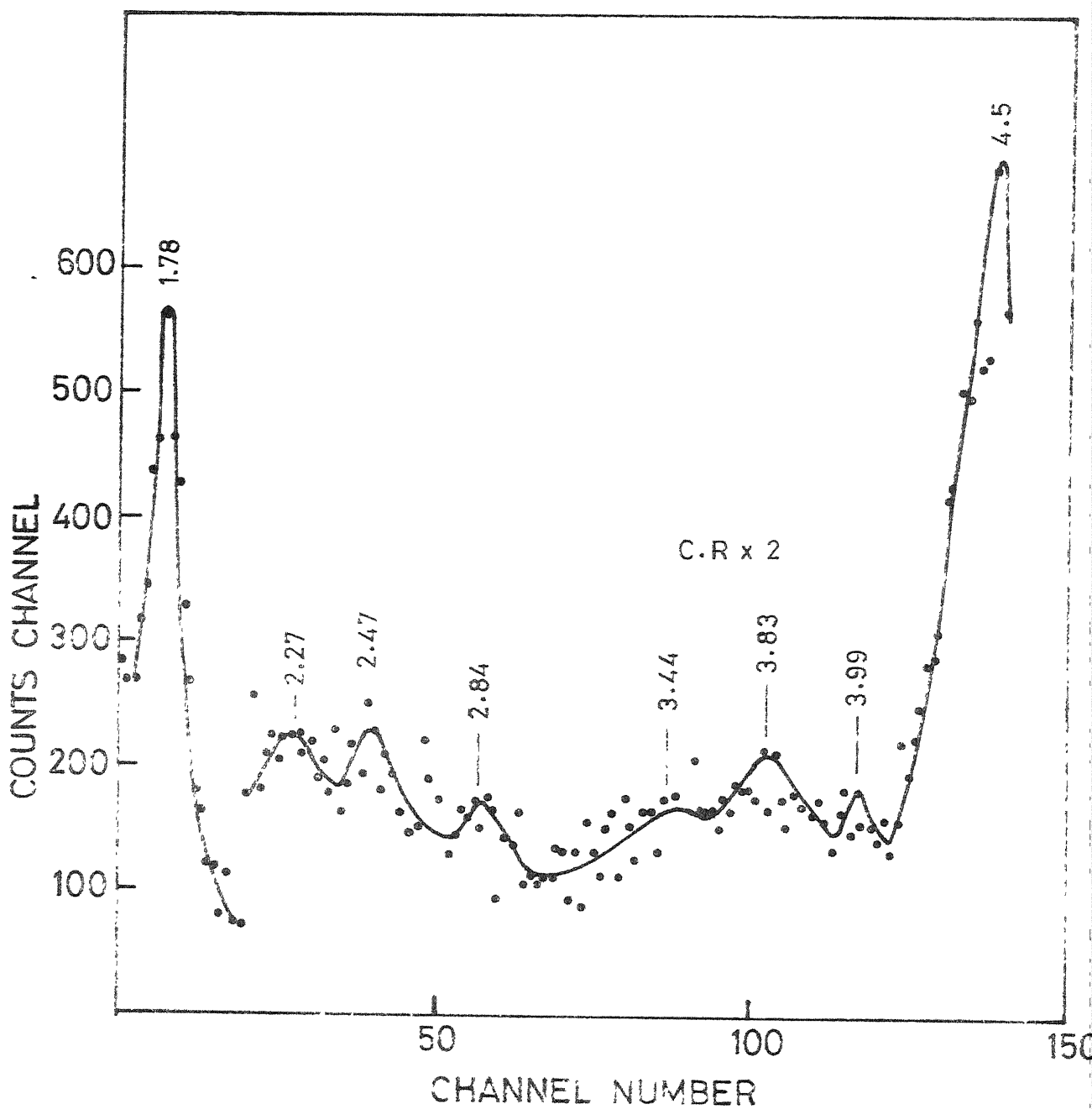


FIG 8.10 SJM-COINCIDENCE SPECTRUM OF 992 KeV RESONANCE  
IN  $^{27}\text{Al}(p,\gamma)^{28}\text{Si}$  WITH GATE AT 6.28 MeV

Table 8.1. Summary of sum-coincidence Measurements at  
the Resonance for  $E_p = 992$  keV

Energy gate (MeV)	Pairs of peaks Observed	Interpretation
10.76	1. 1.78, 8.98	compt 12.54 $\xrightarrow{10.76}$ 1.78 $\xrightarrow{1.78}$
	2. 2.3, 8.46	12.54 $\xrightarrow{2.27}$ 10.27, compt. 1
	3. 2.84, 7.92	12.54 $\xrightarrow{7.92}$ 4.62 $\xrightarrow{2.84}$ 1.78
	4. 3.88, 6.88	compt 12.54 $\xrightarrow{3.88}$ 6.88, 6.8
	5. 4.61, 6.15	12.54 $\xrightarrow{4.61}$ 7.93 $\xrightarrow{6.15}$ 1.78
	6. 4.74, 6.02	12.54 $\xrightarrow{4.74}$ 7.8 $\xrightarrow{6.02}$ 1.78
	7. 5.66, 5.1	12.54 $\xrightarrow{5.66}$ 6.88 $\xrightarrow{5.1}$ 1.78
6.28	1. 4.5, 1.78	6.28 $\xrightarrow{4.5}$ 1.78 $\xrightarrow{1.78}$ 0
	2. 2.27, 3.99	12.54 $\xrightarrow{2.27}$ 10.27 $\xrightarrow{3.99}$ 6.28
	3. 2.47, 3.83	10.27 $\xrightarrow{2.47}$ 7.8, compt 7.8 $\xrightarrow{3.83}$ 1.78
	4. 2.84, 3.44	compt 9.42 $\xrightarrow{3.44}$ 4.62, 4.62 $\xrightarrow{2.84}$ 1.78

gamma ray. An attempt was made to detect 2.27 MeV gamma ray which must be occurring due to  $12.54 \rightarrow 10.27$  MeV transition. There is an indication of the 2.27 MeV gamma ray in the spectrum of 1-3 MeV energy range.

Besides the singles spectra, the sum-coincidence spectra also provide evidence for the existence of 10.27 MeV level. The spectrum with gate at 10.76 MeV shows a pair of peaks with energies 2.3 and 8.4 MeV, which can only be understood as due to the 2.27 MeV gamma ray arising from  $12.54 \rightarrow 10.27$ , getting summed with the compton of 10.27 MeV gamma ray. The spectrum with gate at 6.28 MeV also offers evidence for this level. Two pairs of peaks at energies 2.3, 4.0 and 2.5, 3.8 MeV were observed. The pair of 2.3 and 4.0 MeV can be explained as due to  $12.54 \rightarrow 10.27 \rightarrow 6.28$  MeV mode of decay. The other pair is explained as due to 2.47 MeV gamma ray from  $10.27 \rightarrow 7.8$  MeV transition, summing with the compton of 6.02 MeV gamma ray arising from  $7.8 \rightarrow 1.78$  MeV transition. The gamma ray of energies 2.47 and 3.99 MeV were observed in Ge(Li) spect also, thus confirming the  $10.27 \rightarrow 7.8$  MeV and  $10.27 \rightarrow 6.28$  MeV decay modes. We, therefore, conclude that 10.27 MeV level exists and it populates 6.28 and 7.8 MeV levels, in addition to having a crossover mode of decay.

In singles spectra, two gamma rays of energies 1.05 and 1.65 MeV are observed, which are most probably due to



$7.93 \rightarrow 6.88$  MeV and  $7.93 \rightarrow 6.28$  MeV transitions. The decay scheme incorporating the present results is shown in Fig. 8.11.

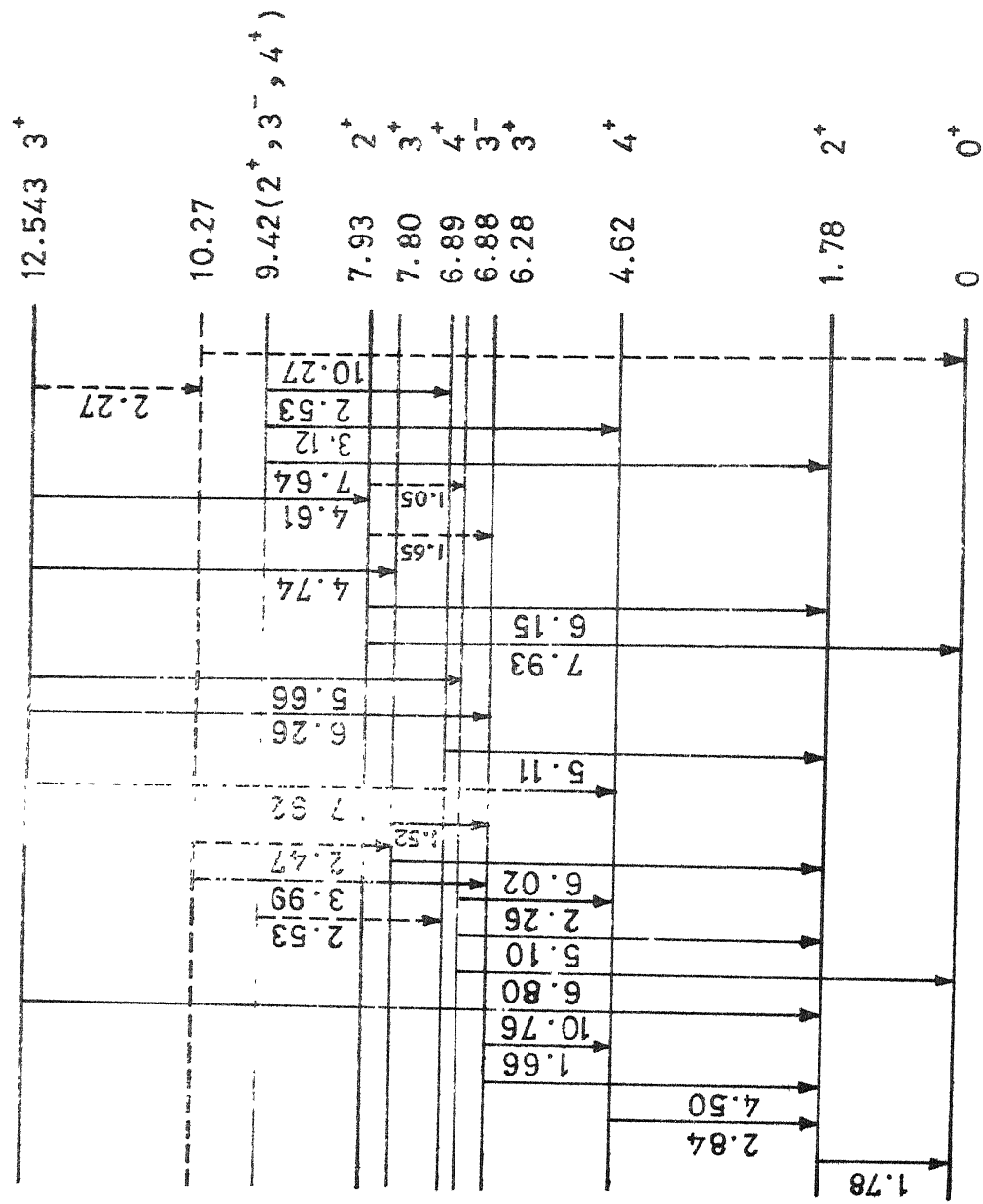
#### VIII.5 Gamma Decay of 1261 keV Resonance

In this case also, first a Ge(Li) spectrum was recorded upto 12 MeV energy to cover the entire region of interest. The spectrum is shown in Figs. 8.12(a) and 8.12(b). Two sum-coincidence spectra were recorded with gates at 11.02 and 8.1 MeV to observe the double cascades in  $12.8 \rightarrow 1.78$  and  $12.8 \rightarrow 4.62$  MeV decays. The two spectra are shown in Figs. 8.13 and 8.14 and the results are summarized in Table 8.2.

It was not possible to resolve the discrepancies from singles spectra. However, the sum-coincidence spectrum with gate at 11.02 MeV showed a pair of peaks at 3.1 and 7.9 MeV, which can be explained as the compton of 4.9 MeV gamma ray arising from the  $12.8 \rightarrow 7.9$  MeV decay, summing with the 7.9 MeV gamma ray. Thus, this spectrum provides an indication for the population of 7.9 MeV level. The decay scheme, including the level at 7.9 MeV, is shown in Fig. 8.15.

#### VIII.6 Summary

The results of the studies at 992 and 1261 keV resonances are summarized below:



(NOT TO SCALE)

FIG. 8.11 GAMMA DECAY SCHEME OF RESONANT CAPTURING STATE IN  $^{27}\text{Al}(p, n)^{28}\text{Si}$  AT  $E_p = 992 \text{ KeV}$

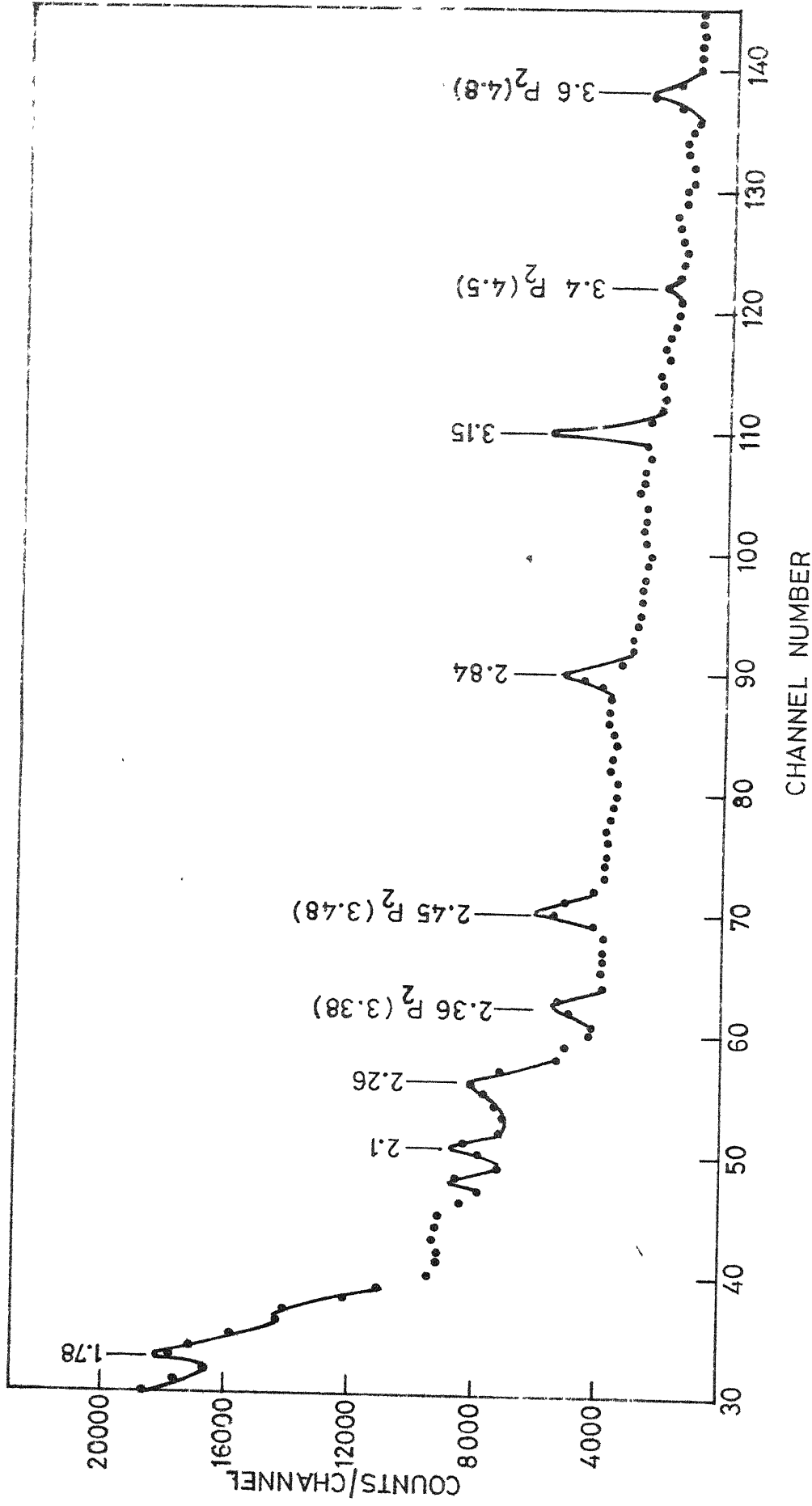


FIG. 8.12a Ge(Li) SPECTRUM OF  $E_p = 1261$  KeV RESONANCE IN 0-4 MeV GAMMA ENERGY RANGE

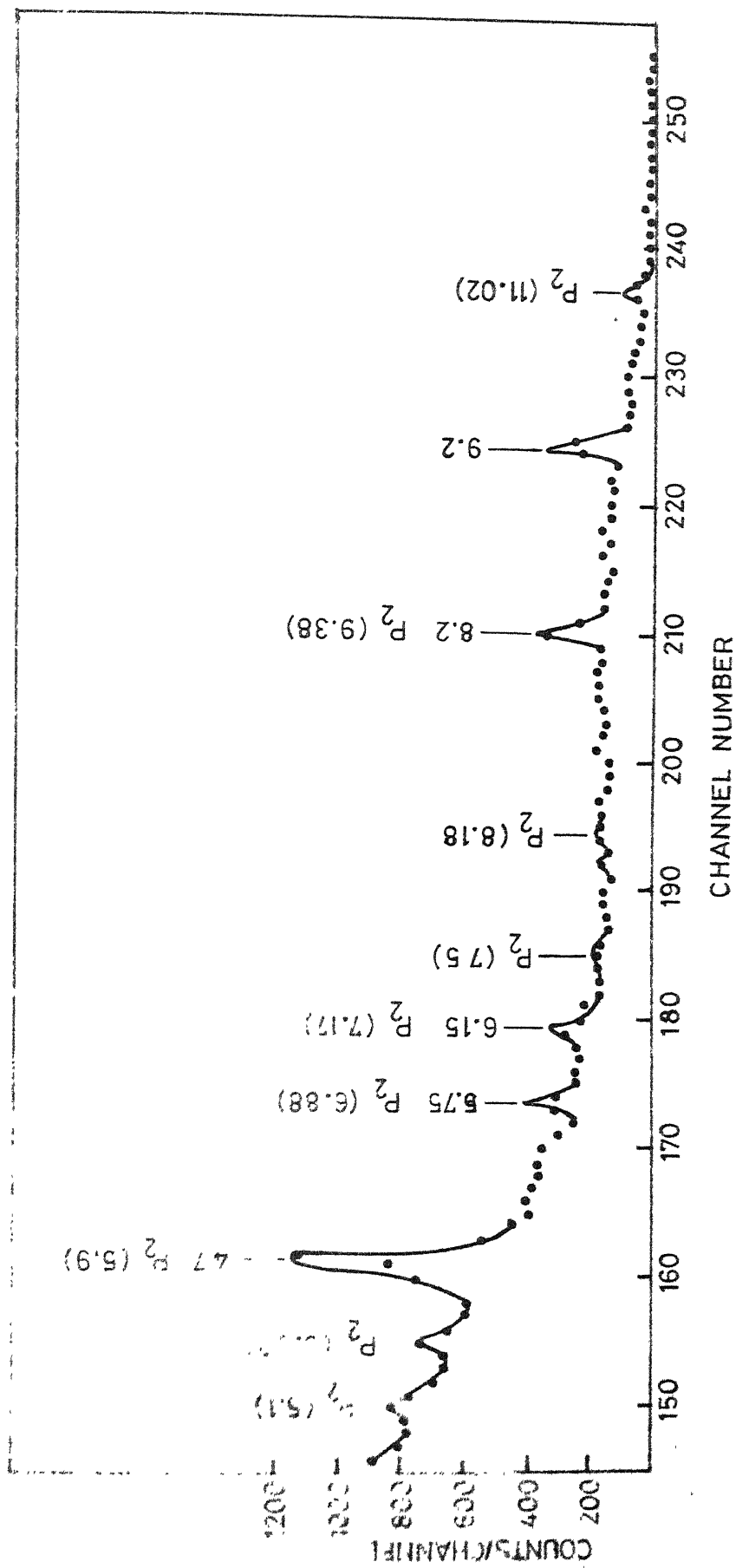


FIG.8.12b Ge(Li) SPECTRUM OF  $E_p = 1261$  KeV RESONANCE IN 4-11 MeV ENERGY RANGE

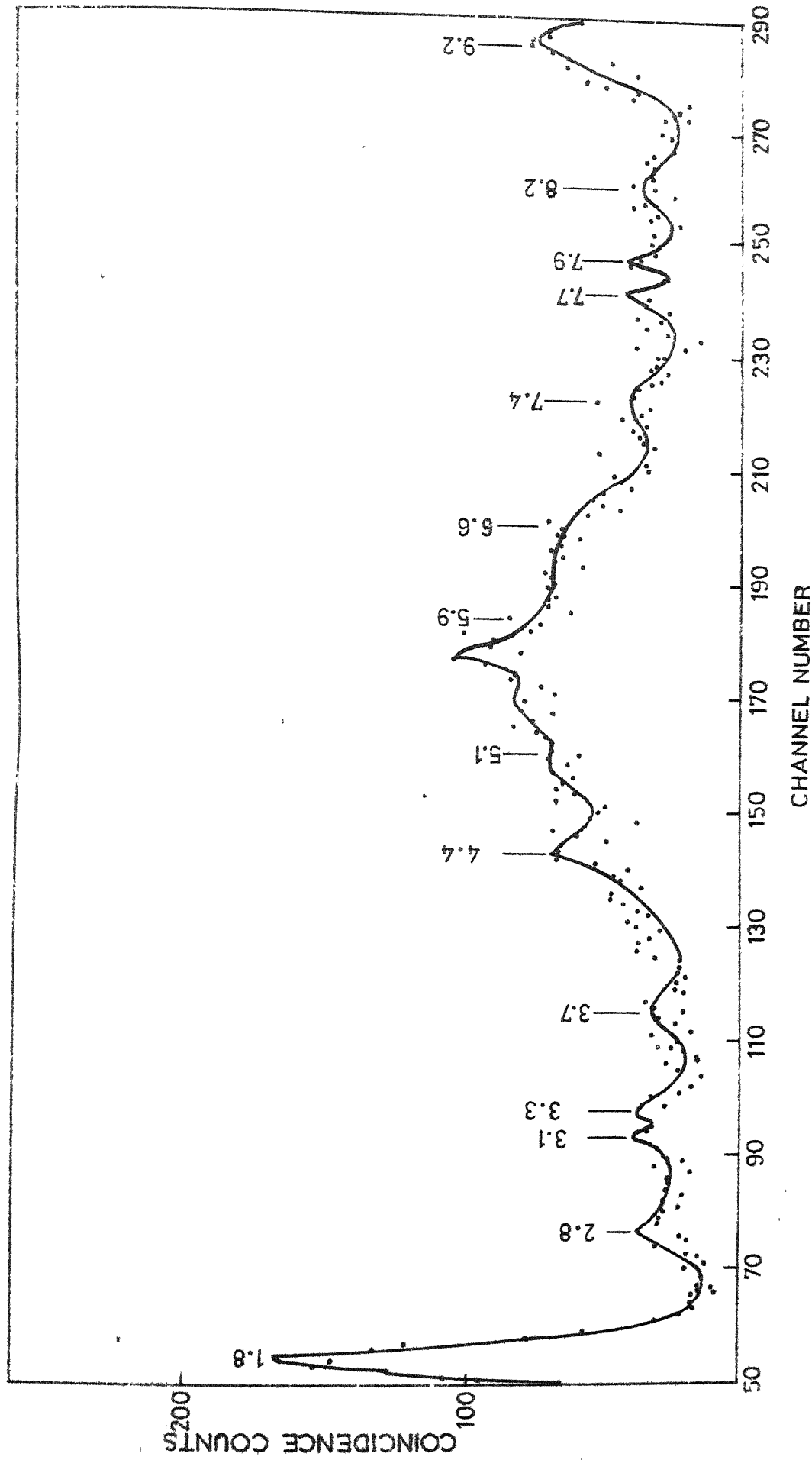


FIG. 8.13 SUM COINCIDENCE SPECTRUM WITH GATE AT 11.02 MeV FOR  $E_p \approx 1261$  KeV  
 RESONANCE IN  $^{27}\text{Al}(p,\gamma)^{28}\text{Si}$  REACTION

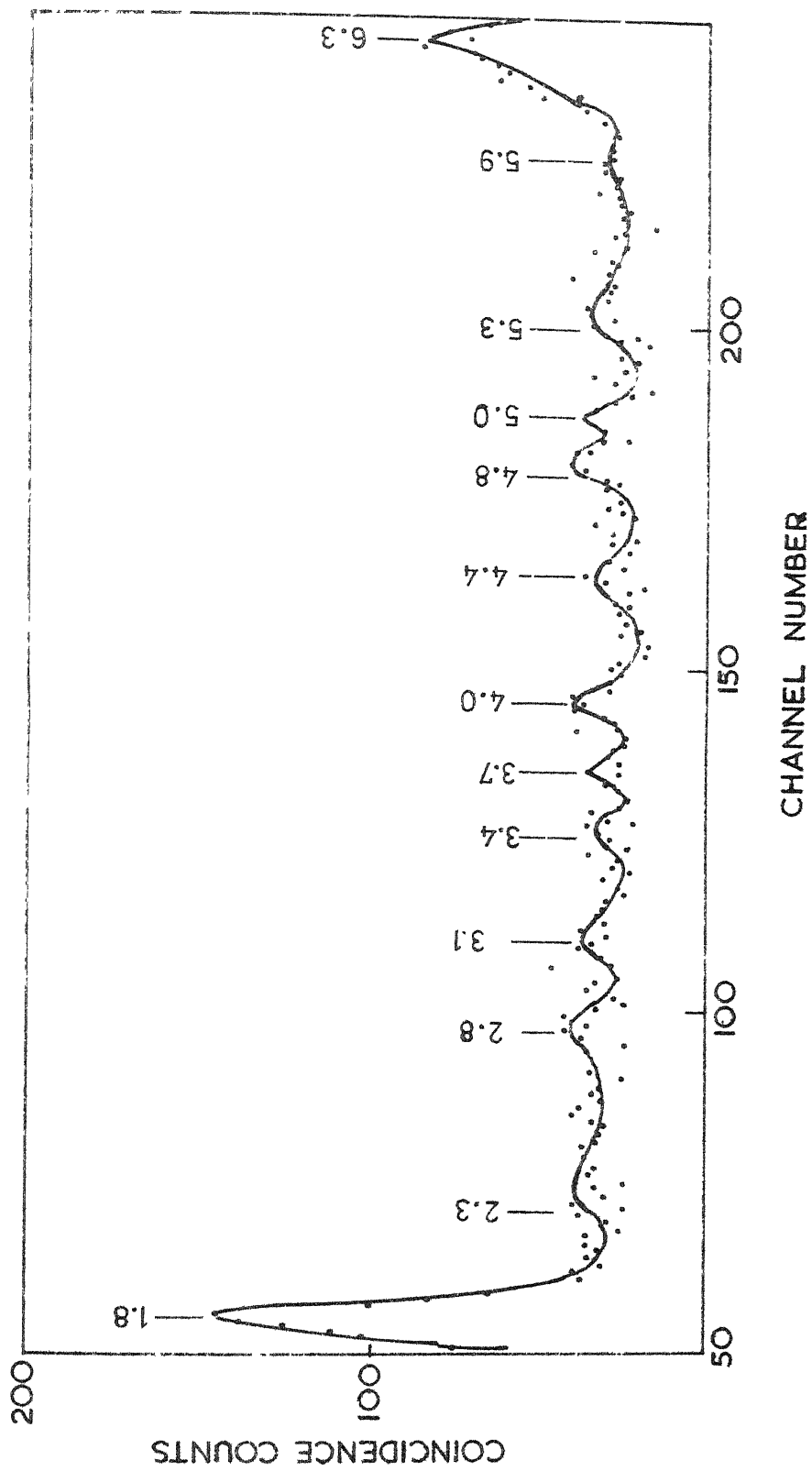


FIG. 8.14 SUM-COINCIDENCE SPECTRUM WITH GATE AT 8.1 MeV FOR  
 $E_p = 1261$  KeV RESONANCE IN  $^{27}\text{Al}(p,\gamma)^{28}\text{Si}$  REACTION

Table 8.2. Summary of Sum-coincidence Measurements at  
the Resonance for  $E_p = 1261$  keV

Energy gate (MeV)		Pairs of peaks Observed	Interpretation
8.1	1.	1.8, 6.3	compt 12.8 $\rightarrow$ 1.78, 1.78 $\rightarrow$ 0
	2.	2.3, 5.9	12.8 $\rightarrow$ 6.88 $\rightarrow$ 4.62
	3.	2.84, 5.3	compt 12.8 $\rightarrow$ 4.62, 4.62 $\rightarrow$ 1.78
	4.	3.1, 5.0	compt 12.8 $\rightarrow$ 6.88, 6.88 $\rightarrow$ 1.78
	5.	3.4, 4.8	12.8 $\rightarrow$ 9.42 $\rightarrow$ 4.62
	6.	3.7, 4.4	compt 12.8 $\rightarrow$ 6.28, 6.28 $\rightarrow$ 1.78
11.02	1.	1.8, 9.2	compt 12.8 $\rightarrow$ 1.78, 1.78 $\rightarrow$ 0
	2.	2.8, 8.2	12.8 $\rightarrow$ 4.62 $\rightarrow$ 1.78
	3.	3.3, 7.6	12.8 $\rightarrow$ 9.32 $\rightarrow$ 1.78 12.8 $\rightarrow$ 9.38 $\rightarrow$ 1.78 12.8 $\rightarrow$ 9.42 $\rightarrow$ 1.78
	4.	3.7, 7.4	compt 12.8 $\rightarrow$ 7.4, 7.4 $\rightarrow$ 0
	5.	4.4, 6.6	12.8 $\rightarrow$ 8.4 $\rightarrow$ 1.78
	6.	5.1, 5.9	12.8 $\rightarrow$ 6.88 $\rightarrow$ 1.78
	7.	7.9, 3.1	compt 12.8 $\rightarrow$ 7.9, 7.9 $\rightarrow$ 0

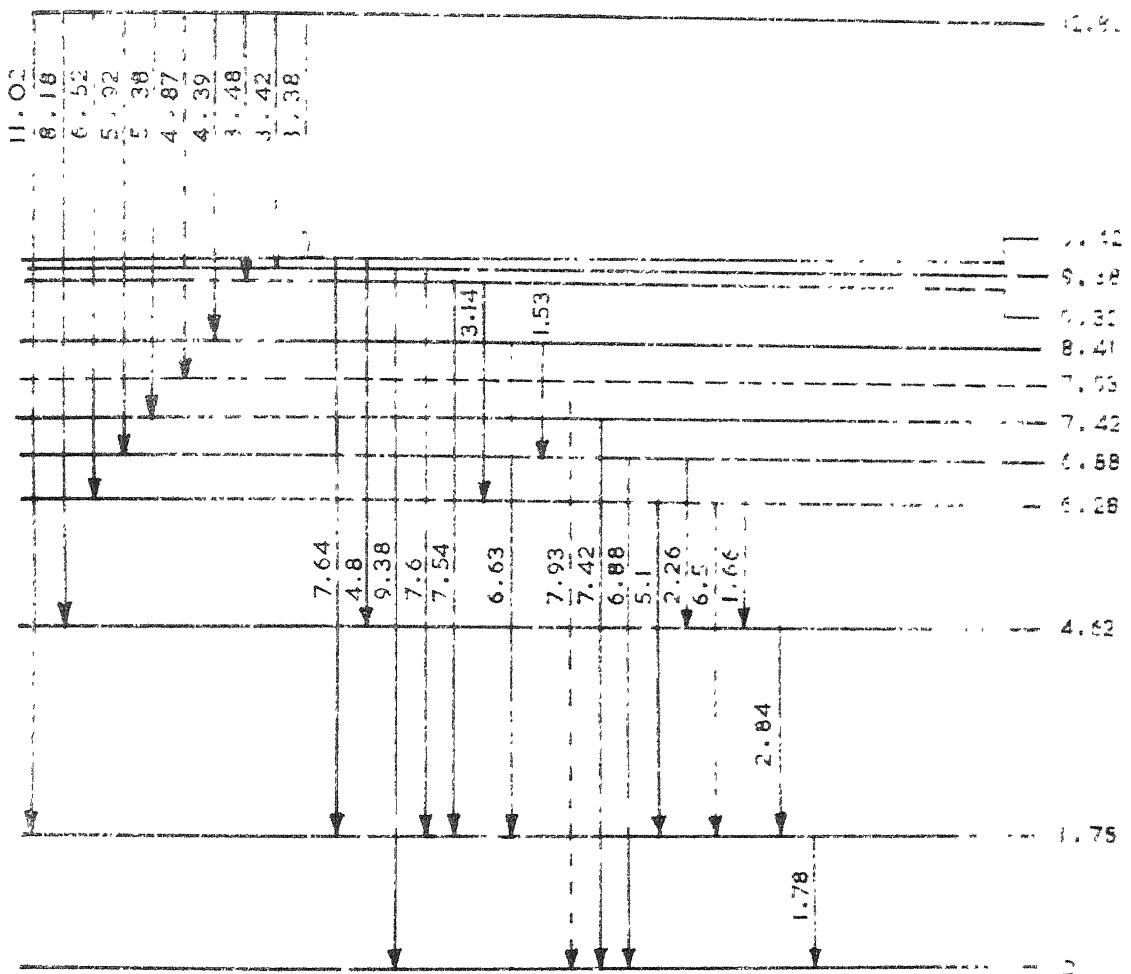


FIG.8.15 DECAY SCHEME OF RESONANT CAPTURING STATE IN  $^{27}\text{Al}(p,\gamma)^{28}\text{Si}$  AT  $E_p = 1261 \text{ KeV}$



- (i) The population of 10.27 MeV level in the 992 KeV resonance decay is confirmed from the singles as well as sum-coincidence measurements.
- (ii) The results indicate that the 10.27 MeV level populates 7.8 and 6.28 MeV levels and also the ground state in its deexcitation process.
- (iii) The 7.93 MeV level, in its deexcitation, populates 6.88 and 6.28 MeV levels also, besides the established ground state population.
- (iv) The results of the experiments at 1261 keV resonance are in fair agreement with the measurements of Meyer et al. except for an indication that 7.9 MeV level is also populated in this resonance decay.

REFERENCES

1. J.B. Marion, Rev. Mod. Phys. 33 (1961) 139.
2. T.R. Ophel and D.R. Osgood, Proc. Phys. Soc. 85 (1965) 1093.
3. R.E. Azuma, L.E. Carlson, A.M. Charlesworth, K.P. Jackson, N. Anyas-Weiss and B. Lavalic, Can. J. Phys. 44 (1966) 3075.
4. M.A. Meyer and N.S. Wolmarans, Nucl. Phys. A136 (1969) 663.
5. M.A. Meyer, N.S. Wolmarans and D. Reitmann, Nucl. Phys. A144 (1970) 261.
6. E.F. Gibson, K. Battleson and D.K. McDaniels, Phys. Rev. 172 (1968) 1004.
7. Y.P. Antoufiev, L.M. El-Nadi, D.A.E. Darwish, O.E. Badawy and P.V. Sorokin, Nucl. Phys. 46 (1963) 1.